



SAPIENZA
UNIVERSITÀ DI ROMA

UNIVERSITÀ LA SAPIENZA DI ROMA
FACOLTÀ DI SCIENZE MATEMATICHE, FISICHE E NATURALI

Corso di Laurea Magistrale in Fisica

Comparison between Direct and Indirect Detection of Dark Matter

**Dark matter particles: motivations and
observable manifestations, with a focus on the
electroweak mass range**

Relatore interno:
Prof. Antonio Capone

Candidata:
Vanessa Zema
matricola 1420488

Relatore esterno:
Dott. Francesco Vissani

Anno Accademico 2015/2016
Dipartimento di Fisica

Ai miei genitori

Contents

Introduction	1
1 Cosmological and Astrophysical Evidences of Dark Matter	3
1.1 Galaxy rotation curves	3
1.2 Gravitational lensing: the Bullet Cluster	4
1.3 Structure formation	5
1.4 CMB anisotropy and Λ CDM model	7
1.4.1 Dark energy	7
1.5 Thermal and non-thermal cosmologic relics	8
1.6 Primordial black holes	10
Appendix A.1	11
2 Motivations and Candidates for Dark Matter from Particle Physics	14
2.1 The Standard Model proposals and limits	15
2.1.1 Neutrinos	15
2.2 Axions	16
2.3 Sterile Neutrinos	19
2.4 Mirror Models	24
2.5 WIMPs	25
2.5.1 Neutralino	27
2.5.2 Kaluza-Klein photon	28
2.6 WIMPZILLAS	29
Appendix A.2	30
Appendix B.2	34
Appendix C.2	40
3 The Phenomenology of WIMP Candidates	46
3.1 The Milky Way dark matter halo	46
3.2 Direct detection	48
3.2.1 The halo velocity relative to the Earth	48
3.2.2 Recoil rate	50
3.2.3 WIMP elastic scattering cross section	51
3.2.4 Annual modulation	53
3.2.5 Inelastic-scattering	54
3.3 Indirect detection	54
3.3.1 WIMP capture and annihilation processes	55

CONTENTS

3.3.2	Event rate for neutrino fluxes	56
3.3.3	Event rate for γ -ray or cosmic ray fluxes	58
Appendix A.3	58
4	Experimental Search for Dark Matter Particles	61
4.1	Direct detection experiments	61
4.1.1	DAMA	63
4.2	Indirect detection experiments	67
4.3	Experimental results and comparison	69
5	Numerical Results	74
5.1	Numerical limits on elastic scattering off nuclei	74
5.2	Direct detection event rate in different targets	78
5.2.1	Differential rate for scalar couplings	80
5.2.2	The form factor contribution to the differential rate	83
5.3	Numerical limits on inelastic scattering off nuclei	87
5.4	Numerical limits on neutrino telescope sensitivity	88
	Conclusions	91
	Bibliography	94

Introduction

The scientific research is inspired by the unknown and unresolved, by the need to unravel and explain the physical reality. In the present time one of the most intriguing issue of physics is the evidence that a massive, non-interacting and non-baryonic form of matter constitutes about the 26% of the Universe. The nature of this matter, usually referred as Dark Matter, is unknown. This enormous blank in the knowledge of the physical reality is embarrassing and the necessity to provide an explanation is becoming more and more impelling. As a consequence several efforts led by the scientific community are dedicated to the dark matter search. In the last years many experiments are focusing on the solution of the missing mass problem. The main branches of physics involved in this challenge are cosmology, astrophysics and particle physics. Cosmology and astrophysics can boast the unique certain dark matter evidence at the present time, therefore are favoured tools. However particle physics actively contributes to this search through the elaboration of several hypotheses and experimental probes. Starting from theories beyond the Standard Model, elaborated to answer to the issues that afflict the affirmed theory, possible dark matter candidates are proposed, supported by the existence of plausible cosmological production processes. From these theoretical suggestions, experiments focusing on the different frameworks are realised. In this picture the deep ignorance on the dark matter nature causes the proliferation of hypothesis, models and convictions that are usually misleading and counter-productive. Scope of this thesis is to clarify what are the confirmed data and what are the proposals, to establish what are the conditions under which a comparison between the available results is allowed and in addition to contribute to the reconciliation among the apparent contrasting data, published by several research groups in the last years. To deal with this vast field, an accurate analysis of the available models is required, to reach an aware approach to the theoretical and experimental search. For this reason the initial part of this work is devoted to the theoretical study of some of the dark matter particle candidates. For a criterion of simplicity, the attention has been focused on minimal models, chosen also according to the strength of the arguments supporting the relative theories. The simple accommodation in the cosmological framework is another motivation. After this horizontal analysis, the popular model, relative to a dark matter mass in the electroweak mass range, is discussed. A particular attention is addressed to the different type of experimental searches carried out so far, that is to direct and indirect detection experiments. Usually the popular cross section plots are shown considering several sets of results, in order to compare the available data. However the conditions under which the comparisons are allowed are often not illustrated and the confusion that can arise from this omission invalidates

Introduction

the comparison. One of the aims of this work is to clarify these assumptions. The last section is devoted to the evaluation of the typical behaviour of the counting rate relative to the dark matter interaction occurring within the detectors. The simulation of the differential counting rate in different detectors, together with the evaluation of the nuclear form factors contribution, allows to predict the expected signal. A final challenge is to assess which are the reasons of tension among the experiments that claim a dark matter signature detection and the experiments that would exclude the same signal. The demonstration of the agreement between the results would play the fundamental role to strengthen the hypothesis that the signal detected by some experiments corresponds really to the first dark matter signature.

Chapter 1

Cosmological and Astrophysical Evidences of Dark Matter

The literature dealing with the dark matter problem starts off by listing the astrophysical and cosmological proofs of the dark matter existence, because it needs to demonstrate, or remember, that the dark matter, in any of the possible shapes, does exist.

1.1 Galaxy rotation curves

The main and oldest astrophysical proof of the dark matter existence originates from the measure of the galaxy rotation velocity within the galaxy clusters. In the rough approximation of spheric and self-gravitating galaxies, of equal mass m and orbital velocity v , the cluster is considered a virially bound system, described by:

$$2K + U = 0 \rightarrow v(r) = \sqrt{\frac{GM(r)}{2r}} \quad (1.1)$$

where K is the kinetics energy, U is the potential energy and $v(r)$ is the orbital velocity of a galaxy at a distance r from the center. G is the gravitational constant while $M(r) = \int_0^r d^3r' \rho(r')$ is the mass contained within the distance r , where ρ is the mass density. From the measure of the galaxy orbital velocity an estimation of the total mass content can be inferred regardless of the luminous matter content, making possible a comparison.

The first observation that let to a similar calculation dates back to F. Zwicky (1933), who studied the galaxy velocity in the Coma cluster [1]. The two contributions in the Coma cluster results in a ratio of $O(10^2)$. This estimation leads to the conclusion that a dark missing mass component must exist.

A similar estimation holds to smaller scales, such as at the galactic scale. The measure of the orbital velocity as a function of the radius allows the construction of the rotation curve of the objects in a galaxy, whose behaviour is expected to be decreasing for greater distances from the center according to:

1.2 Gravitational lensing: the Bullet Cluster

$$m \frac{v^2(r)}{r} = \frac{GmM(r)}{r^2} \rightarrow v \propto \frac{1}{\sqrt{r}} \quad (1.2)$$

Indeed the experimental results provide flat rotation curve up to large radii that does not fit the expected threshold, that is the curve obtained considering only the galactic disk and the gas contribution, as shown for example in fig. (1.1).

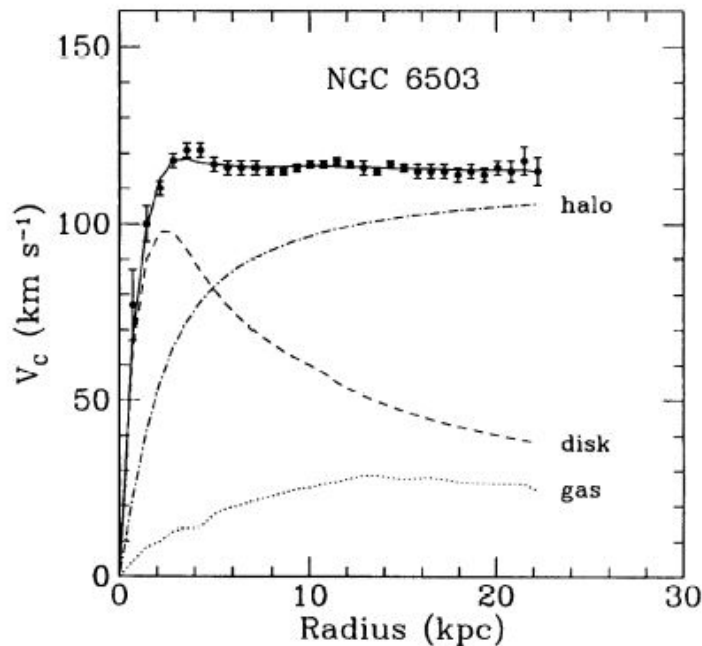


Fig. 1.1: Rotation curve for the dwarf spiral galaxy NGC 6503, located in the Local Void. The dashed and pointed line are the expected curve for the disk and gas contribution, while the data are fitted considering the dark matter contribution. Taken from K.Freese, (2009), *Review of Observational Evidence for Dark Matter in the Universe and in upcoming searches for Dark Stars*.

1.2 Gravitational lensing: the Bullet Cluster

The gravitational lensing is the fascinating phenomenon of deviation of the light path as a consequence of the distortion of the spacetime geometry, due to the presence of a large gravitational field. Since the spacetime curvature modifies the null geodesic, the light emitted by sources behind the massive object are deviated and the source images appear projected around the massive object. Indeed this is the rare *strong* lensing, that occurs when the light source is close to a very massive object and the emitted light is projected into multiple images. It is called *weak* lensing instead the common stretching of the light source image, that occurs almost to all the astrophysical observed objects.

The lensing phenomenon, since it is related only to gravity, allows to identify matter whose unique detectable interaction is gravitational. An example is the observed gravitational lensing around the so called Bullet cluster, evidence that confirmed the existence of a dark matter component of our universe.

1.3 Structure formation

The Bullet cluster (1E0657-56) was observed by the NASA Chandra X-ray telescope in 2006 and it is the most energetic event known from the Big Bang. It is the result of the two galaxy cluster merge and its popularity is due to its contribution as proof of the dark matter existence.

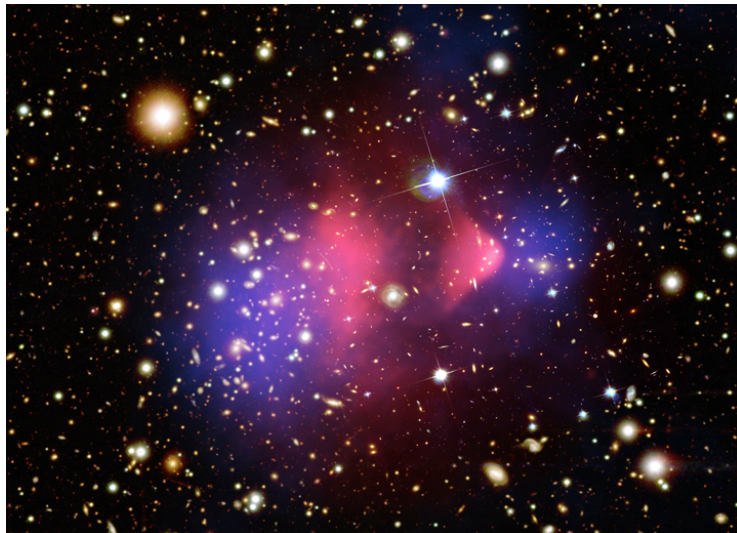


Fig. 1.2: NASA X-ray Chandra composite image of the galaxy cluster 1E0657-56, also known as Bullet cluster. The pink clouds represent baryonic gas, while the blue regions represent the dark matter content, estimated from measures of gravitational lensing.

The pink shadows represents the baryonic gas content; the right pink cloud shape suggests a friction effect. The blue clouds represents instead the two cluster matter content that does not interact neither with the gas or with itself and that, therefore, passes undisturbed through the gas. The signature of this non-interactive mass content is only the gravitational lensing of the light source nearby. As a consequence of this observation, the two blue regions are identified as dark matter.

1.3 Structure formation

The cosmology branch that studies the structure formation mechanisms participates to a great extent to the dark matter nature identification. The Jeans theory on cosmological perturbations asserts that a local inhomogeneity $\delta\rho$ can evolve towards a structure formation if the ratio with the average background density $\bar{\rho}$ is $\delta\rho/\bar{\rho} \gg 1$. The first baryonic density fluctuations, that survive against the radiation pressure, are impressed on the Cosmic Microwave Background (CMB), which is the surface of last scattering originated by the photon decoupling age. Since then, the density fluctuations have been growing as the cosmic scale factor a , such that:

$$\frac{\delta\rho_0}{\bar{\rho}} = \frac{a(t_0)}{a(t_{dec})} \frac{\delta\rho_{dec}}{\bar{\rho}} = (1 + z_{dec}) \frac{\delta\rho_{dec}}{\bar{\rho}} \quad (1.3)$$

where 'dec' refers to the decoupling age, $z_{dec} \sim 10^3$ is the redshift at recombination and $\frac{\delta\rho_{dec}}{\bar{\rho}} \simeq 10^{-4}$ from CMB experimental data. From the simple estimation

1.3 Structure formation

of eqs. (1.3), we conclude that today the ratio between the baryonic density fluctuations and the background density would be equal to $\delta\rho/\bar{\rho} \sim 10^{-1} < 1$, that clearly implies that the luminous baryonic content alone would not allow the reaching of the observed galaxy distribution. Since the washing out of the previous-CMB baryonic density fluctuations is due to the coupling with photons (it is the radiation pressure content that contrasts the gravitational collapse), then a matter content that does not couple with photons, i.e. a *dark* matter content, is required [5].

Since the dark matter nature is unknown, its couplings with ordinary matter are mysterious as well. No information about its production mechanism is available, therefore, as a matter of principle, the dark content of the universe could be hot (relativistic), cold (non-relativistic) or warm. But again the matching with the structure formation theory contributes to constrain the field.

- The **hot dark matter** hypothesis would require that larger structures form before smaller structures. The reason is that the relativistic particles *free streaming*, that is the particle displacement between different density regions of the fluid, smoothes the bumpy inhomogeneities that are below a characteristic length. For this reason structure with initial density fluctuations below this characteristic length are avoided. This ordering, called 'top-down' process, is excluded by the experiments and, as a consequence, the hot dark matter hypothesis is excluded as well⁽¹⁾.
- The **cold dark matter** paradigm is instead related to the ordering called 'bottom-up', that assumes a natural hierarchical structure formation starting from the smallest to the largest objects. This scheme is confirmed by experiments that figure out that small structures are older than large structures. Many of the dark matter particle candidates belong to this framework, such as axions and WIMPs.
- Between these two limits there is the intermediate case of **warm dark matter**. The hypothesis is that the dark matter decouples when it is still relativistic but before the decoupling of the neutrino species, such that its temperature is now below that of neutrinos. In this condition the dark matter free streaming is compatible with the structure formation observed today and both the top-down and the bottom-up schemes are possible. The main candidate that can be described as warm dark matter is the keV sterile neutrino.

Hence the theory of the structure formation provides a determining proof of the dark matter existence and furthermore contributes to the dark matter nature identification, for instance excluding the hot dark matter candidates. However the possibility that a smaller fraction of the dark matter content is hot is not excluded: these are called *dark matter mixed models*.

¹As we will discuss later, this is the reason of the standard neutrino exclusion from the possible dark matter candidates.

1.4 CMB anisotropy and Λ CDM model

The baryon matter density fluctuations are impressed on the CMB, due to the baryon coupling with photons, that for instance allows indirect conclusions about the dark matter existence, as discussed before. The dark matter density fluctuations are not directly observable on the CMB because dark matter does not emit any signal.

Indeed through the gravitational attraction that exerts, the escaping matter directly leaves a mark on the CMB. The CMB temperature fluctuations carry the information about the gravitational redshift experienced by photons; such redshift is a consequence of the gravitational field originated by the *whole* present matter content. Thanks to this effect, studied by Sachs and Wolfe in 1967 [6], the dark matter content can be inferred by the CMB study. Indeed the most compelling constraints on the dark matter properties are imposed exactly by the CMB study.

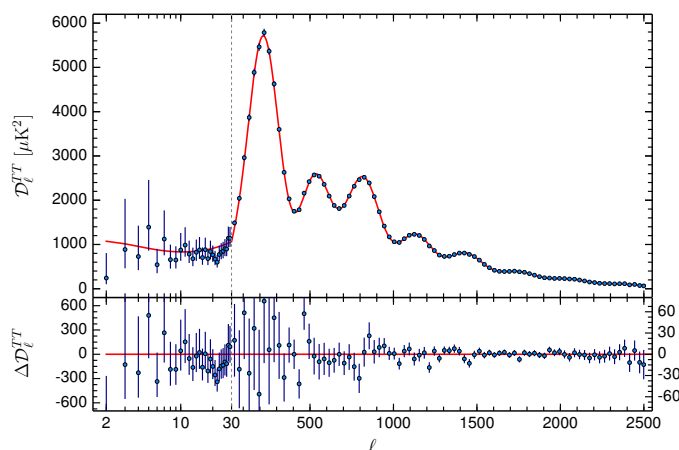


Fig. 1.3: The Planck 2015 temperature power spectrum. The Λ CDM is the best-fit of the experimental data. In the lower panel the residuals with respect this model are shown [4].

The so called Λ CDM (Λ Cold Dark Matter) model, is the minimal model of cosmology corrected for the dark matter contribution, involving also the inflationary mechanism and the dark energy. Λ is the historic cosmological constant, the scalar field that was proposed wrongly by Einstein to preserve the Universe stationarity and that, after the evidence of the universe expansion, was again introduced as possible explanation of the present universe expansion acceleration. The Λ CDM model fortune is due to its capability to describe the experimental results, as recently confirmed by the Planck collaboration [4]. They affirms that the data are so consistent with the Λ CDM model that if there is new physics beyond the standard cosmology, it is very difficult to detect it. The power spectrum describing the coefficients of the temperature anisotropy multipole expansion shows clearly the perfect consistency between the CMB data and the Λ CDM expectation.

1.4.1 Dark energy

The Λ CDM model is characterized by six parameters: the Hubble constant H_0 , two of the three density parameters (the third is fixed by the equation $\Omega_b + \Omega_c + \Omega_\Lambda =$

1.5 Thermal and non-thermal cosmologic relics

1), the reionization optical depth τ , the scalar density fluctuation amplitude A_s and the spectral index n_s [3]. The experiments constrain the density parameters and the result is that about the 69% of our universe is made of dark energy.

Dark energy is the unknown form of energy that is responsible for the universe acceleration. Consider standard cosmology acceleration equation:

$$\left(\frac{\ddot{a}}{a}\right) = -\frac{k}{6}(\rho + 3p) = -\frac{k}{6}\rho(1 + 3w) \quad (1.4)$$

where a is the expansion scale parameter, k is a positive constant, ρ is the energy density and p is the pressure and w derives from the equation of state $p = w\rho$. This equation in order to describe the expansion acceleration requires the presence of a negative pressure component $p \leq \frac{\rho}{3}$, such that $\ddot{a} > 0$.

There two main candidate for the solution of the dark energy problem:

- the cosmological constant Λ , that is the most popular;
- the dynamical scalar field $\phi(t)$, named *quintessence*.

The cosmological constant belong to the standard cosmology framework. The experimental results are consistent with the hypothesis that there is a constant energy component in our Universe and this is the reason of the popularity of the Λ CDM model. However, from the theoretical point of view, the matching between cosmology and quantum field theory fails. The cosmological constant is commonly associated to the quantum vacuum energy, whose order of magnitude is computed as $\rho_{vac} \simeq M_P^4 \simeq (10^{112}\text{eV}^4)$, where M_P is the Planck mass; instead the dark energy density is $\rho_{de} \simeq (10^{-11}\text{eV}^4)$. This absurd discrepancy between the two order of magnitude is the so called "cosmological constant problem".

The quintessence is instead a scalar field ϕ , that is time-dependent. The hypothesis is that at the beginning or at the end of its time evolution it recovers the behaviour of the cosmological constant. As the cosmological constant, this proposal encounters a difficulty when compared with quantum field theory. Cosmology would fix a scalar mass $m_\phi \simeq 10^{-33}\text{eV}$, while the expectation value ϕ is $\sim M_P$.

1.5 Thermal and non-thermal cosmologic relics

- This section refers to [2].

A particle is defined as a *thermal relic* if it was produced by the decoupling from the primordial thermal bath with which it was previously in equilibrium. At the beginning all the known particles were merged in this primordial plasma. What is named as the *thermal history of our Universe* is marked by epochs associated to the different time of particle decoupling from the equilibrium. The equilibrium holds until the different species density number is conserved, i.e. until the high temperature allows "bilateral" interactions. Each particle destroyed is restored by

1.5 Thermal and non-thermal cosmologic relics

the inverse reaction. In a static Universe this ideal condition would hold in any time and the thermal relics would have never produced. The evidence of an expanding Universe, described by a time dependent spacetime geometry, implies instead that many physical quantities, such as the distances, the energy density, the temperature, are time-dependent and, as a consequence, the interaction amplitude as well. The decoupling condition occurs when the thermal bath temperature T drops with respect the particle mass m , i.e. when:

$$T \ll m \tag{1.5}$$

When the mass is greater than the temperature, its production is forbidden and its number density drops due to its annihilation or decay into lighter particles. But the thermal relic number density depends also on the relation between the particle interaction amplitude Γ and the expansion rate $H = \frac{\dot{a}}{a}$. When the interaction amplitude Γ drops with respect to the expansion rate $H = \frac{\dot{a}}{a}$ as much that:

$$\Gamma \ll H \tag{1.6}$$

then the particle number density "freezes-out", because also the annihilation or decay interactions are now forbidden. The species that experience these two mechanisms are what is defined *thermal relics*.

The difference between relativistic and non-relativistic thermal relics originates from the balance between the decoupling and the freeze-out mechanisms:

- if the particle decoupling occurs before the freeze-out than the resulting species is **non-relativistic**⁽²⁾;
- if the freeze-out occurs when the particle is in equilibrium with the thermal bath then the resulting species is **relativistic**.

From the dark matter problem point of view, under the assumption that it is a thermal relic, its distinction in hot, cold or warm depends on the temporal order between decoupling and freeze-out.

An example of hot thermal relic is the neutrino. Since it is light and coupled to ordinary matter only through the weak interactions, it freezes out before the temperature becomes smaller than its mass, therefore it is a relativistic, hot, thermal relic. For the reasons discussed above, regarding the structure formation, it is excluded from the list of possible dark matter candidates.

An example of thermal warm dark matter is instead the sterile neutrino with keV mass range. The sterile neutrino is assumed to be not coupled with ordinary matter, expect for a small mixing with active neutrinos. Hence its interaction amplitude is smaller than that associated to the weak interactions and as a consequence it decouples before active neutrino decouple. The departure from the thermal bath allows their temperature drop and the possibility that the sterile neutrino today can be considered warm.

Finally the thermal cold dark matter is associated to the hypothesis that the dark particle is so massive that the thermal bath temperature becomes smaller than

²For more details see the Appendix A.1.1

1.6 Primordial black holes

the mass before the freeze-out occurs. As a consequence the thermal relic is non-relativistic and therefore cold. This is the case of the Weakly Interactive Massive Particles.

During its thermal history, the Universe experiences also phase transitions, due to mechanisms similar to the quantum field theory Spontaneous Symmetry Breaking (SSB). These phase transitions could contribute to the cosmologic production of massive scalar fields, that today are among the possible solutions of the missing mass problem, for instance the axions⁽³⁾. The axions could be thermally produced as the other particles, but the condition of Universe closing imposes for them a mass of 130 eV; such axions would decay very quickly and astrophysical constraints (concerning for example the star energy loss) exclude this possibility. The conclusion is that thermal axions are ruled out from the dark matter candidates.

Let us briefly illustrate how the SSB process introduces the axion non-thermal production. Given a scalar field ϕ , its potential is:

$$V_\phi(T) = \frac{1}{2}m_\phi^2(T)\phi^2 + \frac{\lambda}{4!}\phi^4 \quad (1.7)$$

where $\lambda > 0$ is the self-interaction coupling. The mass m_ϕ depends on temperature in such a way that when the temperature drops and reaches a characteristic value, the squared mass changes sign (the mass becomes complex). Then the potential assumes the typical "wine bottle" behaviour. The minimum potential point does not depend on the $\Theta \equiv \arg\langle|\phi|\rangle$ and the free choice of one of the possible minima is the cause of the symmetry breaking. Θ is the massless scalar field produced by the SSB. For the axion the experiments suggest that the chosen minimum is $\bar{\Theta} = 0$, as we will discuss later.

A non-thermal relic can be produced by the coherent oscillations that the massless scalar field experiences when roll toward the minimum; in fact at high temperature there is no reason for Θ to be in the minimum. This process is called *misalignment production* because deals with the displacement of the 'misaligned' Θ from its high temperature generic value Θ_1 towards the minimum $\bar{\Theta}$. The equations that rule the misalignment production are beyond the purposes of this work; the relevant aspect of this non-thermal process is that for low temperatures, as that of today, the axion produced is estimated to be cold. In the dark matter optic this is a favorable point for the axion candidate, since the cold dark matter is the framework suggested by the cosmologic observations. Furthermore among the allowed windows of mass that can account for the dark matter density there is the $10^{-5} - 10^{-3}$ eV mass range, that so far has not been ruled out by any experiments.

1.6 Primordial black holes

Primordial Black Holes (PBH) are the gravitational collapse of overdensity region of the primordial Universe. Since they are expected to form before the Big Bang

³The axion arises by the spontaneous symmetry breaking of the Peccei and Quinn new gauge symmetry, the $U(1)_{PQ}$, proposed to provide an explanation to the strong-CP problem. We shall talk about this topic in the next chapter.

Appendix A.1

Nucleosynthesis (BBN) they are not constrained by the baryon-to-photon ratio $\eta \simeq 10^{-10}$. For this reason they are considered to participate to the non-baryonic and non-luminous matter content. Furthermore PBH should be collisionless and non-relativistic, therefore they could account for *cold* dark matter or at least for a fraction of it[6]:

$$f_{pbh} = \frac{\Omega_{pbh}}{\Omega_c} \quad (1.8)$$

where Ω_{pbh} is the hypothesized PBH parameter density and Ω_c is the dark matter parameter density. The abundance of PBH is estimated to be in four allowed mass windows:

- the intermediate mass range with $M_\odot < M < 10^3 M_\odot$;
- the sublunar between $10^{20} - 10^{24}$ g;
- the subatomic-size⁽⁴⁾ between $10^{16} - 10^{17}$ g;
- the last, less popular, of 10^{-5} g;

where $M_\odot \simeq 10^{33}$ g is the solar mass and M is the PBH mass [8]. In the other mass ranges f_{pbh} is less than 10^{-1} , therefore could account only for a fraction of the total missing mass.

These constraints are imposed by observations. For example PBH smaller than 10^{15} g would evaporate due to the Hawking radiation [7] and the null detection of γ -rays compatible with this phenomenon limits their abundance. Another example is the non-observed microlensing in the Magellanic clouds that rules out the more massive mass range between 10^{26} g and $15M_\odot$.

Due to their gravitational interactions, PBH, if exist, should mark the CMB through the processes described above, therefore the CMB experiments are an useful tool to probe this hypothesis.

A new stronger interest on PBH originates from the recent detection by the LIGO (Laser Interferometer Gravitational-Wave Observatory) and Virgo Collaboration of the gravitational waves produced by two merging black holes, that could open a new way for dark matter Primordial Black Holes search [9][10].

Appendix A.1

A.1.1 The Boltzmann equation: non-relativistic thermal relics

The early Universe thermal history reveals the features of the origin of all the species [2][3]. Just after the Big Bang, the Universe is dominated by the radiation, a plasma of relativistic particles in a dynamical equilibrium kept by the annihilation and production rate balance. This equilibrium depends on the mass-temperature ratio and holds until $T \gg m$. Since the expanding Universe causes a temperature decrease, when $m \gg T$ the energy loss inhibits the heaviest particles production and the relative number densities reduce. The particle phase space distribution function

⁴The Schwarzschild radius is $r_{BH} = \sqrt{\frac{2GM}{r}} \simeq 10^{-15}$ m for $10^{16} < M < 10^{17}$ g

Appendix A.1

evolves according to the Boltzmann equation ($L[\hat{f}] = C[f]$). In the Friedmann-Robertson-Walker (FRW) model of an isotropic and homogeneous Universe, the number density evolution equation is [1]:

$$\dot{n}_\chi + 3Hn_\chi = \langle \sigma_{\chi\bar{\chi} \rightarrow f\bar{f}} |v| \rangle [(n_{EQ})^2 - n^2] \quad (1.9)$$

where n_{EQ} is the number density of particles in thermal equilibrium, given by the integration of the Fermi-Dirac (or Bose-Einstein) distribution for the relativistic species ($T \gg m$) and the Maxwell-Boltzmann distribution for the non-relativistic ones ($m \gg T$), H is the expansion rate and $\langle \sigma_{\chi\bar{\chi} \rightarrow f\bar{f}} |v| \rangle$ is the annihilation rate times the velocity, averaged over the $\chi\bar{\chi}$ distribution functions⁵. A more compact form is:

$$a^{-3} \frac{d(n_\chi a^3)}{dt} = \langle \sigma_a |v| \rangle [(n_{EQ})^2 - n^2] \quad (1.11)$$

where a is the cosmological scale parameter. Since $(aT)^3$ is constant in the time, the left hand side can be written as:

$$a^{-3} \frac{d(n_\chi a^3 \frac{T^3}{T^3})}{dt} = a^{-3} (a^3 T^3) \frac{d(\frac{n_\chi}{T^3})}{dt} = T^3 \frac{d(\frac{n_\chi}{T^3})}{dt} \quad (1.12)$$

Considering the density number of particles per comoving volume:

$$Y = \frac{n}{T^3} \quad (1.13)$$

that is a convenient expression since $n/s \propto N/(aT)^3$ is adimensional and $(aT)^3$ is constant, the Boltzmann equation become:

$$\frac{dY}{dt} = T^3 \langle \sigma_{\chi\bar{\chi} \rightarrow f\bar{f}} |v| \rangle [Y_{EQ}^2 - Y^2] \quad (1.14)$$

Now define the adimensional quantity $x = \frac{m}{T}$, such that:

$$\frac{dY}{dx} = \frac{T^3}{Hx} \langle \sigma_{\chi\bar{\chi} \rightarrow f\bar{f}} |v| \rangle [Y_{EQ}^2 - Y^2] \quad (1.15)$$

Since we are interested in the dark matter abundance today, we consider a later time, when $x \gg x_F$ (where x_F is the m_χ/T ratio at the freeze-out) and $Y \gg Y_{EQ}$ (since $Y_{EQ} \propto e^{-m_\chi/T}$), as the common plot shows:

⁵The annihilation cross section times the relative velocity between the two initial particles, averaged over the $\chi\bar{\chi}$ distribution functions is:

$$\langle \sigma_{\chi\bar{\chi} \rightarrow f\bar{f}} |v| \rangle = N \int d\Pi_\chi d\Pi_{\bar{\chi}} d\Pi_f d\Pi_{\bar{f}} (2\pi)^4 \delta^4(p_\chi + p_{\bar{\chi}} - p_f - p_{\bar{f}}) |M|^2 e^{-E_\chi/T} e^{-E_{\bar{\chi}}/T} \quad (1.10)$$

where $N = \int d\Pi_\chi d\Pi_{\bar{\chi}} e^{-E_\chi/T} e^{-E_{\bar{\chi}}/T} = (n_\chi^{EQ})^{-2}$ is the normalization and $d\Pi_i = g_i \frac{d^3p}{(2\pi)^3}$ is the phase space of the species i with g_i degrees of freedom.

Appendix A.1

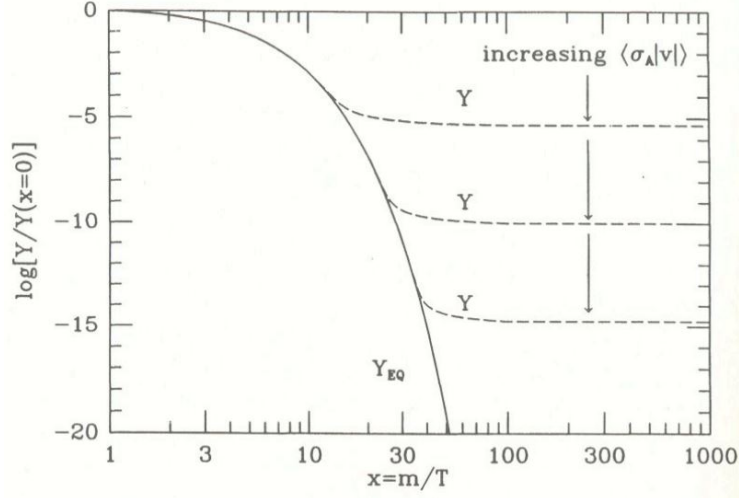


Fig. A.1.1: The number of particle per comoving volume. The solid line represents Y_{EQ} , the dashed line represents Y . The three different curves refer to increasing values of the annihilation cross section, since more particles annihilate, less the residual density is.

Figure taken from [2]

In this limit the Boltzmann equation is:

$$\frac{dY}{dx} \simeq -\frac{T^3}{Hx} \langle \sigma_{\chi\bar{\chi} \rightarrow f\bar{f}} |v| \rangle Y^2 \quad (1.16)$$

This equation has no analytic solution, since $\langle \sigma_{\chi\bar{\chi} \rightarrow f\bar{f}} |v| \rangle$ depends on the temperature. In literature the assumption $\langle \sigma_{\chi\bar{\chi} \rightarrow f\bar{f}} |v| \rangle \simeq \text{const}$ is considered reasonable for non-relativistic particles, at late time after the freeze-out [2]. In this assumption and for $x_F \sim 20$ ⁽⁶⁾, the integration of eqs (1.16) between $x = x_F$ and $x = \infty$ provides:

$$Y_\infty = \frac{1.661 g_*^{1/2}}{m_{Pl} m_\chi \langle \sigma_{\chi\bar{\chi} \rightarrow f\bar{f}} |v| \rangle} \propto \frac{1}{m_\chi \langle \sigma_{\chi\bar{\chi} \rightarrow f\bar{f}} |v| \rangle} \quad (1.17)$$

where $g_{*S} \simeq g_*$ accounts for the degrees of freedom involved and we assume them constant in time and of order $\sim 10^2$ ⁽⁷⁾.

⁶The value $x_F = 20$ often encountered in literature arises from the simplest parameterization $\langle \sigma_{\chi\bar{\chi} \rightarrow f\bar{f}} |v| \rangle \approx \text{const}$.

⁷See [2] for more details

Chapter 2

Motivations and Candidates for Dark Matter from Particle Physics

The baryon number density computation, constrained by the Big Bang Nucleosynthesis [2], suggests that the matter parameter density of the universe, i.e. the ratio between the matter energy density and the critical density, is constituted by both a baryonic and non-baryonic contribution. From the data provided by the Planck Collaboration [4]:

$$\Omega_m h^2 = 0.1415 \pm 0.0019 = \Omega_c h^2 (= 0.1186 \pm 0.0020) + \Omega_b h^2 (= 0.02226 \pm 0.00023) \quad (2.1)$$

where $h = 0.678 \pm 0.009$ and as consequence $\Omega_m = 0.308 \pm 0.005$ is the total matter density parameter, $\Omega_c = 0.258 \pm 0.006$ the cold dark matter density parameter and $\Omega_b = 0.0484 \pm 0.0008$ the baryonic one. Some theories are studying the existence of a non-luminous baryonic dark matter component said MACHOs (Massive Compact Halo Objects), but it would contribute only to the baryonic parameter density and therefore would not explain the more abundant non-baryonic dark matter content. The hypothesis that the dark matter constituent is an elementary particle is proposed by many models.

After a brief comment on the attempt to provide a solution for the missing mass problem without invoking new physics, this chapter is dedicated to the study of some of the particle dark matter candidates that are hypothesized by extensions of the Standard Model. The particles discussed along the chapter are summarized in table (2.1) and in fig. (2.1), as a function of the relative masses.

2.1 The Standard Model proposals and limits

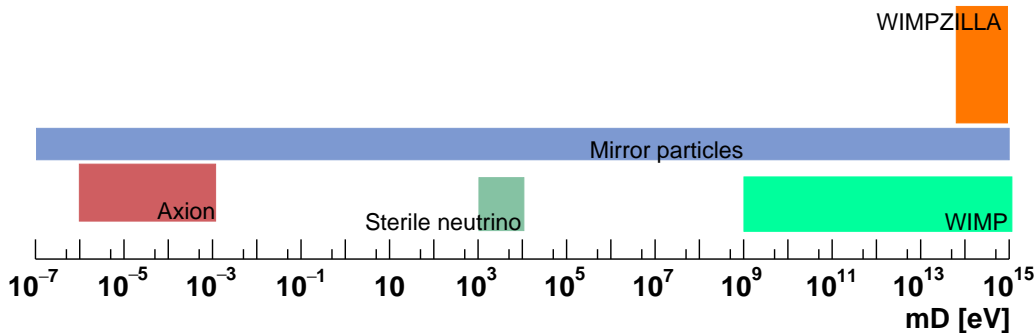


Fig. 2.1: Some of the dark matter candidates proposed in literature as a function of the hypothesized mass

	Mass Range	Detection
Axions	$\sim \mu\text{eV}-\text{meV}$	-Direct -Indirect
Sterile ν	keV	-Direct ^(*) -Indirect
Wimp	Gev-Tev	-Direct -Indirect -Collider
Mirror Particles	/	/
WIMPZILLAS	$\gtrsim 200 \text{ TeV}$	Direct -Indirect -Collider

Table 2.1. The dark matter candidates discussed in this work, in order of increasing mass.

(*): possible but not confirmed detection method. /: not defined mass range or detection method.

The large mass range of the particles that are proposed as dark matter content is due to the different processes that can cause the cosmologic production and to the possible different couplings that are hypothesized for each candidate, as we discuss below.

2.1 The Standard Model proposals and limits

Dark matter predicted abundance implies that it is stable (i.e. the lightest particle of the particle model spectrum) and its "darkness" implies either it is neutral or that the possible couplings are lower than the actual experimental sensitivities. Among the particle standard model zoo, only the neutrino survives.

2.1.1 Neutrinos

Neutrinos were the first dark matter candidates hypotized. Today we know they cannot solve the missing mass problem because of their relativistic nature that would contribute to hot dark matter, today ruled out by the cosmological constraints discussed above. Furthermore in 2015 the Planck collaboration provided the best neutrino mass sum and energy density parameter upper limit:

$$\sum m_\nu < 0.23 \text{ eV} \quad (2.2)$$

2.2 Axions

$$\Omega_\nu h^2 = \frac{\sum m_\nu}{93eV} < 0.0025 \quad (\Omega_\nu = 0.0054) \quad (2.3)$$

which compared with the dark matter density parameter $\Omega_c h^2 = 0.1186 \pm 0.0020$ ($\Omega_c = 0.258 \pm 0.006$), shows the neutrinos do not provide the value required [4].

The particle Standard Model does not provide any good dark matter candidate, therefore a complete description of the physical reality needs a theory beyond the Standard Model.

The Standard Model failure in the resolution of the missing mass problem is not the unique flaw in the theory. There are other issues that we shall discuss along the chapter, that are example of our inevitable and exciting resignation at the actual knowledge incompleteness. A theory built to solve any of these issues becomes more plausible if it naturally provides a dark matter candidate.

2.2 Axions

The axions are pseudoscalar fields introduced by Weinberg [12] and Wilczek [13] as result of Peccei and Quinn's extension of the Standard Model [14], proposed to solve the CP violation of the strong interactions.

In the limit of massless quarks, the QCD theory is symmetric under $U(2)_R \otimes U(2)_L$ or, similarly, under $U(2)_V \otimes U(2)_A$ ⁽¹⁾. According to the Goldstone theorem, the spontaneous global symmetry breaking leads to the production of as many Nambu-Goldstone bosons as the number of transformation parameters. Since $m_q \neq 0$, the $U(2)_A$ Spontaneous Symmetry Breaking (SSB) should be associated to four *pseudo* Nambu-Goldstone bosons. Indeed the effective theory foresees only three light candidates, the three pions π^\pm, π^0 , associated to the $SU(2)_A$ SSB; this means the $U(1)_A$ cannot be spontaneously broken. Indeed it is explicitly broken due to the axial-vector current anomaly, that affects the current quadrivergence:

$$\partial_\mu J^{\mu 5} = \frac{g^2 N}{32\pi^2} F_a^{\mu\nu} \tilde{F}_{\mu\nu}^a \quad (2.4)$$

where N is the number of flavors and g is the strong coupling constant⁽²⁾.

¹Consider the right and left currents $J_R^{\mu a} = \bar{q}_R \gamma^\mu \frac{\sigma^a}{2} q_R$ and $J_L^{\mu a} = \bar{q}_L \gamma^\mu \frac{\sigma^a}{2} q_L$. Then $J_V^{\mu a} = J_R^{\mu a} + J_L^{\mu a} = \bar{q} \gamma^\mu \frac{\sigma^a}{2} q$, while $J_A^{\mu a 5} = J_R^{\mu a} - J_L^{\mu a} = \bar{q} \gamma^\mu \gamma^5 \frac{\sigma^a}{2} q$, therefore $U(2)_R \otimes U(2)_L \rightarrow U(2)_V \otimes U(2)_A$, i. e. the chiral currents are strictly connected to vector-axial currents.

²The QCD is asymptotically free in the ultraviolet. At the lowest order of the perturbation theory the renormalized coupling constant is:

$$g^2 = \frac{48\pi^2}{33 - 2N} \ln\left(\frac{Q}{\Lambda}\right)^2 \quad (2.5)$$

where N is the number of flavors, Q is the energy scale of the process considered and Λ is the cut-off.

2.2 Axions

This term, within the 't Hooft gauge theory of the vacuum structure, introduces in the lagrangian the dangerous term:

$$L_\theta = \theta \frac{g^2}{32\pi^2} F_a^{\mu\nu} \tilde{F}^{\mu\nu a} \quad (2.6)$$

that violates the strong-CP conservation, as shown in Appendix A.2.1 [15]. θ is a dimensionless parameter (L_θ is a 4-dimensional operator, i.e. is renormalizable) that arises from the vacuum structure theory ⁽³⁾.

There are experiments that are searching for the neutron electric dipole moment (NEDM) to probe the strong CP violation. The experiments actually impose a NEDM upper limit equal to $|d_n| < 2.9 \times 10^{-26}$ e-cm [17], that requires $\theta \lesssim 10^{-10}$, as discussed in Appendix A.2.2.

Peccei and Quinn [14] propose a theory that solves this fine tuning, suggesting an extension of the Standard Model with the introduction of a new global chiral symmetry $U(1)_{PQ}$, as called by Weinberg. By the breaking of this new symmetry, due to instanton effects [18] ⁽⁴⁾, they absorb the CP violation term, restoring the CP-symmetry. So far Peccei and Quinn's theory is the most popular explanation of the strong-CP problem.

To inspect the consequences of Peccei and Quinn's theory, Weinberg [12] considers a "minimal" extension of the Standard Model that includes the usual $SU(2) \otimes U(1)$ chiral doublets and singlets of quarks and fermions and adds two complex scalar fields $\{\psi_i^+, \psi_i^0\}$, doublets under $SU(2) \otimes U(1)$, that furthermore carry the $U(1)_{PQ}$ quantum number. The $U(1)_{PQ}$ spontaneous symmetry breaking, together with that of $SU(2) \otimes U(1)$, would produce four massless neutral pseudoscalar Nambu-Goldstone bosons, i.e. π^0, η^0, ψ_1^0 and ψ_2^0 . The presence of small quark masses causes an explicit symmetry breaking, that forces the NG bosons to acquire a mass and to turn into pseudo-NG bosons. Their squared-mass matrix diagonalization produces the axion neutral field a^0 as a linear combination of π^0 and η^0 , with a π^0 dominant weight and with a mass $m_a \geq 23 \text{ keV} \times N$, where N was the quark flavor number. For $N = 3$ the lower limit was $m_a = O(10^2)$ keV. The original Weinberg mass term was:

$$m_a = \frac{Nm_\pi f_\pi}{\sqrt{m_u^2 + m_d^2}} \left[\frac{m_u m_d m_s}{m_u m_d + m_d m_s + m_s m_u} \right]^{1/2} \frac{2^{1/4} G_F^{1/2}}{\sin 2\alpha} \quad (2.7)$$

where N is the number of flavors, $m_\pi \approx 135 \text{ MeV}$ and $f_\pi \approx 93 \text{ MeV}$ are the pion mass and decay constant, m_i , with $i=u,d,s$, the light quark masses, G_F the Fermi coupling constant and α is an unknown angle fixed by the expectation values of the two higgs fields, i.e. $\langle |\psi_1| \rangle = 2^{-1/4} G_F^{-1/2} \cos \alpha$ and $\langle |\psi_2| \rangle = 2^{-1/4} G_F^{-1/2} \sin \alpha$ [12].

This initial model was based on a $U(1)_{PQ}$ SSB scale f_a equal to the electroweak one ($f_a \approx v_{EW} = O(250 \text{ GeV})$), but this hypothesis was ruled out by the experiments; then, during the years, the model has been reexamined and now $f_a \gg v_{EW}$.

³In a gauge theory the vacuum state is defined as the superposition $|\theta\rangle = \sum_n e^{in\theta} |n\rangle$ of n -vacuum states $|n\rangle$, obtained from one another through a phase transformation. From the path integral formula of the transition amplitude ${}_+\langle\theta|\theta\rangle_-$ the lagrangian term (2.6) arises [16].

⁴For a review on instanton in QCD see also [19]

2.2 Axions

A priori, omitting the actual experimental constraints, the strong-CP solving theory admits an axion mass range of $10^{-12} - 10^6$ eV [16][20].

The attractive feature of this version of the PQWW theory (Peccei, Quinn, Weinberg and Wilczek) is that in addition to its resolution of the strong-CP problem it naturally offers a candidate for the challenging dark matter issue. The extra requirement of accounting for the missing mass problem, in addition to the constraints by laboratory and astrophysical experiments (that are discussed below), restricts the predicted axion mass window, that is confined to the range $10^{-5} - 10^{-3}$ eV (and $f_a \sim 10^9 - 10^{11}$ GeV). A common way to express the axion mass is⁽⁵⁾:

$$m_a = \frac{m_\pi f_\pi}{f_a} \approx 6eV \frac{10^7 GeV}{f_a} \quad (2.8)$$

where the $m_a - f_a$ relation is in evidence.

Generically the axion lagrangian interaction terms are proportional to f_a^{-1} ; this implies that the light axions, that are characterized by an f_a in a range of order $\sim 10^9 - 10^{11}$ GeV, are feeble coupled to electromagnetic and matter fields (from that "invisible axions").

From the cosmological and astrophysical point of view the axion-photon coupling is important, both for the present axion density and for the stellar energy loss. Due to their lightness, the invisible axions have only the two-photons decay channel, described by the 5-dimensional lagrangian term ⁽⁶⁾:

$$L_{a\gamma\gamma} = -\frac{g_{a\gamma\gamma}}{4} \phi_a F^{\mu\nu} \tilde{F}^{\mu\nu} \quad (2.9)$$

where ϕ_a is the pseudoscalar axion field, $F^{\mu\nu}$ is the electromagnetic field-strength tensor, $\tilde{F}^{\mu\nu}$ its dual and $g_{a\gamma\gamma}$ is the adimensional coupling constant:

$$g_{a\gamma\gamma} = \frac{\alpha}{2\pi f_a} \left(c - \frac{2}{3} \frac{4+z}{1+z} \right) = \frac{\alpha}{\pi f_a} g_\gamma \quad (2.10)$$

with c a model-dependent constant of order $O(1)$ ⁽⁷⁾ and $z = \frac{m_u}{m_d}$, with u and d the light quarks. The light axion life-time is [21]:

$$\tau(a \rightarrow 2\gamma) = \frac{0.8 \times 10^7 t_U}{g_\gamma^2} \left(\frac{eV}{m_a} \right)^5 \quad (2.11)$$

with $g_\gamma \sim O(1)$ adimensional and defined above and $t_U = O(10^{17})$ s is the age of the Universe. The (2.11) implies that $\tau(a \rightarrow 2\gamma) < t_U$ if $m_a \gtrsim 24.02$ eV; since we

⁵In this work we call *axion* both the Weinberg particle and the lighter particle we are searching for, while in literature the latter is indicated by the terms "axion-like particle" or "invisible axion" to distinguish it from the original one.

⁶We are concerning with an effective low-energy theory, therefore higher dimensional lagrangian terms can be involved.

⁷There are two main models built on the axion paradigm: the KSVZ(Kim-Shifman-Vainshtein-Zakharov), that introduce the axions and new heavy quarks that carry the $U(1)_{PQ}$ charge and that are electrically neutral, and the DFSZ (Dine-Fischler-Srednicki-Zhitnitsky) that associates to the standard quarks and leptons the $U(1)_{PQ}$ charge and requires at least two higgs doublets. For the KSVZ $c=0$ while for the DFSZ $c=8/3$.

2.3 Sterile Neutrinos

are concerning with light axions, with $m_a \lesssim \text{meV}$, the invisible axions are stable within the age of the universe, as necessary to constitute the dark matter. Many laboratory, astrophysical and cosmological experiments are dedicated to the axion search. Their results are compared into the mass exclusion graph[22]:

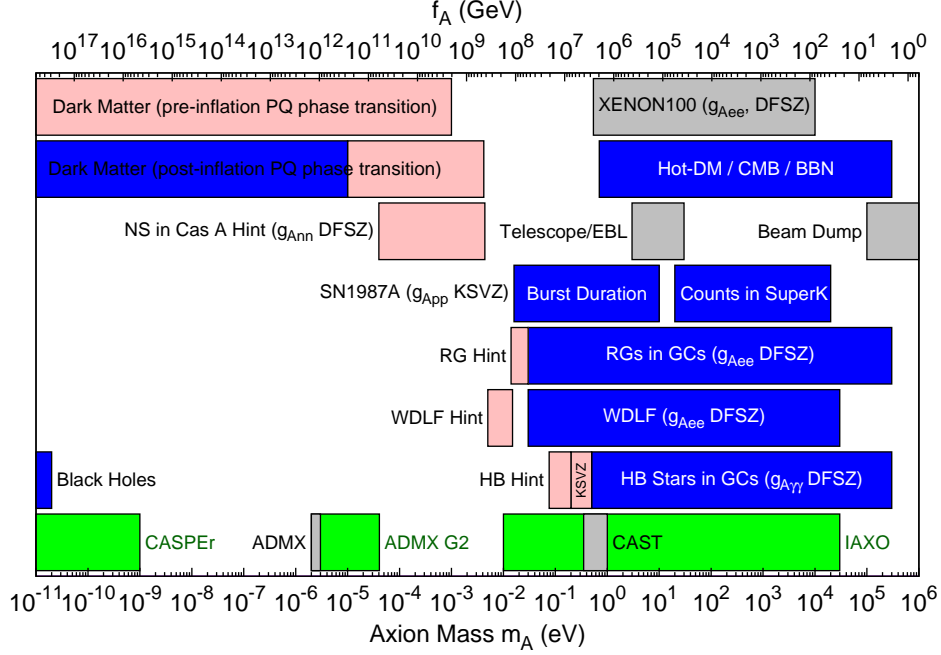


Fig. 2.2.1: The blue bar are exclusion ranges from astrophysical and cosmological experiments and models. The grey bars are exclusion ranges from experiments searching for axions from the Sun and the halo (the Beam Dump bar refer to the experiments that ruled out the original PQWW axion). Green bars are the range that future experiments are searching for. Rose bars are open ways of search.

pdg.lbl.gov/2015/reviews/rpp2015-rev-axions.pdf.

where the remaining $10^{-5} - 10^{-3}$ eV axion mass range is shown. The most intriguing region of search is $m_a \sim \text{meV}$, because there are hints concerning stellar energy loss in Red Giants (RG), White Dwarf (WD) and Neutron Stars (NS) that constrain the emitted axion masses to be of this order, as shown in fig. (2.2.1) [22].

2.3 Sterile Neutrinos

The sterile neutrino is a particle beyond the standard model, that does not interact with any gauge boson of the electroweak theory (for this reason "sterile"). It is the right handed projection of the neutrino field. This extension of the standard model seems quite natural, because it relaxes the artificial constraint of the right handed neutrino exclusion from the particle content, not supported by any theoretical argument. Similarly to the right handed projection of the charged leptons, the right handed neutrino can take part in the generation of the neutrino mass term

2.3 Sterile Neutrinos

and, as a consequence, it can be involved in the mechanism that causes the discrepancy between the neutrino and the charged lepton masses [27]⁽⁸⁾; it could take part also in the generation of the baryon asymmetry of the Universe [28]. Furthermore the sterile neutrino, if accommodated by ad hoc hypothesis, can account for dark matter.

Clearly the last application is the most interesting one for our purpose and we shall discuss it in the following, but the cognition of the right handed neutrino versatility in the solution of different issues makes it a more attractive object of study.

Because of the LEP results on Z decay width, that provide a number of invisible channel equal to $N_\nu = 2.984 \pm 0.009$ [29] (ν_e, ν_μ, ν_τ , with amplitude $\propto \bar{\nu}_L \gamma^\mu \nu_L$), the right-handed neutrinos must be either not coupled to the Z gauge bosons or more massive than $m_Z/2$. In order to get a stable particle⁽⁹⁾, consider the first condition and introduce the gauge singlet, right-handed neutrino N_R . Since it is not coupled with gauge bosons, the number of generations is not constrained by the anomaly cancellations, therefore a priori the number of generations is arbitrary. This freedom characterized also the masses, because the physics on the neutrino mass generation is not well established⁽⁸⁾ and the sterile neutrino a priori can have almost any mass (from eV to an arbitrary scale M_R smaller than the Planck scale) [28]. The effect is that many models has been proposed, as a function of the parameter choice.

In this thesis, we are interested in the case when one or more sterile neutrino can be relevant as a candidate to address the dark matter problem. For this reason, we are particularly interested in sterile neutrinos with masses of O(keV). As discussed below, this is the range suggested by cosmological and astrophysical constraints. Let us introduce immediately the terminology we use in the following; we suppose that we have several heavy neutrinos, with masses $M_1 < M_2 < M_3 \dots$. The standard case is the one when we have 3 neutrinos, and one of them, the lightest one, has mass around keV.

The *models* proposed to provide a mechanism to explain the imposed framework, for the most part, agree with two main mass shifting schemes, the bottom-up and the top-down, shown in the fig. (2.3.1):

⁸At this time it is not established if the neutrino is a Dirac or Majorana particle and several models are been proposed to explain the generation of the neutrino mass term. More details are discussed in Neutrino mass, Appendix B.2

⁹A sterile neutrino of $m_s \sim 45$ GeV and weakly interacting would be highly unstable.

2.3 Sterile Neutrinos

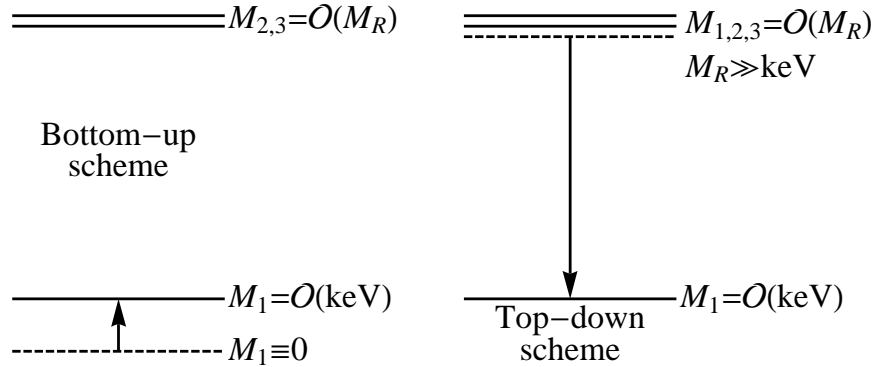


Fig. 2.3.1: Left: The bottom-up scheme. The light neutrino mass initially is $M_1 = 0$ and is increased at the keV by some mechanism. The two heavier neutrino mass M_2, M_3 are of $O(M_R)$, where M_R is some high energy scale. Right: the top-down scheme. The all three right handed neutrino masses initially are of $O(M_R)$ and some mechanism suppresses M_1 at the keV scale. Taken from [31].

where M_1 is the light sterile neutrino mass, M_2, M_3 are the heavier sterile neutrino masses and $M_R \gg \text{keV}$ is some high energy scale. These schemes refer to a total of three sterile neutrinos, but it can be generalized to an arbitrary number. The common tendency is to consider a starting configuration, in which M_2 and M_3 are of $O(M_R)$ and M_1 is either zero or $O(M_R)$; then some mechanism increases or suppresses the N_1 sterile neutrino mass up to the keV scale.

A particularly interesting example of this scenario is the one called νMSM (Neutrino Minimal Standard Model) proposed by Asaka, Blanchet and Shaposhnikov in 2005[30] as a minimal extension of the actual theory. It works within the $SU(2)_L \otimes U(1)_Y$ symmetry group and extends the standard model particle content by only three right singlets (N_1, N_2, N_3) ⁽¹⁰⁾. It accounts for:

1. neutrino masses consistent with the oscillation paradigm;
2. warm dark matter, through the accommodation of a light sterile neutrino of $O(\text{keV})$;
3. the baryon asymmetry, through the accommodation of two heavier right handed neutrinos in the range (150 MeV-100 GeV).

The many issues that find a solution in this *scenario*⁽¹¹⁾ make it attractive; how-

¹⁰A comment on notation: in this work we use equivalently *right handed* and *sterile* to distinguish the three N_1, N_2, N_3 from the standard, left handed (or *active*) neutrinos. To identify instead the N_i from each other, in particular the keV neutrino from the others that are heavier, we specify *light* or *heavy*. Moreover, in the same way as the literature, N_1 is associated to the light sterile neutrino and N_2, N_3 to the heavier neutrinos.

¹¹On terminology: Alexander Merle, in [31], classifies a sterile neutrino approach relative to the keV mass scale as a "[...]scenario, whenever it can accommodate for a keV sterile neutrino, but does not give any explanation for the appearance of the keV scale" and as a "[...]model whenever there is an explanation for the appearance of the keV scale or, rather, for a suitable mass hierarchy or the existence of a suitable new scale". In this optic, the νMSM would be an interesting *scenario*.

2.3 Sterile Neutrinos

ever it is a phenomenological theory that does not provide any explanation for the appearance of the keV scale and for the shift between the light and the two heavier right handed neutrino masses, therefore other approaches (*model*) are required [31].

Since these *models* aim to provide a more complete theory on neutrino physics, they have to account also for the difference between neutrino and charged lepton masses. This task is commonly achieved involving the popular *seesaw mechanism*, whose simplest version is discussed in Appendix B.2. Besides the explanation of the charged lepton-neutrino mass departure, the seesaw mechanism implies the fundamental active - *light* sterile neutrino mixing, that makes the light right handed neutrino not completely sterile and opens experimental probes. For example it could have a main decay channel $N_1 \rightarrow \nu_a \nu_a \nu_a$, where ν_a is the active neutrino, of amplitude[32]⁽¹²⁾:

$$\Gamma_{N_1 \rightarrow \nu_a \nu_a \nu_a} = \frac{G_F^2 M_1^5 \theta_1^2}{96\pi^3} \quad (2.13)$$

where G_F is the Fermi coupling constant and θ_1 is the active - light sterile neutrino mixing angle⁽¹³⁾. The required stability (necessary for the sterile neutrino to constitute dark matter), imposed by:

$$\tau_{N_1} = 5 \times 10^{26} s \left(\frac{M_1}{1keV} \right)^{-5} \left(\frac{\theta_1^2}{10^{-8}} \right)^{-1} \gtrsim 10^{17} s \quad (2.14)$$

where τ_{N_1} is the lightest sterile neutrino decay time, puts an upper limit on a relation between the mixing angle and the mass (M_1, θ_1) [6]:

$$\left(\frac{M_1}{10keV} \right)^5 \left(\frac{\theta_1^2}{10^{-4}} \right) \lesssim 1 \quad (2.15)$$

A very interesting decay channel is $N_1 \rightarrow \gamma \nu_a$ [6]:

$$\Gamma_{N_1 \rightarrow \gamma \nu_a} = \frac{9\alpha_{EM} G_F^2}{256 \cdot 4\pi^4} \sin^2(2\theta_1) M_1^5 \quad (2.16)$$

¹²In [32], §12.2.1, this amplitude is written as:

$$\Gamma_{N_1 \rightarrow \nu_a \nu_a \nu_a} = \frac{G_F^2 M_1^5 \theta_1^2}{96\pi^3} = 10^{14} years \left(\frac{10keV}{M_1} \right)^5 \left(\frac{10^{-8}}{\theta_1^2} \right) \quad (2.12)$$

In the third member maybe there is an error. It is likely to refer to the decay time $\tau_{N_1 \rightarrow \nu_a \nu_a \nu_a}$ rather than to the amplitude; the correct form should be the inverse one.

¹³For more details see The active-sterile neutrino mixing, Appendix B.2

2.3 Sterile Neutrinos

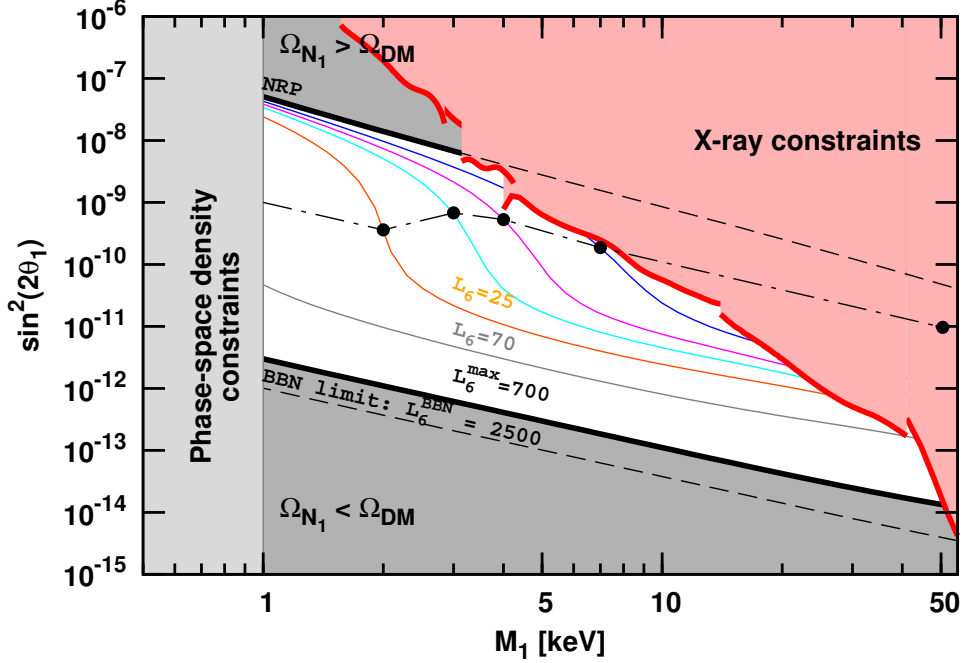


Fig. 2.3.2: The exclusion graph of the ν MSM sterile neutrino mass as a function of the active-sterile neutrino mixing angle. The upper right corner is the X-ray exclusion region.

The left grey region is the dwarf spheroidal limit. The two black solid lines are the non-resonant production limit (the upper line NRP, with null lepton asymmetry) and the maximal resonant production limit (the lower line, with a maximal lepton asymmetry).

The colored lines between the two solid lines are production curves relative to different lepton asymmetries. This figure is taken from [33].

where α_{EM} is the fine-structure constant. The photon produced by this latter decay was searched by a spectrometer on board of INTEGRAL (International Gamma-Ray Astrophysics Laboratory) satellite, pointed toward the Galactic Center [34]. The non-observation of the expected photon line bounds the (M_1, θ_1) parameter space, where θ_1 is the active-sterile neutrino mixing angle, and fixes an upper limit $M_1 < 50$ keV (the upper right corner in Fig. 2.3.2). In addition the phase-space distribution of the dwarf spheroidal galaxies in the Milky Way fixes a lower mass bound $M_1 > 1$ keV [35] (the left grey region in Fig. 2.3.2). The other bounds derive from the sterile neutrino production mechanism, that involved the lepton asymmetry [36]. The lepton asymmetry rises from the difference between the lepton and anti-lepton number densities ($L_\alpha = \frac{n_{\nu_\alpha} - n_{\bar{\nu}_\alpha}}{n_\gamma}$). It depends on the primordial production of sterile neutrino and today it is not well established; different values lead to different curves on the (M_1, θ_1) parameter space⁽¹⁴⁾ (colored curves between solid lines in Fig. 2.3.2).

The recent observation of an X-ray line at $E \approx 3.55$ keV from cluster galaxy spectra could be interpreted as an annihilation dark matter signal from a neutrino of this type [37, 38]. If it is a two-body decay product, then $M_1 \approx 7.1$ keV, in agreement

¹⁴For example in [4] is reported the allow mass range $2 \text{ keV} < M_1 < 5 \text{ keV}$ for $L_\alpha \approx 0$.

2.4 Mirror Models

with the sterile neutrino mass window (with $\theta_1 \approx 10^{-11}$). However the uncertainties due to other possible astrophysical sources or to the instrumental background, or the plasma emission origin of the line require more investigations.

2.4 Mirror Models

The *mirror models* date back to the attempt of restoring the universe symmetry under parity transformation, spoiled by the weak interactions. A first proposal was suggested by Lee and Young at the end of their popular article[41], as chance to restore the right-left symmetry. They proposed that there could exist two protons, left p_L and right p_R , with an interaction time-scale greater than the age of the universe and likely coupled to the same electromagnetic field; the asymmetric preponderance of the left handed proton is ascribed to a some cosmological process, similarly to the matter-antimatter asymmetry. Later this hypothesis was revised by Landau and re-elaborated by his students Pomeranchuk, Okun and Kobzarev [42]. Since then mirror models have been captured theorists' attention, thanks also their potential success in the dark matter problem resolution⁽¹⁵⁾.

The main feature of this theory is the building of a "mirror world", an exact copy of the ordinary one, whose fields interact only gravitationally with the standard particles. Another theoretical possibility is that there could be non-gravitational mixed interactions between the ordinary world and its mirror image, in particular a small electromagnetic coupling, as discussed below.

The symmetry group would be $SU(3)_c \otimes SU(2)_L \otimes U(1)_Y \otimes SU(3)_c \otimes SU(2)'_R \otimes U(1)'_Y$. The particle content is extended to include the mirror fields, associated to each standard particle and antiparticle. The dynamics is described by the lagrangian[44]:

$$L = L(e, \nu, u, d, W, Z, \gamma, \phi..) + L(e', \nu', u', d', W', Z', \gamma', \phi'..) + L_{mix} \quad (2.17)$$

where L_{mix} involves terms coupling the two sectors. This lagrangian is invariant under the discrete $Z_2 = P \times R$ symmetry transformation, where P is the usual parity reflection and R represents the reflection into the mirror space, i.e. the substitution of the standard fields with the correspondent mirror one and viceversa:

$$\begin{aligned} L_L(1, 1, -1/2) \otimes (1, 1, 0) &\leftrightarrow L'_R(1, 1, 0) \otimes (1, 2, -1/2) \\ e_R(1, 1, -1) \otimes (1, 1, 0) &\leftrightarrow e'_L(1, 1, 0) \otimes (1, 1, -1) \end{aligned}$$

...

The mirror theory provides a resolution to the missing mass problem because all the astrophysical objects (stars, planets, interstellar gas,..) or simple stable mirror particles (such as mirror electrons, protons, etc..) could be dark matter constituents. Among the admissible mixing interaction terms, there is the electromagnetic coupling $-\frac{\epsilon}{2} F^{\mu\nu} F'_{\mu\nu}$, where ϵ is the small coupling constant, supposed to be of $O(10^{-9})$; beyond the possible astrophysical and cosmological effects, this

¹⁵See [43] for a detailed review on the published papers.

2.5 WIMPs

term opens the possibility of direct test of the mirror model, since it would produce a detectable nuclear recoil [44]. The mirror charged particles could acquire a small ordinary electric charge $\pm e$, that would causes a mirror nucleus Rutherford scattering off an ordinary nucleus:

$$\frac{d\sigma}{dE_R} = \frac{2\pi\epsilon^2 Z^2 Z'^2 \alpha^2 F_A^2 F_{A'}^2}{m_A E_R^2 v^2} \quad (2.18)$$

where Z and A are the atomic and mass number of the ordinary nucleus, Z' and A' the atomic and mass number of the mirror nucleo, F_A and $F_{A'}$ are the two form factors, m_A is the ordinary nucleus mass and v is the mirror nucleus velocity (while the ordinary one is considered at rest). This model is still in agreement with the available direct detection result [45].

2.5 WIMPs

The historical hypothesis that the cosmological origin of the dark matter is thermal [2],[3], i.e. that it is the frozen out relic of a species in a previous thermodynamical equilibrium, implied the proposal of the dark matter Weakly Interacting Massive Particles (WIMPs).

The WIMP characterization is often ambiguous, because many candidates proposed by the particle physics seems to share the same properties:

- the stability and the massivity, necessary to explain the missing mass at this time;
- the weak interactions, where by weak interaction we intend any type of coupling lower than the actual experimental sensitivities, since otherwise we would have already detected them;

The thermal origin is the feature that distinguishes the dark matter candidates that are indicated traditionally as WIMPs, from the others.

Consider a dark matter content of (i) particle nature and produced by a (ii) thermal mechanism and assume the hypothesis that (iii) all the dark matter is of an unique type. In these hypotheses the experimental value of the dark matter parameter density Ω_χ constrains the *thermally averaged annihilation cross section times the relative velocity* $\langle\sigma_{\chi\bar{\chi}\rightarrow f\bar{f}}|v|\rangle$ at the order of $3 \times 10^{-26} \text{ cm}^3\text{s}^{-1}$ ⁽¹⁶⁾:

$$\Omega_\chi \simeq 0.1 \cdot \frac{3 \cdot 10^{-26} \text{ cm}^3\text{s}^{-1}}{\langle\sigma_{\chi\bar{\chi}\rightarrow f\bar{f}}|v|\rangle} \quad (2.19)$$

Through a rough estimate, $\sigma_a \simeq 10^{-36} \text{ cm}^2 \equiv 1 \text{ pb}$ (1 picobarn= $10^{-12} \times 10^{-24} \text{ cm}^2$) for $v \simeq c$ and $\sigma_a \simeq 10^{-33} \text{ cm}^2$ for $v \simeq 10^{-3}c$, that is the typical mean halo velocity assumed for practical purpose⁽¹⁷⁾. The typical orders of the annihilation cross section channels for the e^+e^- as a function of $s = (p_1 + p_2)^2$ are shown in the graph for a comparison:

¹⁶See What is the 'WIMP miracle' in Appendix C.2 for more details.

¹⁷In the next chapter the halo density profile models and the velocity distributions are discussed

2.5 WIMPs

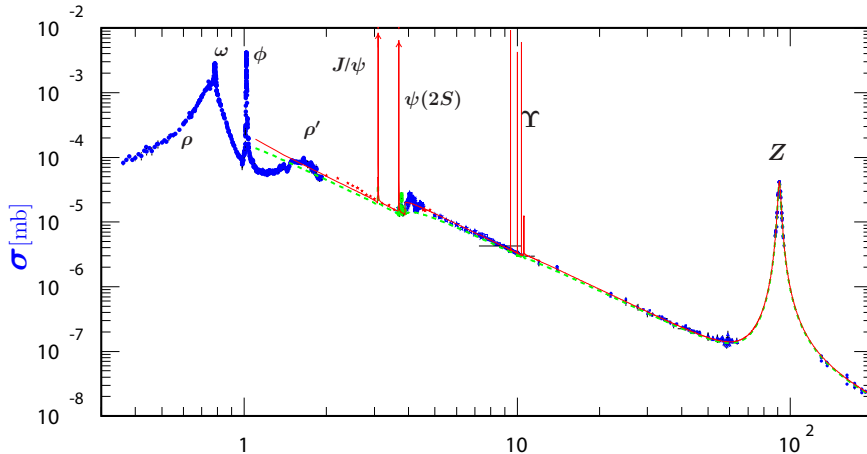


Fig. 2.5.1: The e^+e^- annihilation cross section as a function of $s = (p_1 + p_2)^2$. $\sigma[\text{mb}] \sim 10^{-6}$ is the order of the WIMP σ_a estimate for $v \simeq 10^{-3}c$. The figure is taken from <http://pdg.lbl.gov/2015/reviews/rpp2015-rev-cross-section-plots.pdf>

The parameter density estimate discussed in Appendix C.2 implies that the experimental value $\Omega_\chi \simeq 0.2$ imposes a limit on $\langle \sigma \cdot v \rangle$, regardless of the parameters of the particle involved in the process. Therefore we know the order of magnitude of the dark matter annihilation cross section in the hypothesis of a thermal production, but we cannot establish the interaction type. To associate this interaction to the electroweak scale we should know that the mediator mass is of order of the Z^0 and of the W^\pm , i.e. $O(10^2)$ GeV, while we have no information about the mediator. If we want to speculate on the hypothesis that this is an electroweak interaction⁽¹⁸⁾, i.e. that:

$$\sigma \sim G_F^2 m_\chi^2 = \frac{g^4 m_\chi^2}{M^4} \quad (2.20)$$

with $M \sim O(10^2)$ GeV, where $G_F \sim 10^{-5}$ GeV⁻² in natural units is the Fermi constant, M is the mediator mass, m_χ the dark matter particle mass and g the coupling constant. Within this speculation a lower limit on the WIMP mass can be imposed, i.e. the 'Lee-Weinberg limit'. In [47] Lee and Weinberg show that for a stable heavy neutrino produced as a thermal relic, the condition to avoid the universe overclosing imposes a lower limit on the mass at about 2 GeV. If we consider the dark matter parameter density Ω_χ , rather than the total parameter density, this limit becomes $m_\chi \gtrsim 10$ GeV.

Go back to the general WIMPs, masses lower the Lee-Weinberg limit could be possible and for this reason there are many experimental efforts that try to probe the lower mass region⁽¹⁹⁾, while an upper limit equal to $m_\chi < 7$ TeV is provided by Edsjo and Gondolo in 1997 as result of a study including coannihilation processes⁽²⁰⁾ [48]. This is the reason of the WIMP mass upper limit often encountered, ex-

¹⁸A *speculation* that is defined as the 'WIMP miracle'.

¹⁹In particular the direct detection experiments, as we shall discuss later.

²⁰Coannihilation is a process that corrects the thermal relic abundance and that occurs if there is a degeneration in mass between different relic species that share also the quantum numbers. This

2.5 WIMPs

pecially in experimental probes, that commonly focus on the range 10 GeV-1 TeV. The lower limit of 10 GeV instead is an experimental limit and there are many efforts to probe lower mass scales.

There exist different Grand Unified Theories (GUT), such as the Supersymmetry (SUSY) and the extra dimension models (arised as a Kaluza-Klein theory elaboration), that, in their attempt to solve in an unique picture the physical reality, provide a possible *explanation* to the dark matter problem, condicio sine qua non the unified theory cannot be considered complete.

2.5.1 Neutralino

The *neutralino* is the Lightest neutral Supersymmetric Particle (LSP) of many supersymmetric models⁽²¹⁾.

From the most general gauge invariant supersymmetric effective lagrangian by Girardello and Grisaru [50], the lagrangian terms dealing with the neutralino field are:

$$L = -\frac{1}{2}[\psi_i^{0T} M_{ij} \psi_j^0] \quad (2.21)$$

where with ψ^0 we intend the four SUSY neutral fields $\psi^0 = (\tilde{B}^0, \tilde{W}^0, \tilde{H}_u^0, \tilde{H}_d^0)$, and M_{ij} is a non diagonal mass matrix. The fields in the ψ^0 basis are gauge-eigenstates, while the fields obtained by the diagonalization of the mass matrix M_{ij} are mass-eigenstates. This spin-1/2 mass-eigenstates are said neutralinos, $\tilde{\chi}_i^0$, with $i = 1, \dots, 4$, and are a linear combination of the ψ_i^0 fields:

$$\tilde{\chi}_i^0 = N_{ij} \psi_j^0 = N_{i1} \tilde{B}^0 + N_{i2} \tilde{W}^0 + N_{i3} \tilde{H}_u^0 + N_{i4} \tilde{H}_d^0 \quad (2.22)$$

where N_{ij} is the unitary diagonalizing matrix. The generic N_{ij} coefficient can be roughly considered as the fraction of the j - ψ^0 field that enters in the i - $\tilde{\chi}^0$ field. A mass hierarchy order is commonly imposed, for example $m_{\tilde{\chi}_1} < m_{\tilde{\chi}_2} < m_{\tilde{\chi}_3} < m_{\tilde{\chi}_4}$ ⁽²²⁾, such that the hierarchy lightest particle is the Lightest Supersymmetry Particle (LSP) of the spectrum. Indeed the lightest neutralino is the lightest particle of the supersymmetric spectrum thanks to the imposed R-parity, that makes the neutralino stable avoiding its decay into Standard Model particles⁽²³⁾.

Under these assumptions, the neutralino can be considered a dark matter candidate. The range of mass usually probed is 10 – 1000 GeV, in agreement with the constraints imposed by the thermal production hypothesis. This is also the reason of the old expectation of a SUSY signature at the O(TeV). The neutralino has been considered for long time the most plausible solution of the missing mass problem. All the detection techniques can contribute to the neutralino search and the most part of the experimental results had been interpreted as a function of this hypothesis. The lack of a supersymmetric signature at collider motivates the search

process was pointed out by Griest and Seckel [49].

²¹For a discussion on the Supersymmetry see Appendix C.2

²²The convention is that the *B-ino* mass is lighter than the *W-ino* mass, therefore the hierarchy depends on the content of the four neutralinos. For more details see [51].

²³For more details see SUPerSYmmetry in Appendix C.2.

2.5 WIMPs

of new hypothesis. The energy upper limit within which supersymmetry signs are expected to appear is increased after each failure and this is a discouraging proof of the large arbitrariness left by this *theory*.

Other SUSY dark matter candidates The supersymmetric particles that are commonly considered as potential content of the dark matter are the gravitino and the lightest neutralino. Also the sneutrino was studied as a possible candidate but it was ruled out because if it is light does not provide the right dark matter energy density, if it is heavier it should have been directly detected [52]. The gravitino belongs to more general frameworks than the MSSM, while the neutralino is included also in this simple model. The *gravitino* is the spin-3/2 fermion superpartner of the spin-2 graviton. It arises in supersymmetric approaches involving gravity, where the global supersymmetry is promoted to a local symmetry. The gravitino interactions are only gravitational, therefore it can produce only cosmological and astrophysical effects. The direct and indirect particle searches are blind to this candidate, therefore we do not further discuss about it.

2.5.2 Kaluza-Klein photon

- *This part is taken from [55].*

The Kaluza-Klein photon is the most valued dark matter candidate within the minimal version of the Universal-Extra Dimension (UED) models. The UED models are a re-elaboration of the original Kaluza-Klein (KK) effort to unify gravity and electromagnetism through the extension of general relativity to 5-dimensions. Although there exist other versions of the original KK theory, here we will discuss the UED model proposed by Appelquist, Cheng and Dobreanu in 2001 [53], because it can accommodate a dark matter candidate, at cost of some arbitrary impositions. In general the UED models consider $4 + D$ -dimensions, where D are compactified dimensions of size $\sim R$. For a minimal criterion we consider $D = 1$. In analogy with the Klein proposal, the smallness of R avoids the observation of this extra dimension and increases the energy scale at which the Standard Model states can propagate in it, since the energy scale is $\propto 1/R$, that is assumed to be $\sim \text{TeV}$ in the theory here considered. The UED model proposal is that the particle spectrum is a "tower" of excited modes whose Standard Model is the fundamental one. The squared mass of the n th excited state of a generic particle X at the tree level is:

$$m_{X^{(n)}}^2 = \frac{n^2}{R^2} + m_{X^{(0)}}^2 \quad (2.23)$$

where $m_{X^{(0)}}^2$ is the Standard Model mass. From eqs. (2.23) the Standard Model spectrum correspond to $n = 0$, i.e. in this scenario it is the Kaluza-Klein fundamental mode.

The dark matter content would be the lightest particle of the spectrum of the considered model. Since all the Standard Model particles are ruled out, the Lightest Kaluza-Klein Particle (LKP) of dark matter must belong to the $n = 1$ excited state.

2.6 WIMPZILLAS

To avoid the $n = 1$ particle decay into SM (Standard Model) particles, a so called Kaluza-Klein Parity conservation is imposed, whose quantum number can be written as $P = (-1)^n$, where n is the n th KK mode.

The KK-Parity role is quite similar to that of the SUSY R-Parity: they are both an imposed unbroken symmetry, introduced to make plausible the discussion of a dark matter candidate within the respective model.

A constraint on the LKP masses derives from the thermal production hypothesis. Servant and Taint in 2002 [54] fixed the mass range for the LKP at 900 – 1200 GeV, as a consequence of the thermal production and of the coannihilation processes. The mass range spreads out if we take into account other possible mechanisms that can occur, therefore to include all the minimal cases we will consider the range 500–2700 GeV. Similarly to the other WIMP candidates, this is the reason of the mass range often encountered in the experimental search for dark matter. Furthermore this mass range encouraged the search, because the signature of this minimal KK-model were expected to be observed at the next generation of colliders. Unfortunately, today this signature should have already been observed. However the model is not ruled out since other production mechanism can be considered and the mass range can be translated to higher upper limits.

The KK-photon is the LKP that requires the minimal effort. More precisely the KK-photon is usually identified to the hypercharged gauge boson $B^{(1)}$, i.e. the first Kaluza-Klein excited mode of the standard U(1) gauge boson.

Other Kaluza-Klein dark matter candidates Another popular Kaluza-Klein dark matter candidate is the KK-neutrino, that, however, as Profumo and Hooper assert [55], is not favored by the direct detection results. Another KK-particle that can account for dark matter is the KK-graviton, but this proposal involves gravity, while here we are referring only to minimal models⁽²⁴⁾.

2.6 WIMPZILLAS

The WIMPZILLAs, as the eccentric name evokes, are heavy WIMPs, where the WIMPs are the historic and popular Weakly Interactive Massive Particles. They were proposed by Kolb, Chung and Riotto in 1996 [59], who concluded their article affirming: "[...] WIMPZILLAS may surprise and be the dark matter, and we may learn that size does matter!".

Consider first the WIMPs: they are hypothesized to be a *thermal relic*, where a thermal relic is the result of the freeze-out of a species in thermodynamical equilibrium⁽²⁵⁾. Under this hypothesis the parameter density is forced by the Boltzmann equation to depend mostly upon to the mass of the species frozen out. As a consequence the dark matter parameter density ($\Omega_\chi h^2 = 0.1187 \pm 0.0021$, recently measured by the Planck Collaboration [4] and denoted with Ω_c in the paper), imposes an upper limit to the allowed WIMP mass. For example Griest and

²⁴The UED minimal model is also said the flat UED model, because does not include the gravity.

²⁵For more details see 'The Boltzmann equation: non-relativistic thermal relics' in Appendix A.1

Appendix A.2

Kamionkowski in 1990 [60], for an $\Omega_\chi \lesssim 1$, found an upper limit $m_\chi \lesssim 10^2$ TeV.

The WIMPZILLAs are the WIMP *non-thermal relic* version, not constrained by the Boltzmann equation and therefore characterized by any large mass. This is the main property of these candidates, that makes them the heavier dark matter candidate proposed. The two necessary conditions are only the stability and the non-equilibrium. The first can result somehow from supersymmetric theories while the second derives from an interaction rate Γ smaller than the expansion rate H at the production temperature T^* . This condition is codified in the limit:

$$\left(\frac{200\text{TeV}}{M_\chi}\right)^2 \left(\frac{T^*}{M_\chi}\right) < 1 \quad (2.24)$$

where the capital M distinguishes the WIMPZILLA mass M_χ from the WIMP mass m_χ . This bound implies $M_\chi \gtrsim 200$ TeV.

If the dark matter is so massive, then its numerical abundance would be less than the WIMP one, i.e. given a ρ_χ , it can be $\rho_\chi \propto m_\chi n_\chi \propto M_\chi n'_\chi$, with $M_\chi \gg m_\chi$ and $n'_\chi \ll n_\chi$.

This hypothesis is not so popular, but we have discuss it because it proves the weakness of the arguments that support also one of the most friendly and pursued model, i.e. the WIMPs, and shows the arbitrariness of the admissible theoretical resolutions of the missing mass problem.

Appendix A.2

A.2.1 Strong CP violation

The lagrangian term proportional to the parameter θ violates CP due to the presence of the F-tensor dual \tilde{F} :

$$L_\theta = \theta \frac{g^2}{32\pi^2} F_a^{\mu\nu} \tilde{F}^{\mu\nu a} \quad (2.25)$$

Consider first the Abelian case. The QED strength tensor is:

$$F^{\mu\nu} = \partial^\mu A^\nu - \partial^\nu A^\mu \quad (2.26)$$

and its dual:

$$\tilde{F}^{\mu\nu} = \frac{1}{2} \epsilon^{\mu\nu\alpha\beta} F_{\alpha\beta} \quad (2.27)$$

Consider a lagrangian term proportional to $F_{\mu\nu} \tilde{F}^{\mu\nu}$. Because of the $F^{\mu\nu}$ antisymmetry, only the off-diagonal terms are non-null, with $F^{0i} = -E^i$ and $F^{ij} = -\epsilon^{ijk} B_k$. The $F^{\mu\nu} \tilde{F}_{\mu\nu}$ contraction selects the terms:

$$F^{0i} \tilde{F}_{0i} = (-E^i) \left(\frac{1}{2} \epsilon_{0ijk} F^{jk}\right) = -\frac{1}{2} \epsilon_{0ijk} \epsilon^{jkl} (-E^i) B_l = \delta_i^l E^i B_l = \vec{E} \cdot \vec{B} \quad (2.28)$$

Appendix A.2

and

$$F^{ij}\tilde{F}_{ij} = (-\epsilon^{ijl}B_l)\left(\frac{1}{2}\epsilon_{ijk0}F^{k0}\right) = -\frac{1}{2}\epsilon^{ijl}\epsilon_{ijk0}B_l(E^k) = -\delta_k^l B_l E^k = -\vec{E} \cdot \vec{B} \quad (2.29)$$

where $\epsilon_{0ijk}\epsilon^{jkl} \equiv \epsilon_{ijk}\epsilon^{jkl} = \epsilon_{ijk}\epsilon^{ljk} = 2\delta_i^l$

Therefore:

$$F^{\mu\nu}\tilde{F}^{\mu\nu} = F^{0i}\tilde{F}_{0i} + F^{i0}\tilde{F}_{i0} + F^{ij}\tilde{F}_{ij} = 2\vec{E} \cdot \vec{B} - \vec{E} \cdot \vec{B} = \vec{E} \cdot \vec{B} \quad (2.30)$$

Since E and B are characterized by:

	P	T	C
E	-	+	-
B	+	-	-

their scalar product is T-odd (or equivalently CP-odd), therefore the associated lagrangian term is CP violating.

Now consider the non-Abelian theory:

$$G_a^{\mu\nu} = \partial^\mu A_a^\nu - \partial^\nu A_a^\mu + ig\epsilon_{abc}A^{\mu b}A^{\nu c} \quad (2.31)$$

$$\tilde{G}_a^{\mu\nu} = \epsilon_{\mu\nu\alpha\beta}(\partial^\alpha A_a^\beta - \partial^\beta A_a^\alpha + ig\epsilon_{abc}A^{\alpha b}A^{\beta c}) \quad (2.32)$$

with $G_a^{\mu\nu}$ antisymmetric and only G^{0i} and G^{ij} ($i \neq j$) non-null (similarly for its dual). At the leading order the non-Abelian field theory reduces to the Abelian one, therefore $G^{\mu\nu a}\tilde{G}_{\mu\nu a}$ ($\vec{E}_a \cdot \vec{B}_a$) violates CP as well.

A.2.2 The Electric Dipole Moment(EDM) connection with the strong CP-problem

The non-observation of the Electric Dipole Moment(EDM) imposes a fine-tuning for the parameter θ , appeared in the lagrangian as a consequence of the QCD vacuum-structure theory. The reason is that if the EDM was observed, it would be a proof of the strong CP violation. Let us see why.

The Maxwell's equations are⁽²⁶⁾:

$$\vec{\nabla} \cdot \vec{E} = \rho \quad (2.33)$$

$$\vec{\nabla} \cdot \vec{B} = 0 \quad (2.34)$$

$$\vec{\nabla} \times \vec{E} + \frac{\partial \vec{B}}{\partial t} = 0 \quad (2.35)$$

$$\vec{\nabla} \times \vec{B} - \frac{\partial \vec{E}}{\partial t} = j \quad (2.36)$$

where ρ is the electric charge density and $j = \rho v$ is the electric charge current. Then, considering the following eigenvalue scheme ⁽²⁷⁾:

²⁶This part refers to [23]

²⁷To check the discrete symmetry eigenvalues refer to [24]

Appendix A.2

	P	T	C
E	-	+	-
B	+	-	-
ρ	+	+	-
\mathbf{j}	-	-	-

the Maxwell's equations are invariant under discrete symmetries.

The Dirac's proposal of the existence of a "magnetic charge", as the electric one, led to the search for the electric dipole moment, that would arise in the same way as the magnetic dipole moment. In 1949 [25] he wrote "I do not believe there is any need for physical laws to be invariant under these rejections, although all the exact laws of nature so far known do have this invariance." and in effect he proposed the modification of the Maxwell's equations (2.34) and (2.35):

$$\vec{\nabla} \cdot \vec{B} = \rho_m \quad (2.37)$$

$$\vec{\nabla} \times \vec{E} + \frac{\partial \vec{B}}{\partial t} = \mathbf{j}_m \quad (2.38)$$

where ρ_m and \mathbf{j}_m would be the magnetic charge density and the magnetic charge current, with $\mathbf{j}_m = \rho_m \mathbf{v}$. Under parity reflection and time reversal the two equations (2.37) and (2.38) are not invariant, therefore Ramsey (1958) proposed an additional operation of magnetic charge conjugation M, to obtain the PM and TM conservation. In any case P and T are destroyed.

Note that in this way the Maxwell equations would appear completely symmetric between the electric and the magnetic part. The hamiltonian term relative to the electric dipole moment would be:

$$H_e = -\vec{d}_e \cdot \vec{E} \quad (2.39)$$

To leave H_e invariant under P, d_e should change sign $\vec{d}_e \rightarrow -\vec{d}_e$. But since it is projected on the angular momentum direction \vec{J} (the \vec{d}_e orthogonal components average to zero):

$$\vec{d}_e = \alpha \vec{J} \quad (2.40)$$

where α is some constant, and:

	P	T	C
J	+	-	+

i.e. \vec{J} is a pseudo-vector, then the parity conservation is violated.

The time-reversal reflection is similarly violated. Since under T $\vec{J} \rightarrow -\vec{J}$, then $\vec{d}_e \rightarrow -\vec{d}_e$, while $\vec{E} \rightarrow \vec{E}$ as shown in the previous tables. This implies that H_e is not invariant under time-reversal, or equivalently under CP (since for the CPT theorem, CPT is conserved).

Today many efforts are working for improving the EDM bounds. The main searches are dedicated to the EDMs of paramagnetic atoms and molecules, the

Appendix A.2

EDMs of diamagnetic atoms and the EDMs of hadrons ⁽²⁸⁾.

Focusing on nucleon EDM, the generalization of H_e in eqs. (2.39) in relativistic terms is:

$$L_{dim=5} = -d_e \frac{i}{2} \bar{\psi} \sigma_{\mu\nu} \gamma_5 \psi F_{\mu\nu} \quad (2.41)$$

where dim=5 stay for the energy dimension of the lagrangian density, that implies $[d_e] = E^{-1}$. This lagrangian term, of course, violates CP as well. We can separate L in three parts, (i) d_e , (ii) $A_{\mu\nu} = \frac{1}{2} \bar{\psi} \sigma_{\mu\nu} \gamma_5 \psi$ and (iii) $F_{\mu\nu}$.

d_e changes sign under T. For $\mu, \nu = 0, i \rightarrow F_{0i} = -E_i$, that does not change sign under T ($E_i \rightarrow -E_i$). In order to violate CP, A^{0i} should have eigenvalue +1 under T. Neglecting the factor 1/2:

$$\begin{aligned} T \left(\bar{\psi} \sigma_{0i} \gamma_5 \psi \right) T^\dagger &= T \left(\bar{\psi} \frac{i}{4} [\gamma^0, \gamma^i] \gamma_5 \psi \right) T^\dagger = \\ &= T \bar{\psi} \left(\frac{i}{4} [\gamma^0, \gamma^i] \gamma_5 \right) \psi T^\dagger = T \bar{\psi} \left(\frac{i}{2} \gamma^0 \gamma^i \gamma_5 \right) \psi T^\dagger \end{aligned} \quad (2.42)$$

Inserting TT^\dagger conveniently, $T \bar{\psi} T^\dagger = \bar{\psi} (\gamma_1 \gamma_3)$, $T \psi T^\dagger = (-\gamma_1 \gamma_3) \psi$ $T i T^\dagger = -i$ since T is antiunitary ⁽²⁹⁾, and $T \gamma^0 \gamma^i \gamma_5 T^\dagger = \gamma^0 \gamma^i \gamma_5$, since T is a spatio-temporal operator, therefore it does not act on γ matrices, except γ^2 , that in Dirac representation is pure imaginary, therefore $T \gamma^2 T^\dagger = -\gamma^2$. Hence:

$$\begin{aligned} \bar{\psi} (\gamma_1 \gamma_3) (-i) (\gamma^0 \gamma^i \gamma_5) (-\gamma_1 \gamma_3) \psi &= i [\bar{\psi} \gamma^0 \gamma_1 \gamma_3 \gamma^i \gamma_5 \gamma_1 \gamma_3 \psi] = \\ &= -i [\bar{\psi} \gamma^0 \gamma^i \gamma_1 \gamma_3 \gamma_5 \gamma_1 \gamma_3 \psi] = \bar{\psi} \gamma^0 \gamma^i \gamma_5 \psi \end{aligned} \quad (2.43)$$

where $\gamma_5 = i\gamma_0\gamma_1\gamma_2\gamma_3$, $\{\gamma^\mu, \gamma^\nu\} = 2g^{\mu\nu}$ and $(\gamma^i)^2 = 1$. Therefore:

$$T \left(\bar{\psi} \sigma_{0i} \gamma_5 \psi \right) T^\dagger = \left(\bar{\psi} \sigma_{0i} \gamma_5 \psi \right) \quad (2.44)$$

as expected. Now for $\mu, \nu = i, j \rightarrow F_{ij} = -\epsilon_{ijk} B_k$, where $B_k \rightarrow -B_k$ under T. With similar considerations (paying attention to the substitution $\gamma^0 \rightarrow \gamma^j$):

$$T \left(\bar{\psi} \sigma_{ij} \gamma_5 \psi \right) T^\dagger = \left(\bar{\psi} \sigma_{ij} \gamma_5 \psi \right) \quad (2.45)$$

Finally:

$$T L_{dim=5} T^\dagger = -L_{dim=5} \quad (2.46)$$

The effective lagrangian at low energy can be therefore written as:

$$L_{eff} = L_{dim=4} + L_{dim=5} + \dots = \theta \frac{g^2}{32\pi^2} F_a^{\mu\nu} \tilde{F}^{\mu\nu a} - d_e \frac{i}{2} \bar{\psi} \sigma_{\mu\nu} \gamma_5 \psi F_{\mu\nu} + \dots \quad (2.47)$$

where $L_{dim=4}$ refer to (2.25). The connection between the parameter θ and the electric dipole moment d_e lies in this lagrangian density. Handling these terms, one can infer [17]:

²⁸This section refers to [26]

²⁹An antiunitary operator θ satisfies the antilinear condition: $\theta(a|\alpha\rangle + b|\beta\rangle) = a^* \theta(|\alpha\rangle) + b^* \theta(|\beta\rangle)$.

Appendix B.2

$$d_e \sim e\theta \frac{m}{\Lambda_{had}^2} \quad (2.48)$$

where m is the spin 1/2 particle mass and $\Lambda_{had} \sim 4\pi f_\pi$, with $f_\pi = 93$ MeV. From the experimental results on the Neutron Electric Dipole Moment (NEDM), the "fine-tuning" of the θ parameter arises [13]:

$$d_e \leq 2.9 \cdot 10^{-26} e \cdot cm \rightarrow \theta \leq 10^{-10} \quad (2.49)$$

Appendix B.2

B.2.1 Fermion representations

- This appendix refers to [27][39].

A *Dirac spinor* is the linear combination of plane waves whose positive frequency part annihilates ($\pm\frac{1}{2}$) polarized particles and the negative frequency part creates ($\pm\frac{1}{2}$) polarized antiparticles.

If we use the anticommutation relations between oscillator operators:

$$\{a_r(p), a_s^\dagger(p')\} = \{b_r(p), b_s^\dagger(p')\} = \delta_{rs} \delta^3(p - p') \quad (2.50)$$

and the spinor normalization⁽³⁰⁾:

$$u_r^\dagger(p)u_r(p) = v_r^\dagger(p)v_r(p) = \frac{E_p}{m} \quad (2.53)$$

the Dirac spinor is:

$$\Psi^D(x) = \sum_{r=1,2} \int \frac{d^3p}{(2\pi)^{3/2}} \sqrt{\frac{m}{E_p}} \{a_r(p)u_r(p)e^{-ipx} + b_r^\dagger(p)v_r(p)e^{ipx}\} \quad (2.54)$$

A Dirac field can be decomposed into two-component chiral spinors, Ψ_R and Ψ_L (where R and L indicate right and left). In the massless limit, these two-components chiral spinors that are mixed by the mass term, become independent solutions of the Dirac equation of motion. In this limit they are called *Weyl spinors* and the Fourier expansion is:

$$\Psi_{L,R}^W(x) = \int \frac{d^3p}{(2\pi)^3 2E_p} \{a(p)u_{L,R}(p)e^{-ipx} + \hat{a}^\dagger(p)v_{L,R}(p)e^{ipx}\} \quad (2.55)$$

³⁰Another common normalization is:

$$u_r^\dagger(p)u_r(p) = v_r^\dagger(p)v_r(p) = 1 \quad (2.51)$$

These spinors, unlike that above, reabsorb the square-root $\sqrt{\frac{E_p}{m}}$, such that the Dirac field become:

$$\Psi^D(x) = \sum_{r=1,2} \int \frac{d^3p}{(2\pi)^{3/2}} \{a_r(p)u_r(p)e^{-ipx} + b_r^\dagger(p)v_r(p)e^{ipx}\} \quad (2.52)$$

Appendix B.2

$$a(p) = N \int d^3x e^{-ipx} u_L^\dagger(p) \Psi_{L,R} \quad (2.56)$$

$$\hat{a}^\dagger(p) = N \int d^3x \gamma^0 C (e^{ipx} (\Psi_{L,R}^\dagger u_L(p)))^* = N \int d^3x e^{-ipx} v_L^\dagger(p) \Psi_{L,R} \quad (2.57)$$

where $u(p) = \gamma^0 C v^*(p)$ and $v(p) = \gamma^0 C u^*(p)$.

Since this is a massless limit, the normalization (2.53) fails, therefore for the Weyl spinor we have used:

$$\{a_r(p), a_s^\dagger(p')\} = \{\hat{a}_r(p), \hat{a}_s^\dagger(p')\} = (2\pi)^3 2E_p \delta_{rs} \delta^3(p - p') \quad (2.58)$$

and:

$$u_r^\dagger(p) u_r(p) = v_r^\dagger(p) v_r(p) = 2E_p \quad (2.59)$$

A *Majorana spinor* is a Dirac field that satisfy the reality condition. The simple $\Psi = \Psi^*$ condition is not Lorentz invariant, as shown in the following:

$$\Psi'(x') = e^{-\frac{i}{4} \sigma_{\mu\nu} \omega^{\mu\nu}} \Psi(x) \quad (2.60)$$

Consider now the Lorentz-trasformation of the $\Psi^*(x)$:

$$\Psi^{*'}(x) = e^{-i\sigma_{\mu\nu}^* \omega^{\mu\nu}} \Psi^*(x) \quad (2.61)$$

that is not the same trasformation law because $\sigma_{\mu\nu}$ is not purely imaginary. Therefore we defined the conjugate field:

$$\hat{\Psi}(x) = \gamma^0 C \Psi^*(x) \quad (2.62)$$

such that the trasformation law is:

$$\hat{\Psi}'(x') = (e^{-i\sigma_{\mu\nu} \omega^{\mu\nu}}) \hat{\Psi}(x) = (e^{-i\sigma_{\mu\nu} \omega^{\mu\nu}}) \gamma^0 C \Psi^*(x) \quad (2.63)$$

we can find a general condition for the unitary C matrix by equating $\Psi'(x') = \hat{\Psi}'(x')$:

$$C \sigma_{\mu\nu}^* C^{-1} = -\gamma_0 \sigma_{\mu\nu} \gamma_0 \quad (2.64)$$

For the Dirac γ -matrices:

$$C = i\gamma_2 \gamma_0 \quad (2.65)$$

In general the unitary trasformation:

$$\hat{\Psi}_{R,L} = \Psi_{L,R} \quad (2.66)$$

rotates a chiral state into the other. Both Dirac and Majorana field can be obtained as a combination of Weyl fields. Consider two Weyl fields, Ψ_1, Ψ_2 , that can be left or right handed respectively. Dirac and Majorana are massive fields, therefore both the chirality must be present in the combination. The difference between Dirac and Majorana fields is that the first is complex and the second is real. This implies that the Dirac field is the combination of two different Weyl fields with different chirality, while the Majorana field is the combination of the same Weyl field with

Appendix B.2

different chirality. Exploiting the unitary transformation (2.66), if we consider Ψ_1 and Ψ_2 with a fixed chirality, the Dirac and Majorana fields can be written as:

$$\Psi^D = \Psi_1^W + \hat{\Psi}_2^W \quad (2.67)$$

and:

$$\Psi^M = \Psi_1^W + \hat{\Psi}_1^W \quad (2.68)$$

We remark that the Dirac field is a general combination of different fields, right and left, while the Majorana is the combination of the right and left part of the same field, because it is constrained by the reality condition. The Weyl condition imposes the existence of only one of the two chiral components (left-handed particles and right-handed antiparticles or viceversa). Therefore Weyl field is a particular case of Dirac fields, while the Majorana and Weyl conditions are not compatible.

Another feature that distinguishes Dirac and Majorana particles is the boost. If a Dirac particle is boosted, since it is massive, an observer can travel at an upper velocity. He will observe a particle with the opposite helicity. To discern particles and antiparticles he needs to look at the charge. But if the particle is uncharged, as the neutrino, then he cannot distinguish them. For this reason the neutrinos could be Majorana particles. This hypothesis is very interesting, but at this time we do not know if the neutrino is a Dirac or Majorana particle.

B.2.2 Neutrino mass

Within the Standard Model the observation of only one neutrino helicity (the left handed projection) and the requirement of the lagrangian gauge invariance imply that the neutrinos are massless:

- a Dirac mass term would involve two helicities and therefore would require the introduction of gauge singlet right handed neutrinos;
- a Majorana mass term would involve only one helicity at a time, being $\propto \nu_L^T C^{-1} \nu_L$, where ν_L is the left handed neutrino field and C the charge conjugation matrix, therefore it would be favoured. But the total hypercharge of this term is -1, since that of the left handed neutrino is $Y = -\frac{1}{2}$. The Higgs doublet $\phi^T = (\phi^+ \ \phi^0)$ has $Y = \frac{1}{2}$ (or $-\frac{1}{2}$ for the conjugate $\hat{\phi}$), therefore any Yukawa type coupling leads to a lagrangian term with total hypercharge different from zero and hence that violates the correspondent $U(1)_Y$ gauge symmetry.

For these reasons, within the standard model, the neutrinos are considered massless.

The recent results on neutrino oscillations prove that the neutrinos are massive and therefore definitively imply that a standard model extension is required. To allow a Dirac mass term it is sufficient to introduce a gauge singlet right handed neutrino ν_R . To allow a Majorana mass term through minimal extensions of the standard model, we can:

Appendix B.2

1. introduce an Higgs triplet ϕ^T with hypercharge $Y = 1$, so that, coupled to $\nu_L^T C^{-1} \nu_L$, the gauge invariance is restored;
2. consider a non-renormalizable 5-dimensional operator $\frac{C}{\Lambda}(L\phi)(L\phi)$, where C is a dimensionless constant and Λ is a large energy scale; this term restores the hypercharge conservation involving only standard model particles and, below the electroweak spontaneous breaking, it provides a Majorana mass term, suppressed by the energy scale Λ . This hypothesis can occur if the standard model is the low energy manifestation of an higher energy theory, whose energy scale is $E \sim \Lambda$.

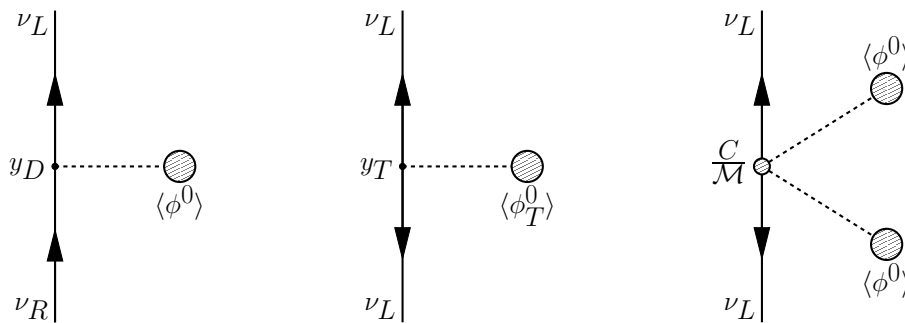


Fig. B.2.1: Left: the Dirac mass term, that involves neutrinos ν of both the helicities, right (R) and left (L), coupled to the neutral component ϕ^0 of the standard Higgs doublet and that therefore requires the introduction of a right handed neutrino (y_D is the Yukawa coupling). Center: the Majorana mass term, whose gauge invariance under $U(1)_Y$ is obtained introducing an higgs triplet ϕ^T , coupled to left handed neutrinos (y_T is the Yukawa coupling). Right: the Majorana mass term provided by a gauge invariant non renormalizable 5-dimensional operator, in which the two left handed neutrinos are coupled to the neutral components ϕ^0 of two standard higgs doublets (C is a dimensionless constant and M is the large energy scale associated to the unexplored higher energy theory, Λ in the text.). This figure is taken from [28].

3. introduce the gauge-singlet right-handed neutrinos and consider a mass term $\propto \hat{\nu}_R^\dagger \nu_R$. Since the total hypercharge of this term is $Y=0$, it could be coupled to a non standard Higgs singlet ϕ_s .

The Majorana mass terms would violate the lepton number conservation. Since the lepton number is not a gauge quantum number, its violation is admissible.

To show briefly how the seesaw mechanism works, let us consider a simple framework that involves a Yukawa type coupling term and a Majorana mass term, i.e. that introduce the right handed neutrino without specifying the possible physics beyond the standard model that produces the masses. This is the framework under which the *seesaw type I mechanism* works. There is a notation change: the right handed neutrinos so far indicated with ν_R , below are indicated with N_R , the Yukawa coupling y_D with a generic matrix λ and the standard Higgs doublet with

Appendix B.2

ϕ , in the same way as the literature cited. Within this condition the dynamics at low energy is described by the lagrangian:

$$L = L_{SM} + \sum_i N_{R,i} \hat{\phi} N_{R,i} + L_Y^D + L_{mass}^M \quad (2.69)$$

where L_Y^D is the Yukawa interaction term:

$$L_Y^D = \sum_{ij} (\lambda_{ij} \bar{\psi}_{L,i} \hat{\phi} N_{R,j} + h.c.) \quad (2.70)$$

with λ_{ij} a coupling matrix with flavor indices and $\hat{\phi} = i\tau_2 \phi^*$; note that $Y_{N_R} = 0$, $Y_\phi = 1/2$ and $Y_{\psi_L} = -1/2$, therefore the term conserves the hypercharge. After spontaneous symmetry breaking, the Dirac mass term is:

$$L_{mass}^D = \sum_{ij} (m_{ij} \bar{\nu}_{L,i} N_{R,j} + h.c.) \quad (2.71)$$

where $m_{ij} = \lambda_{ij} \frac{v}{\sqrt{2}}$ is the Dirac mass matrix ($v = \langle \phi \rangle$).

L_{mass}^M is the Majorana mass term:

$$L_{mass}^M = \sum_{ij} \left(\frac{1}{2} M_{ij} \bar{\tilde{N}}_{L,i} N_{R,j} + h.c. \right) \quad (2.72)$$

where again M_{ij} is the Majorana mass matrix.

Then the total neutrinos mass term is:

$$L_{mass} = \frac{1}{2} \begin{pmatrix} \bar{\nu}_L & \bar{\tilde{N}}_L \end{pmatrix} \begin{pmatrix} 0 & m \\ m^T & M \end{pmatrix} \begin{pmatrix} \hat{\nu}_R \\ N_R \end{pmatrix} + h.c.$$

where it is used the identity $\bar{\tilde{N}}_L \hat{\nu}_R = \bar{\nu}_L N_R^{(31)}$ such that the two terms $\propto M$ add up to the Dirac mass term. Note that m is a 3×3 matrix, equal to the number of charged lepton generations, M is in general a $N \times N$ matrix and the sterile neutrino field is a N -dimensional vector, where N is the number of sterile neutrino generations (the cancellation of chiral anomalies does not constrain the number of generations because sterile neutrinos are not coupled to gauge bosons). Since the chiral projections are not eigenstates of mass, the diagonalization process leads to the active-sterile neutrino mixing, with a mixing angle $\theta \sim O(\frac{m}{M})$, and provides the mass eigenvalues we are searching for⁽³²⁾. Then the block-diagonalization in the $M \gg m$ limit, leads to:

$$m_a = -m M^{-1} m^T \quad (2.73)$$

such that, if $m \sim v = O(100 \text{ GeV})$, as expected, and M is somehow $M \sim O(10^{14} \text{ GeV})$, then:

$$m_a \sim \frac{m^2}{M} \sim \frac{100^2}{10^{14}} \text{ GeV} = 10^{-10} \text{ GeV} = 0.1 \text{ eV} \quad (2.74)$$

below the cosmological experimental limit $\sum_i \nu_{a,i} \lesssim 0.23 \text{ eV}$ [2].

³¹ $\bar{\tilde{N}}_L \hat{\nu}_R = ((i\gamma^0 C N_R^*)^\dagger \gamma^0) i\gamma^0 C \nu_L^* = -i N_R^{*\dagger} C^\dagger \gamma^{0\dagger} i C \nu_L^* = N_R^T \gamma^0 \nu_L^* = (\nu_L^* \gamma^0 N_R^T)^T = \nu_L^\dagger \gamma^0 N_R = \bar{\nu}_L N_R$

³²For the diagonalization details we recommend the appendix A of [31], that includes also other possible mass terms.

B.2.3 The active-sterile neutrino mixing

- This appendix refers to [40]

The active-sterile neutrino mixing is employed by the diagonalization of the mass matrix discussed above. In a simplified version of the mixing in which there are only one active and one sterile neutrino, the diagonalization is made by an orthogonal rotational matrix O :

$$O = \begin{pmatrix} \cos(\theta) & -\sin(\theta) \\ \sin(\theta) & \cos(\theta) \end{pmatrix} \quad (2.75)$$

such that $OO^T = 1$ and:

$$L_{mass} = \frac{1}{2} (\bar{\nu}_L \quad \bar{N}_L) OO^T \begin{pmatrix} 0 & m \\ m^T & M \end{pmatrix} OO^T \begin{pmatrix} \hat{\nu}_R \\ N_R \end{pmatrix} + h.c. \quad (2.76)$$

Then:

$$O^T \begin{pmatrix} 0 & m \\ m^T & M \end{pmatrix} O = \begin{pmatrix} \cos(\theta) & \sin(\theta) \\ -\sin(\theta) & \cos(\theta) \end{pmatrix} \begin{pmatrix} 0 & m \\ m^T & M \end{pmatrix} \begin{pmatrix} \cos(\theta) & -\sin(\theta) \\ \sin(\theta) & \cos(\theta) \end{pmatrix} =$$

$$\begin{pmatrix} M\sin^2(\theta) + 2m\sin(\theta)\cos(\theta) & \frac{M\sin(2\theta)}{2} + m\cos(2\theta) \\ \frac{M\sin(2\theta)}{2} + m\cos(2\theta) & M\cos^2(\theta) - 2m\sin(\theta)\cos(\theta) \end{pmatrix}$$

To be diagonal, $\frac{M\sin(2\theta)}{2} + m\cos(2\theta) = 0 \Rightarrow \tan(2\theta) = -2\frac{m}{M}$, therefore, since θ -mixing is small:

$$\theta \approx \frac{m}{M} \quad (2.77)$$

and in the $m \ll M$ limit:

$$\begin{pmatrix} -\frac{m^2}{M} & 0 \\ 0 & \sim M \end{pmatrix} \quad (2.78)$$

In these conditions the rotated sterile neutrino eigenstate is:

$$N'_R = O_{12}\nu + O_{22}N = -\sin(\theta)\nu + \cos(\theta)N \approx N + \theta\nu \quad (2.79)$$

This mixing opens the important radiative decay channel $N_1 \rightarrow \nu_a\gamma$ on which many experiments are based, whose 1-loop feynman diagrams are shown below:

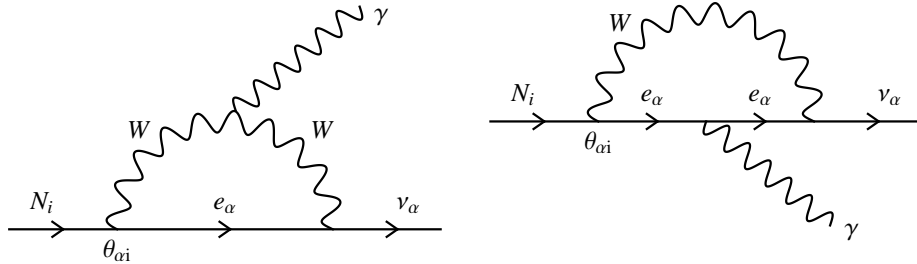


Fig. B.2.2: The Feynman diagram for the sterile neutrino radiative decay, allowed by the active-sterile neutrino mixing. This figure is taken from [31].

where ν_a is the active neutrino.

Appendix C.2

C.2.1 What is the 'WIMP miracle'

Usually in literature dealing with the WIMP paradigm, we bump into the the popular thermally averaged total annihilation cross section of χ into lighter particles times the relative velocity:

$$\langle\sigma_{\chi\bar{\chi}\rightarrow f\bar{f}}|v|\rangle \approx pb \cdot c \approx 3 \cdot 10^{-26} cm^3 s^{-1} \quad (2.80)$$

This value results from the computation of the dark matter parameter density, in the thermic hypothesis.

Exploiting the computation of Y^∞ provided in at the end of 'The Boltzmann equation: non-relativistic thermal relics' in Appendix A.1:

$$Y^\infty = \frac{n_0}{T^3} = \frac{1.661g_*^{1/2}}{m_{Pl}m_\chi\langle\sigma_{\chi\bar{\chi}\rightarrow f\bar{f}}|v|\rangle} \quad (2.81)$$

the Boltzmann equation provides the parameter density equation at this time:

$$\Omega_\chi^0 = \frac{\rho_\chi^0}{\rho_c^0} = \frac{m_\chi n_0}{\rho_c^0} = \frac{m_\chi Y^\infty T_0^3}{\rho_c^0} \quad (2.82)$$

Since:

$$n_0 = Y^\infty T_0^3 = Y^\infty s_0 \frac{45}{2\pi^2 g_{*s}} = 1.12 \times 10^4 \frac{g_*^{1/2}}{g_{*s} m_{Pl} m_\chi \langle\sigma_{\chi\bar{\chi}\rightarrow f\bar{f}}|v|\rangle} cm^{-3} \quad (2.83)$$

with $s_0 = 2970 cm^{-3}$, and:

$$\rho_c^0 = (4.85 \pm 0.13) \cdot 10^{-6} \frac{GeV/c^2}{cm^3} \quad (2.84)$$

then:

$$\Omega_\chi^0 = \frac{1.12 \times 10^4 cm^{-3}}{\rho_c} \frac{g_*^{1/2}}{g_{*s} m_{Pl} \langle\sigma_{\chi\bar{\chi}\rightarrow f\bar{f}}|v|\rangle} \sim 0.1 \cdot \sqrt{\frac{100}{g_*}} \left(\frac{10^{-10} GeV^{-2}}{\langle\sigma_{\chi\bar{\chi}\rightarrow f\bar{f}}|v|\rangle} \right) \quad (2.85)$$

where $\frac{g_*^{1/2}}{g_{*s}} \sim g_*^{-1/2}$.

Since $1 GeV^{-2}$ in natural units is 0.1 mbarn, then:

$$\langle\sigma_{\chi\bar{\chi}\rightarrow f\bar{f}}|v|\rangle \sim 10^{-38} cm^2 \rightarrow \langle\sigma_{\chi\bar{\chi}\rightarrow f\bar{f}}|v|\rangle \sim 10^{-28} cm^3 s^{-1} \quad (2.86)$$

Usually in literature this prediction is claimed as the "WIMP miracle", because the $\langle\sigma_{\chi\bar{\chi}\rightarrow f\bar{f}}|v|\rangle$ is of the same order of the electroweak interaction. Indeed the interaction is not establish, because we have no information about the mediator. The significant result is the estimation of the annihilation cross section in a mass independent way, but this is not enough to be claim as a 'miracle'.

C.2.2 SuperSymmetry

- This part is mostly taken from [51].

The SuperSymmetry (SUSY) is a mathematical proposal that imagines a symmetry between fermions and bosons. Since the SUSY considers the symmetry between particles with different statistics, i.e. with integer and half-integer spin, is a more general symmetry group than the Poincaré ones⁽³³⁾. If Q is the supersymmetry generator, such that:

$$Q|\text{fermion}\rangle=|\text{boson}\rangle \quad Q|\text{boson}\rangle=|\text{fermion}\rangle$$

than the square of the spin generator S^2 cannot be a Casimir for the SUSY group, while P^2 is imposed to be a Casimir adding a superpartners for all the elementary particles with the same mass but different statistics. This framework is supported by the Coleman-Mandula theorem [56], asserting that in theories with chiral fermions and parity-violating interaction, Q and Q^\dagger must satisfy the following anticommutation and commutation relations:

$$\{Q, Q^\dagger\} = 2\sigma_\mu P^\mu \tag{2.88}$$

$$\{Q, Q\} = \{Q^\dagger, Q^\dagger\} = 0 \tag{2.89}$$

$$[P^\mu, Q] = [P^\mu, Q^\dagger] = 0 \tag{2.90}$$

where the spinor indices are omitted. From eqs. (2.90) we can infer that P^2 is the SUSY Casimir and therefore states of the same multiplet must have equal masses.

Hierarchical or naturalness "problem" The mass degeneration just discussed is the supersymmetry property that provides a solution to the so said hierarchy or naturalness *problem*, that is the appearance of quadratic divergences in the radiative corrections of the mass of possible scalar fields contained in the lagrangian. This *problem* does not occur within the Standard Model because, being a renormalizable theory, all the divergences are absorbed by the renormalization procedure. The *problem* would arise only if an energy scale of new physics exists, such as an heavier particle.

³³The Poincaré group counts two Casimir, the length of the Pauli-Lubansky pseudo-vector $W^2 = -mJ^2$, where J^μ is the total angular momentum generator, and the length of the 4-momentum generator P^2 . The Pauli-Lubansky pseudo-vector is the 'moving particle spin generator' because it is defined as:

$$W_\mu = \frac{1}{2}\epsilon_{\mu\nu\rho\sigma}M^{\nu\rho}P^\mu \tag{2.87}$$

where $M^{\nu\rho} = \frac{i}{4}[\gamma^\nu, \gamma^\rho]$ is the infinitesimal rotation generator and P^μ is the traslation generator. For massive moving particles $W^2 = -mJ^2$, where J is the total angular momentum. For particle at rest $W^2 = -mS^2$ and since both W^2 and P^2 commute with all the Poincaré group generators, they are considered as the Casimir of the group. In this way the elementary particles can be collected according their mass and spin in irreducible multiplets under the Poincaré trasformations. At rest the Pauli-Lubansky pseudo-vector is $\propto S^2$, where S^μ is the spin generator, therefore the irreducible multiplets of the Poincaré group are constituted by the particles with the same mass and spin, labelled by $|m, s, s_z\rangle$, where $-s \leq s_z \leq s$.

Appendix C.2

Consider the Higgs potential:

$$V = m_H^2 |H|^2 + \lambda(|H|)^4 \quad (2.91)$$

where m_H is the Higgs mass and λ is the coupling constant. The Standard Model masses are fixed by a unique energy scale, that is the vacuum expectation value of the Higgs field (vev), that is non null if $m_H^2 < 0$ and $\lambda > 0$. The one-loop diagrams involving fermionic or bosonic intermediate states correct the m_H^2

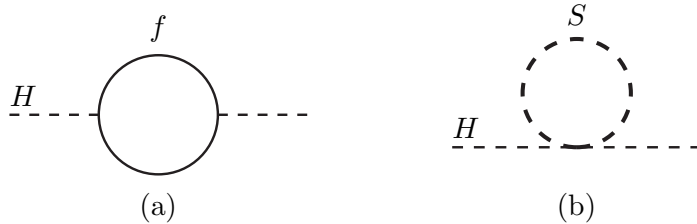


Fig. C.2.1: One-loop corrections to the Higgs squared mass m_H^2 due to (a) a fermionic intermediate state and (b) a scalar intermediate state [51]

The diagram (a) corresponds to the Higgs-fermion coupling lagrangian term $-\lambda_f H \bar{f} f$ and the relative correction to m_H^2 is:

$$\Delta m_H^2 = -\frac{|\lambda_f|^2}{8\pi^2} \Lambda_{UV}^2 \quad (2.92)$$

The diagram (b) corresponds to the Higgs-scalar coupling lagrangian term $-\lambda_S |H|^2 |S|^2$ and the relative correction is:

$$\Delta m_H^2 = -\frac{\lambda_S}{16\pi^2} [\Lambda_{UV}^2 - 2m_S^2 \ln(\Lambda_{UV}/m_S) + \dots] \quad (2.93)$$

where m_S is the scalar field mass. The quadratic divergence $\propto \Lambda_{UV}^2$ is solved by the renormalization procedure and with a different regularization, such as the dimensional, the term Λ_{UV}^2 does not occur. The naturalness problem arises *if* an heavier field exists⁽³⁴⁾, because in order to provide the cancellation of the term $\propto m_S^2$, fine-tuned conditions are required⁽³⁵⁾. The minus sign that occurs between boson and fermion loops can provide the cancellation of the dangerous contributions to all the higher order corrections, but this require that the particle content is constituted by an equal number of bosons and fermions.

The SUSY succeeds in providing this cancellation and this is one of the strongest argumentations that are led in its favor. Since, as known, the standard model matter fields and the gauge bosons, after the electroweak symmetry breaking, have not similar masses, imposing supersymmetry in the quantum field theory framework, as mentioned above, implies the existence of a copy for all the fundamental fields, a *superpartner*, degenerate in mass and with different statistics. Hence the *supermultiplets* contain each field and its superpartner.

³⁴For a review on the experimental hints of the hierarchical problem see [57].

³⁵Here the correction is due to an heavy scalar particle, but at higher order it can be also a fermion heavy particle.

Appendix C.2

Indeed the SUSY does not solve completely the question. Taking into account gravity, the complete lagrangian contains another term, the cosmological constant Λ . We have already encountered the problem connected with the cosmological constant when we discussed dark energy. The SUSY fails in solving this hierarchy problem [58].

Minimal Supersymmetric Standard Model (MSSM) Let us introduce the simplest approach to the supersymmetry theories, the Minimal Supersymmetric Standard Model (MSSM). It extends the Standard Model particle content introducing a superpartner for each standard field, or, more precisely, for each degree of freedom of the standard fields. It is said "Minimal" because it introduces a minimal number of SUSY fields, only to account for all the Standard Model fields.

Since the energy scale of supersymmetry is higher than the electroweak one, the standard particles are massless; hence considering Weyl fermions, there are two degrees of freedom for each fermion, due to the two helicities. Therefore the MSSM particle spectrum contains:

- two real spin-0 superpartners (or equivalently a complex scalar field) for each matter field (spin-1/2). These scalar superpartners are called *s-fermions* (from scalar fermions);
- two non-supersymmetric Higgs doublets and the two relative fermionic superpartners. A new Higgs non-supersymmetric doublet is introduced to avoid spoiling the anomaly cancellation, that requires an even number of fermion (or sfermion) fields. The Higgs superpartners are called *higgsinos*;
- a spin-1/2 fermion superpartner for each spin-1 gauge boson. This fermion superpartner is called as the relative gauge boson, adding -ino at the end of the name. In general they are called *gaug-inos*.

Names		spin 0	spin 1/2	$SU(3)_C, SU(2)_L, U(1)_Y$
squarks, quarks ($\times 3$ families)	Q	$(\tilde{u}_L \tilde{d}_L)$	$(u_L d_L)$	$(\mathbf{3}, \mathbf{2}, \frac{1}{6})$
	\bar{u}	\tilde{u}_R^*	u_R^\dagger	$(\bar{\mathbf{3}}, \mathbf{1}, -\frac{2}{3})$
	\bar{d}	\tilde{d}_R^*	d_R^\dagger	$(\bar{\mathbf{3}}, \mathbf{1}, \frac{1}{3})$
sleptons, leptons ($\times 3$ families)	L	$(\tilde{\nu} \tilde{e}_L)$	(νe_L)	$(\mathbf{1}, \mathbf{2}, -\frac{1}{2})$
	\bar{e}	\tilde{e}_R^*	e_R^\dagger	$(\mathbf{1}, \mathbf{1}, 1)$
Higgs, higgsinos	H_u	$(H_u^+ H_u^0)$	$(\tilde{H}_u^+ \tilde{H}_u^0)$	$(\mathbf{1}, \mathbf{2}, +\frac{1}{2})$
	H_d	$(H_d^0 H_d^-)$	$(\tilde{H}_d^0 \tilde{H}_d^-)$	$(\mathbf{1}, \mathbf{2}, -\frac{1}{2})$

Table C.2.1: The MSSM spin-0,1/2 supermultiplets. The notation \tilde{a} indicates the superpartners [51].

Appendix C.2

Names	spin 1/2	spin 1	$SU(3)_C, SU(2)_L, U(1)_Y$
gluino, gluon	\tilde{g}	g	$(\mathbf{8}, \mathbf{1}, 0)$
winos, W bosons	$\tilde{W}^\pm \tilde{W}^0$	$W^\pm W^0$	$(\mathbf{1}, \mathbf{3}, 0)$
bino, B boson	\tilde{B}^0	B^0	$(\mathbf{1}, \mathbf{1}, 0)$

Table C.2.2: The MSSM spin-1,1/2 gauge supermultiplets. The notation \tilde{a} indicates the superpartners[51].

The particle content of the Minimal Supersymmetric Standard Model is summarized in the two tables above. The two Higgs doublets have the up and down indices because they provide the masses respectively to the up and down doublet components.

Soft symmetry breaking If these fields had masses equal to the standard partners, clearly we would have already detected them. In order to comply with the known phenomenology, the supersymmetry is supposed to be a broken symmetry, but the energy order of this symmetry breaking is not predicted. This is the reason of the large arbitrariness in the parameter space, when we talk about supersymmetric dark matter candidates. Indeed the requirement of solution of the naturalness problem can constrain the mass splitting between particles and the relative superpartner. For example, within the the Minimal Supersymmetric Standard Model (MSSM), one can image a *soft* symmetry breaking, that introduces the correction to the squared Higgs mass:

$$\Delta m_H^2 = m_{soft}^2 \left[\frac{\lambda}{16\pi^2} \ln(\Lambda_{UV}/m_{soft}) + \dots \right] \quad (2.94)$$

that is proportional to m_{soft}^2 , where m_{soft} is the mass scale of the superpartners. As the electroweak symmetry breaking, the SUSY breaking provides SUSY masses proportional to a unique mass scale, in this case m_{soft} . The numerical value of this correction is not so relevant because the value of the Higgs bare mass is unknown. Indeed there are not constraints on the m_{soft} . At the begining m_{soft} was thought to be of O(TeV), to probe an energy scale accessible to experiments: signs of the supersymmetry should have arisen at the TeV scale [2][46][51]. Since the SUSY symmetry breaking energy scale is imposed and not derived, it is arbitrarily and **conveniently** changed as a function of the experimental results.

R-parity Finally, to consider a supersymmetric dark matter candidate, is yet necessary to introduce an important property: the R-parity. The R-parity is the global symmetry:

$$R = (-1)^{3(B-L)+2s} \quad (2.95)$$

where B and L are the baryon and lepton numbers, and s is the spin. For the standard particles $R = 1$, while for the superpartners $R = -1$. To preserve the

Appendix C.2

R-parity, the SUSY particles must be always produced in couple. This new global symmetry is introduced because also the MSSM, that is the simplest approach to the SUSY, allows terms that violates the B and L numbers. This violation is admissible because they are not gauge symmetries, but in these conditions unobserved processes are allowed, such as the proton decay. The R-parity conservation is imposed to avoid these processes.

From the dark matter problem point of view, the R-parity is the symmetry that allows to isolate the SUSY particles by the standard model particles, so that the lightest particle of the SUSY spectrum is stable. Therefore the arbitrary imposition of the R-parity permits the prediction of supersymmetric dark matter candidates.

Chapter 3

The Phenomenology of WIMP Candidates

The WIMP, Weakly Interactive Massive Particle, is the most questioned dark matter hypothesis. This chapter is focused on the phenomenology that characterizes this candidate, i.e. on the physics at the basis of the experimental search. We will discuss the several halo models in section 3.1 and the direct and indirect detection techniques in section 3.2 and 3.3. The aim is to study in depth the analytical form of the observable quantities and furthermore to clarify the conditions under which the comparison between direct and indirect search is possible.

3.1 The Milky Way dark matter halo

An accurate dark matter density profile has not been calculated yet. N-body simulations of hierarchical clustering in cold dark matter scenarios provide some solutions and the Milky Way halo density profile can be inferred by these results.

A general density profile model is [61]:

$$\rho(r) \propto \frac{1}{\left(\frac{r}{a}\right)^\gamma \left[1 + \left(\frac{r}{a}\right)^\alpha\right]^{(\beta-\gamma)/\alpha}} \quad (3.1)$$

where a is the halo core radius and α, β and γ are parameters that identify the different models.

	α	β	γ
Ka	2	3	0.2
Kb	2	3	0.4
FNW	1	3	1
Iso	2	2	0

Table 3.1. The parameters α, β and γ for four different models. Ka is the Kravtsov model, with $\gamma = 0.2$, Kb is the Kravtsov model, with $\gamma = 0.4$, FNW is the Navarro, Frank and White and Iso is the isothermal, spherical symmetry profile.

In table (3.1) we refer to the Kravtsov et al. model as K, to the Frank, Navarro

3.1 The Milky Way dark matter halo

and White as FNW and to the simple isothermal, spherically symmetric halo density as Iso, where Ka and Kb stay for the two $\gamma \sim 0.2 - 0.4$.

The dark matter direct and indirect searches usually adopt the simplest halo model to fit their results, i.e. the isothermal, spherically symmetric halo density, therefore $(\alpha, \beta, \gamma) = (2, 2, 0)$. The normalization constant is choose as the value of the halo density at the Solar System distance R_0 from the galactic centre:

$$\rho(r) = \rho_0 \frac{\left[1 + \left(\frac{R_0}{a}\right)^2\right]}{\left[1 + \left(\frac{r}{a}\right)^2\right]} \quad (3.2)$$

such that ρ_0 is the mean dark matter energy density nearby the solar system. Solving the Jeans equation, the associated distribution velocity function is the Maxwellian [62]:

$$f(v, v_E) d^3v = \frac{1}{k} e^{-(v+v_E)^2/v_0^2} d^3v \quad (3.3)$$

where v is the dark matter halo velocity, v_E is the dark matter velocity relative to the target and v_0 is the galactic rotation velocity and k is the normalization. Indeed the functions $\rho(r)$ and $f(v, v_E)$ just defined are an approximation of the Jeans equation solutions, but the approximation and the exact solution coincide at small and large radii. The model described by the density profile (3.2) and velocity distribution (3.3) is the Standard Halo Model (SHM). This is the simplest model, but different density profiles leads to different velocity distribution [63]. Since the experimental result interpretation is dependent on the velocity distribution, there are attempts to provide halo-independent result analyses [64].

The direct search depends on the halo density near the solar system and we use this recent study result [65]:

$$\rho_{DM}^{local} = (0.39 \pm 0.03)(1.2 \pm 0.2)(1 \pm \delta_{triax}) \frac{GeV}{cm^3} \quad (3.4)$$

where the first factor is the mean dark matter density at R_0 , the second accounts for an enhancement effect due to the galactic baryonic disk and the third is due to a possible deviation from a spherical symmetric halo, with $\delta_{triax} \leq 0.2$. If we maximize this latter, the mean halo density in the solar system is:

$$\rho_{DM}^{local} = 0.47 \pm 0.13 \frac{GeV}{cm^3} \quad (3.5)$$

The indirect search instead depends also on the dark matter density in the core of massive celestial objects, such as the Sun or the galactic center. Besides there are different density profile, there are also uncertainties on the R_0 and a parameters, such that a parameters space region must be considered, as shown by the following plot:

3.2 Direct detection

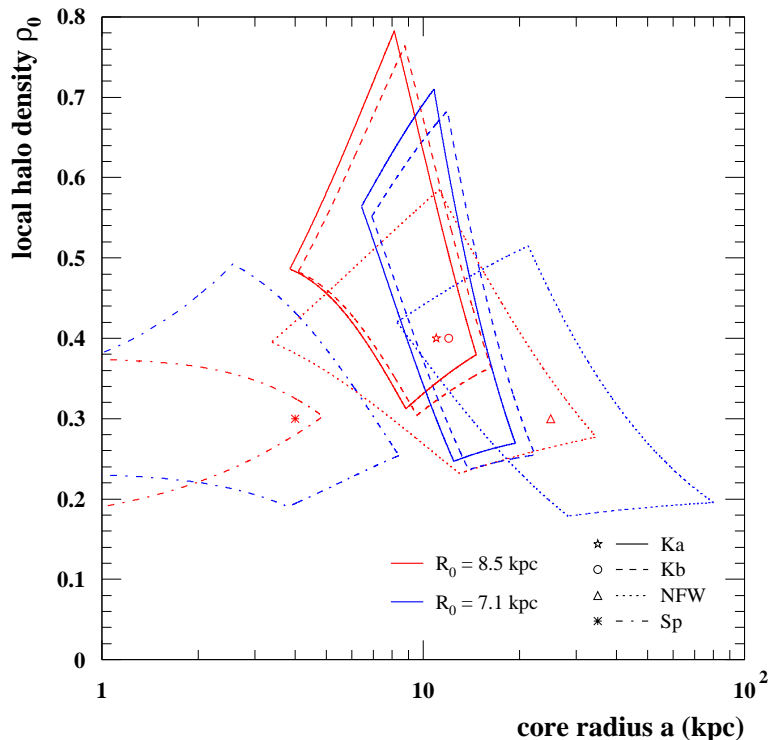


Fig. 3.1.1: The halo density profile ρ_0 is shown as a function of the possible core radius a , for the four density models discussed above, and for two different galactocentric distances $R_0 = 7.1$ kpc and $R_0 = 8.5$ kpc. Taken from Bergstrom L., Ullio P., Buckley J. H. (1998). *Observability of γ -rays from dark matter neutralino annihilations in the Milky Way halo.* *Astroparticle Physics*, 9(2), 137-162

3.2 Direct detection

- This section refers mostly to [66]

The dark matter direct detection is usually performed with a very low background apparatus that aims to observe the potential signal produced by the dark matter interaction with nuclei or electrons within the detector. The most so far exploited phenomenology is the elastic cross section of dark matter with protons and neutrons.

3.2.1 The halo velocity relative to the Earth

The Galaxy is merged in a dark matter halo. The celestial body motion through the halo provides a relative velocity between the halo particles and the Earth. If we define ⁽¹⁾:

- u_E - the Earth rotation velocity around the Sun, with $\langle u_E \rangle \approx 30$ km/s);

¹The notation used is in agreement with [66], while the values are taken from [46]

3.2 Direct detection

- u_S - the Sun proper motion relative to nearby stars;
 - v_0 - the galactic rotation velocity around the Galaxy center and therefore also the Solar System center of mass velocity; $\langle v_0 \rangle \approx 220\text{km/s}$ is taken as the mean dark matter velocity at R_0 ;
- v_{esc} - the escape velocity, i.e. the velocity at which a particle can escape from the gravitational field, that is $498\text{km/s} \lesssim v_{esc} \lesssim 608\text{km/s}$, typically 544km/s ;

then the resulting dark matter halo velocity v_E relative to the target (in the target rest frame) is:

$$\vec{v}_E = \vec{u}_E + \vec{u}_S + \vec{v}_0 \quad (3.6)$$

Since $|\vec{v}_0| \gg |\vec{u}_E|, |\vec{u}_S|$, commonly it is considered $\vec{v}_0 \sim v_E$, unless the annual motion of the Earth around the Sun can be indicative to identify a dark matter signature. The Earth orbit around the Sun is inclined by 60° with respect to the Galaxy plane and, as a consequence, with respect to the plane of the Sun rotation around the Galaxy center, as shown in Fig. (3.1.1). The Earth velocity contribution to the velocity of the WIMP wind is usually considered as a sinusoidal effect with an amplitude of 15km/s , due to the u_E projection on the galactic plane. The maximum projection is reached about in June, the minimum in December. The relative velocity between the target and the incident WIMP particle usually taken for direct detection simulation is:

$$v_E \simeq 220 + 15\cos(2\pi t) \text{ km/s} \quad (3.7)$$

with $0 < t < 1$.

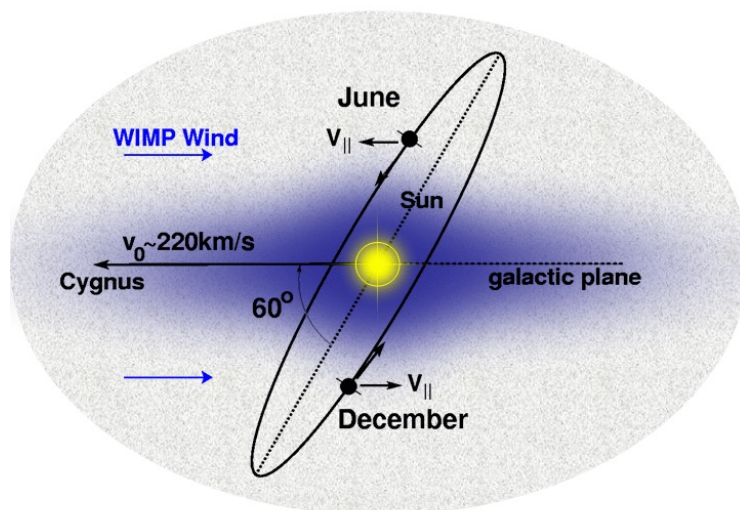


Fig. 3.2.1: A popular representation of the Earth orbit around the Sun, used to show the common model of the target-WIMP relative velocity. The maximum velocity is reached about in June, while the minimum one about in December.

3.2 Direct detection

3.2.2 Recoil rate

Consider the elastic scattering of an halo particle with mass m_D off a target nucleus of mass m_T . The differential number of recoil events dR is proportional to (i) the elastic cross section σ , (ii) the differential flux of incident particles $d\phi$ and (iii) the number of nuclei targets N_T :

(i) for the moment we do not fix the model, hence we assume a not specified elastic cross section and the only interesting property is that it depends on the relative velocity;

(ii) the incident flux depends on the halo number density described by the equation (3.11) and the relative velocity v , i.e. $d\phi = vdn$;

(iii) in a detector of total mass M there are $N_0 \times \frac{M}{A}$ nuclei, where A is the atomic mass expressed in grams, that contains an Avogadro number $N_0 = 6.022 \times 10^{23}$ of nuclei. Therefore in 1kg target of atomic mass A there are $N_T = \frac{N_0 \times 1kg}{A(g)} = \frac{N_0 \times 10^3}{A(uma)}$ target nuclei.

Then the differential recoil rate is:

$$dR = N_T \sigma d\phi = N_T \sigma v dn = N_T \sigma v \frac{n_0}{k} g(v, v_E) d^3v \quad (3.8)$$

where $g(v, v_E) d^3v$ is a generic velocity distribution ⁽²⁾, called g to distinguish it from the maxwellian distribution f mentioned above. Since the detectors have a characteristic energy threshold, to produce a detectable recoil energy, the incoming particle must have a minimal relative velocity v_{min} . Integrating over the range $v_{min} - v_{esc}$, where v_{esc} is the escape velocity from the galactic gravitational field, the total rate per kg×day is:

$$R = N_T n_0 \frac{\int_{v_{min}}^{v_{esc}} \sigma v g(v, v_E) d^3v}{k} = N_T \frac{\rho_D}{m_D} \frac{\int_{v_{min}}^{v_{esc}} \sigma v g(v, v_E) d^3v}{k} \quad (3.9)$$

To give an order of magnitude of the rate, for a simplified model with $\sigma = \sigma_0/v^2$, where σ_0 is velocity independent⁽³⁾, $g = f$ and $v_{esc} = \infty$ and for an ideal detector with $v_{min} = 0$, the counting rate would be [67]:

$$R = R_0 = \frac{5.8/A \text{ events}}{kg \text{ day}} \left(\frac{\sigma_0}{10^{-38} cm^2} \right) \left(\frac{\rho_D}{10^{-24} g/cm^3} \right) \left(\frac{v}{200 km/s} \right) \left(\frac{1 GeV}{m_D} \right) \quad (3.10)$$

where the normalizations of eqs. (3.10) refer to the WIMPs hypothesis, even if this discussion can be valid for all the massive candidates. Observe that since $1g/cm^3 = 5.6 \cdot 10^{23} GeV/cm^3$ than $\rho_D = 10^{-24} g/cm^3 \equiv 0.56 GeV/cm^3$, that is of the order of magnitude of the dark matter density.

²Note that in the following the normalization k is extracted from the velocity distribution function.

³In [5] the calculation is made for the 'zero momentum transfer' cross section σ_0 , but probably, as in [1], in the appendix A of [66] the dependency on $1/v^2$ is assorbed in the integration of the velocity distribution.

3.2 Direct detection

The maxwellian distribution approximation *If we assume a dark matter halo velocity described by the maxwellian distribution $f = f(\mathbf{v}, \mathbf{v}_E)$ of eq. (3.3), that, as said before, is associated to the isothermal, spherical symmetric density profile, then the dark matter number density n would be:*

$$n = \frac{n_0}{k} \int_0^{2\pi} d\phi \int_1^{-1} d\cos(\theta) \int_0^{v'} dv v^2 f(\mathbf{v}, \mathbf{v}_E) \quad (3.11)$$

where k is the normalization constant, such that if $v' = v_{esc} \rightarrow n = n_0$:

$$k = \int_0^{2\pi} d\phi \int_1^{-1} d\cos(\theta) \int_0^{v_{esc}} dv v^2 f(\mathbf{v}, \mathbf{v}_E) = (\pi v_0)^{3/2} \left(\text{erf} \left(\frac{v_{esc}}{v_0} \right) - \frac{2}{\pi^{1/2}} \frac{v_{esc}}{v_0} e^{-\frac{v_{esc}^2}{v_0^2}} \right) \quad (3.12)$$

with $k \rightarrow k_0 = (\pi v_0)^{3/2}$ if $v_{esc} \rightarrow \infty$ ⁽⁴⁾. Defined v_{min} , the counting rate, due to incoming dark matter particles with velocity between v_{min} and v_{esc} , for a target relative velocity v_E , but for a simplified constant cross section and for g equal to the maxwellian distribution f , is:

$$R(v_E, v_{esc}) = R_0 \frac{k_0}{k_1} \left[\frac{R(v_E, \infty)}{R_0} - \left(\frac{v_{esc}^2}{v_0^2} + \frac{1}{3} \frac{v_E^2}{v_0^2} + 1 \right) e^{-\frac{v_{esc}^2}{v_0^2}} \right] \quad (3.13)$$

$$\frac{R(v_E, \infty)}{R_0} = \frac{1}{2} \left[\pi^{1/2} \left(\frac{v_E}{v_0} + \frac{1}{2} \frac{v_0}{v_E} \right) \text{erf} \left(\frac{v_E}{v_0} \right) + e^{-\frac{v_E^2}{v_0^2}} \right] \quad (3.14)$$

where $E_0 = \frac{1}{2} m_D v_0^2$, $\frac{R_0}{E_0} = \frac{4}{\pi^{1/2}} N_T \frac{\rho_D}{m_D^2} \sigma_0$ and k_1 is the normalization constant with the integration extreme v_{min} and R_0 is the counting rate for $v_E = 0$ (zero solar system rotation velocity and zero earth revolution velocity), $v_{esc} = \infty$ (infinite gravitational attraction) and $v_{min} = 0$ (no detector energy threshold):

$$R_0 = \frac{N_0 \cdot 10^3}{A} \frac{\rho_D}{m_D} \sigma_0 \frac{2v_0}{\pi^{1/2}} \quad (3.15)$$

In summary, so far we have considered a zero momentum transfer nuclear form factor $F(|q^2|) \sim 1$ and an efficiency f for each detector equal to 1.

3.2.3 WIMP elastic scattering cross section

- *This section refers to [62][66]*

The elastic dark matter-nucleus scattering cross section is relevant both for the direct and the indirect WIMP searches: the WIMP direct search is based on the

⁴The details of the calculus of the normalization constant k are in the appendix of [66]. The main subtlety to simplify the integration is to put $v_E=0$, since the dark matter number density is independent from the Earth velocity through the halo and therefore the normalization is equal for all the v_E .

3.2 Direct detection

nuclear recoil, while the capture in the celestial bodies consists in the WIMP energy loss due to collisions off nuclei. Assuming that annihilation and capture processes reach the equilibrium there is a strict relation between the annihilation rate and the capture rate. This assumption is the key for the comparison of the results between these two completely different categories of search.

The WIMPs, when they hit a nucleus, interact with quark and gluons. This implies the introduction of unknown parameters related to the couplings and the mediators. Since the WIMPs nature is unknown, both axial-vector and scalar interactions are hypothesized and the cross section is the result of their sum. Often the cross section is classified as *spin-dependent* or *spin-independent*, because an interaction can prevail on the other as a function of the nucleus properties.

Spin dependent cross section The spin-dependent cross section can occur only in nuclei with an odd number of protons and/or neutrons. The form of the differential spin-dependent cross section σ_{SD} of a WIMP-nuclear elastic scattering, for a transferred momentum \mathbf{q} ⁽⁵⁾, is:

$$\frac{d\sigma_{SD}}{d|\mathbf{q}^2|} = \frac{8}{\pi v^2} \Lambda^2 G_F^2 J(J+1) F^2(|\mathbf{q}|) \quad (3.16)$$

where v is the incoming particle velocity, J is the total angular momentum of the nucleus, $G_F = 1.166 \times 10^{-5} GeV^{-2} (\hbar c)^3$ is the Fermi constant, $F^2(|\mathbf{q}|)$ is the nuclear form factor⁽⁶⁾ and Λ is:

$$\Lambda = \frac{1}{J} (a_p \langle S_p \rangle + a_n \langle S_n \rangle) \quad (3.18)$$

where $\langle S \rangle$ is the expectation value of the spin of the unpaired proton or neutron and:

$$a_p = \sum_{q=u,d,s} \frac{d_q}{\sqrt{2} G_F} \Delta q^{(p)} \quad (3.19)$$

$$a_n = \sum_{q=u,d,s} \frac{d_q}{\sqrt{2} G_F} \Delta q^{(n)} \quad (3.20)$$

are unknown parameters, depending on the couplings d_q between WIMPs and sea or valence quarks and on the quantities Δq , resulting by the effective strong interaction theory and numerical computed by experiments. Then the elastic spin dependent cross section can be written as:

$$\frac{d\sigma_{SD}}{d|\mathbf{q}^2|} = \frac{8}{\pi v^2} G_F^2 \frac{(J+1)}{J} (a_p \langle S_p \rangle + a_n \langle S_n \rangle)^2 F^2(|\mathbf{q}|) \quad (3.21)$$

⁵For the kinematics relations relative to the elastic scattering see the Appendix A.3.1

⁶In [66] $F^2(|\mathbf{q}|) = \frac{S(|\mathbf{q}|)}{S(0)}$, with:

$$S(|\mathbf{q}|) = (a_p + a_n)^2 S_{00}(q) + (a_p - a_n)^2 S_{11}(q) + (a_p^2 - a_n^2) S_{01}(q) \quad (3.17)$$

where S_{ij} are form factors whose values are numerically calculated using many models [62], and a_p and a_n are factors referred to proton and neutron respectively. They involve the interaction couplings, therefore are model dependent.

3.2 Direct detection

Spin independent cross section The spin independent or 'coherent' cross section, due to scalar or vectorial couplings, are dominant for heavier nuclei. Scalar or vectorial interactions do not involve the nucleon spin, therefore the proton and neutron couplings are the same and the differential cross section is:

$$\frac{d\sigma_{SI}}{d|\mathbf{q}|^2} = \frac{1}{\pi v^2} [Z f_p + (A - Z) f_n]^2 F^2(|\mathbf{q}|) = \frac{\sigma_0}{v^2} F^2(|\mathbf{q}|) \quad (3.22)$$

where f_p and f_n are unknown WIMP-quark couplings, σ_0 is the velocity-independent part of the cross section and $\mu = \frac{m_D m_T}{(m_D + m_T)}$ ⁽⁷⁾.

Analytic expression of the form factor In the scalar or vectorial interactions the form factor does not depend on the nucleon spin and reduces to the usual charge distribution in the momentum space. The only analytical expression of the form factor comes from the charge density proposed by Helm in 1956 [68]⁽⁸⁾ that leads to [69]:

$$F^2(|\mathbf{q}|) = \left[\frac{3j_1(qR_1)}{qR_1} \right]^2 e^{-(qs)^2} \quad (3.23)$$

where $q = \sqrt{2m_T E_R}$ is the transferred momentum, with E_R the recoil energy, $s = 1\text{fm}$ is a characteristic dimension of the nucleus, $j_1(qR_1) = [\sin(qR_1) - qR_1 \cos(qR_1)] / (qR_1)^3$ and $R_1 = (R^2 - 5s^2)^{1/2}$, with $R \simeq 1.2A^{1/3}\text{fm}$.

Therefore the form factor, that can be written as:

$$F^2(|\mathbf{q}|) = \left[\frac{3(\sin(qR_1(A)) - qR_1(A)\cos(qR_1(A)))}{(qR_1(A))^3} \right]^2 e^{-(qs)^2} \quad (3.24)$$

depends non trivially on the target atomic mass.

Often, even if there exists a difference between the spin-dependent and the spin-independent interaction, the simulation are done in the simpler assumption of a spin independent cross section, whose velocity dependency is in the factor $1/v^2$ and in the form factor. The form factor used for practical purpose is the Helm form factor in eqs. (3.23), but it is worth noting that it approximates a more complicated framework.

3.2.4 Annual modulation

As "annual modulation" we refer to the differential recoil rate annual oscillation, due to the Earth velocity around the Sun, that sums vectorially to the Sun velocity around the Galactic center. The differential rate acquires a period of one year and therefore can be expanded in Fourier:

$$\frac{dR(v_{min}, t)}{dE} = A_0 + \sum_i A_i \cos[nw(t - t_0)] + \sum_i B_i \sin[nw(t - t_0)] \quad (3.25)$$

⁷From eq. (7.34) of [62]

⁸In [66] the authors refer to this form factor as the "Wood-Saxon", because it is very similar.

3.3 Indirect detection

where v_{min} is the minimum velocity that can cause a detectable recoil. In the assumption of an isotropic velocity distribution, such that $B_i = 0$, and of a neglectable variation of the velocity distribution due to the Earth velocity, such that $A_0 \gg A_1 \gg A_2\dots$, then:

$$\frac{dR(E, t)}{dE} \approx S_0(E) + S_m(E)\cos w(t - t_0) \quad (3.26)$$

where $w = 2\pi/year$. The annual modulation depends only on the detectability of the energy recoil. For this reason it is an important signature and its detection by the DAMA collaboration is a fundamental result in the panorama of the dark matter search, though the published data seems in contrast with the results of other experiments.

3.2.5 Inelastic-scattering

The most so far exploited phenomenology is the WIMP-nuclei elastic cross section. Another possible signature could be due to the WIMP inelastic scattering off target electrons or target nuclei. The inelastic scattering consists in a process whose final state content is different from the starting one. They are characterized by a further energy loss, beyond the nuclear recoil, that in the cases of WIMP is due to atomic or nuclear excitation. As a consequence the inelastic cross section is suppressed with respect to elastic cross section.

The two inelastic processes due to a WIMP scattering can occur if[62]:

1. a WIMP hits an orbital electron; this latter can leave the atoms in an excited state and the de-excitation can produce a detectable signal;
2. a WIMP scatters off the nucleus; under certain conditions can cause the nuclear excitation and its de-excitation can produce a detectable signal.

In the first process the excited electron state is expected to decay emitting a photon of several eV. These photons may be easier to be detected than the phonon or electron-hole pairs produced by the nuclear elastic scattering because of the presence of many different excitable energy states whose rate can be predicted and distinguished [70].

The second process was discussed by Ellis, Flores and Lewin in 1988 [71]. They focused on some supersymmetric particles, but their considerations can be generalized. Starting from their results, the numerical limits on this latter process are discussed in the last chapter.

3.3 Indirect detection

The indirect detection aims to study the dark matter properties through the detection of Standard Model particles produced by the dark matter annihilation or decay occurring in over density regions, as the center of celestial bodies.

Consider WIMPs. The fluxes of the interesting particles depends on the WIMP previous capture process, that traps WIMP in the center of the Galaxy, the Sun or the Earth and in the following WIMP annihilation into Standard Model particles.

3.3 Indirect detection

3.3.1 WIMP capture and annihilation processes

When a dark matter halo particle scatters off nuclei near the Sun, the Earth or the Galaxy center, it can be trapped gravitationally with a certain probability and accumulate in the core region. Here the annihilation process can occur, producing primary or secondary particles, whose fluxes are detected on Earth. Due to these processes, the variation in time of the WIMP particle number N_χ in the core region is:

$$\frac{dN_\chi}{dt} = C_C - C_A N_\chi^2 - C_E N_\chi \quad (3.27)$$

where C_C is the capture rate, C_A is the annihilation rate, with $\Gamma_A = \frac{1}{2}C_A N_\chi^2$ and C_E is the evaporation rate⁽⁹⁾.

The evaporation term for masses for the masses of interest can be neglected [72]. The capture rate is time independent because the dark matter halo properties and the composition of the body are considered constant in time. The solution of eqs. (3.27) is:

$$\Gamma_A = \frac{1}{2}C_C \tanh^2\left(\frac{t}{\tau}\right) \quad (3.28)$$

where $\tau = 1/\sqrt{C_C C_A}$ and t can be the solar system age $t \approx t^\odot \simeq 4.5 \cdot 10^9$ years. Commonly the equilibrium condition $dN/dT = 0$, that holds for $t^\odot/\tau \gg 1$ is considered, such that from eq. (3.27):

$$\Gamma_A = \frac{1}{2}C_C \quad (3.29)$$

Under this assumption the physics of the annihilation is not necessary, because it can be evaluated from the physics of the WIMP-nuclei elastic scattering. The capture can be due to the WIMP scatter off any nucleus in the volume dV considered:

$$C_C = \int_0^R dr 4\pi r^2 \sum_i \frac{dC_i(r)}{dV} \quad (3.30)$$

where R is the celestial body radius and $\frac{dC_i(r)}{dV}$ is the capture rate off the nucleus i in a shell of volume. Edsjo and Wikstrom in [9], referring to a Gould article published in 1987 [73], calculate the capture probability for a velocity independent cross section $\sigma_{\chi,i}$. Indeed they consider a generic elastic scattering cross section, but, as in literature [1], it is factorized in a velocity independent factor, usually called σ_0 but here called $\sigma_{\chi,i}$, times a velocity dependent term constituted by the form factor $F(|q^2|)$ times a term $\frac{1}{v^2}$. The velocity dependent term is absorbed in the integrals, while the velocity independent part of the cross section can be factorized:

$$\Gamma_A = \frac{C_C}{2} = \sigma_{\chi,i} \cdot \int_0^R dr 4\pi r^2 \sum_i \frac{1}{\sigma_{\chi,i}} \frac{dC_i(r)}{dV} \quad (3.31)$$

This method is crucial for the direct and indirect detection result comparison, as discussed in the next sections. Since $\sigma_{\chi,i}$ is constituted by a spin-dependent and by

⁹The evaporation process is the particle escape from the gravitational field due to a particle velocity greater than the celestial body escape velocity.

3.3 Indirect detection

a spin-independent part, in agreement with [72] the eqs. (3.31) can be inverted and written as:

$$\sigma^{SI} = \lambda^{SI}(m_\chi)\Gamma_A \quad (3.32)$$

$$\sigma^{SD} = \lambda^{SD}(m_\chi)\Gamma_A \quad (3.33)$$

where σ^{SI} and σ^{SD} are relative to the WIMP-proton elastic scattering, and the difference between the two conversion factors λ^{SI} and λ^{SD} is only the relation between the WIMP-nucleus cross section $\sigma_{\chi,i}$ and the spin-dependent/independent WIMP-proton cross sections.

Annihilation channels The WIMP can annihilate in various final states: considering only those at tree level they are the fermion-antifermion $f\bar{f}$, where f can be charge leptons, neutrinos and quarks, the gauge bosons W^+W^- , Z^0Z^0 and $\gamma\gamma$, and other annihilation channels involving the Higgs boson. In the non-relativistic limit, the thermally average annihilation cross section times the velocity, discussed in 'The Boltzmann equation: non-relativistic thermal relics' in Appendix A.1.1, can be expanded as:

$$\langle\sigma_a v\rangle = a + bv^2 + O(v^4) \quad (3.34)$$

where a corresponds to the s-wave annihilation and b both to the p and s-wave annihilation. In the $v \rightarrow 0$ limit, that holds in the Earth and Sun core, the s-wave annihilation constrains the process, because the two Majorana neutralino interacting spins must be opposite according to the Fermi statistic. The angular momentum conservation leads to outgoing fermions with the same helicity. But in the $m_f \rightarrow 0$ limit the helicity flip is required to get a non-null cross section; as a consequence the lighter the fermion, the rarer the process. This makes the $t\bar{t}$ final state the dominant fermionic annihilation channel for such models where $m_\chi > m_t$ [4]. This is the reason for considering mostly annihilation channels in heavy Standard Model particles, i.e. $t\bar{t}$, $c\bar{c}$, $b\bar{b}$, $\tau^+\tau^-$, W^+W^- , Z^0Z^0 .

3.3.2 Event rate for neutrino fluxes

The annihilation or the decay of dark matter captured in the core of the Galaxy, the Sun or the Earth can produce neutrinos. The neutrino astronomy is a competitive indirect search for dark matter because, unlike charged particles, the produced neutrinos escape from the core and can reach the Earth, preserving the source direction. This favours their distinction from the background. The expected differential neutrino flux is:

$$\frac{d\phi_\nu}{dE} = \frac{\Gamma_A}{4\pi R^2} \sum_f B_f \frac{dN_\nu^f}{dE} \quad (3.35)$$

where Γ_A is the annihilation amplitude, R is the distance from the source, B_f is the branching ratio of the f -channel and $\frac{dN_\nu^f}{dE}$ is the neutrino differential number in the channel f .

This neutrino flux is not directly observed. The neutrino telescope detection principle relies on the detection of the charge leptons produced by the neutrino scattering off nuclei in the detector material or in rock. Since the incoming neutrinos are at

3.3 Indirect detection

high energies, they interact with the quarks of the nucleus, via the deep inelastic scattering:

$$\nu(\bar{\nu}) + N \rightarrow l^{-(+)} + X \quad (3.36)$$

where N is the nucleus, $l^{-(+)}$ is a charge lepton and X is the hadronic shower. Since the detection technique requires a long path length from the interaction point, the $\bar{\nu}_\mu^{cc}$ interactions are the best candidate events to be identified by the μ detection.

Event rate for muon-neutrino induced fluxes The neutrinos, that can escape from the celestial body core, propagate, oscillate and near the detector interact producing detectable muons. The observable is the neutrino-induced muon flux ϕ_μ . If we consider the WIMP annihilation process[72]:

$$\begin{aligned} \phi_\mu = \frac{\Gamma_A \cdot n}{4\pi R^2} \int_{E_\mu^{th}}^\infty dE_\mu \int_{E_\mu^{th}}^\infty dE_\nu \int_0^\infty d\lambda \int_{E_\mu}^{E_\nu} dE'_\mu P(E_\mu, E'_\mu, \lambda) \frac{d\sigma_\nu(E_\nu, E'_\mu)}{dE'_\mu} \\ \cdot \sum_i P(\nu_\mu, \nu_i) \sum_f B_f \frac{dN_i^f}{dE_\nu} = \Gamma_A \cdot \eta(m_\chi) \end{aligned} \quad (3.37)$$

where Γ_A is the annihilation amplitude, R is the distance from the celestial body center, n is the numerical density of targets; $\frac{dN_i^f}{dE_\nu}$ is the number of neutrinos ν_i in energy unity produced starting from the WIMP annihilation in channel f , B_f weighs the probability of the annihilation channel f , $P(\nu_\mu, \nu_i)$ is the probability that the ν_i oscillates in ν_μ in the detector; $P(E_\mu, E'_\mu, \lambda) \frac{d\sigma_\nu(E_\nu, E'_\mu)}{dE'_\mu}$ is the probability of detecting a muon of energy E'_μ , being $\frac{d\sigma_\nu(E_\nu, E'_\mu)}{dE'_\mu}$ the differential $\nu_\mu - \mu$ cross section and $P(E_\mu, E'_\mu, \lambda)$ the probability that starting from a muon energy E'_μ , after a path length λ in the detector, the muon energy is E_μ ; there are than the integral over all the energies and the possible path lengths. Note that the lower integration limit is the detector energy threshold.

Now combine the ϕ_μ expression with the capture rate in eq. (3.32) and (3.33):

$$\sigma^{SI} = \lambda^{SI}(m_\chi)\Gamma_A = \lambda^{SI}(m_\chi)\frac{\phi_\mu}{\eta(m_\chi)} = k^{SI}(m_\chi)\phi_\mu \quad (3.38)$$

$$\sigma^{SD} = \lambda^{SD}(m_\chi)\Gamma_A = \lambda^{SD}(m_\chi)\frac{\phi_\mu}{\eta(m_\chi)} = k^{SD}(m_\chi)\phi_\mu \quad (3.39)$$

This is the direct relation between the observable, i.e. the muon flux, and the elastic scattering cross section, that is crucial for the direct and indirect result comparison. We underline that this direct relation holds only if the equilibrium condition between capture and annihilation rate works. Furthermore if an annihilation channel f is considered dominating, then the conversion factors $k^f(m_\chi)$ are provided by the web tool WimpSim [74].

Appendix A.3

3.3.3 Event rate for γ -ray or cosmic ray fluxes

As neutrinos, also γ -rays can be produced at the end of the dark matter annihilation or decay chain. For the WIMP paradigm, the expected monochromatic γ -ray flux is:

$$\frac{d\phi_\gamma(\psi, \theta)}{dE} = \frac{\langle \sigma_a v \rangle}{8\pi m_\chi^2} \sum_f B^f \frac{dN_\gamma^f}{dE_\gamma} \cdot J(\psi, \theta) \quad (3.40)$$

where:

$$J(\psi, \theta) = \int_0^{\Delta\Omega} \int_{l_{of}} \rho^2(l(\psi, \theta)) dl d\Delta\Omega \quad (3.41)$$

is the astrophysical term that relates the expected γ -ray flux with the dark matter density along the telescope line of sight (los) and within the accessible solid angle $\Delta\Omega$. ψ and θ are the angular distance of the observation point from the galactic center and plane. The density is squared because we are considering the annihilation process. The integral over the line of sight is peculiar of the γ -ray and cosmic ray detection since the detected signal cannot be connected with a specific source, as the neutrinos that can be associated to the center of celestial objects. An analogue approach is exploited for the detection of cosmic rays.

Appendix A.3

A.3.1 Non-relativistic elastic scattering kinematics

Consider two particles in the laboratory frame (LF) with $v_1 \neq 0$ and $v_2 = 0$.

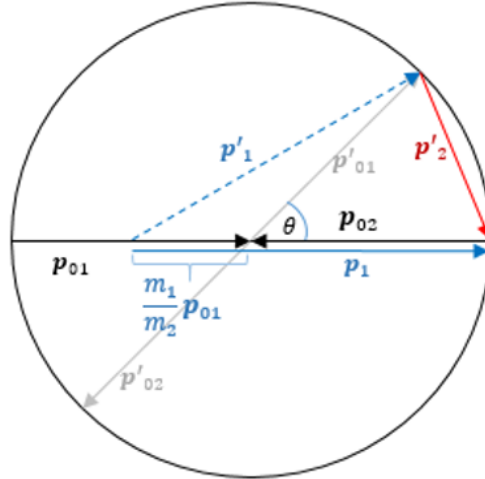


Fig. A.3.1: A schematic representation of the kinematics of the non-relativistic scattering. In black \mathbf{p}_{01} and \mathbf{p}_{02} are the incident momentum in the center of mass, $|\mathbf{p}_{01}| = |\mathbf{p}_{02}|$. In grey \mathbf{p}'_{01} and \mathbf{p}'_{02} are the final momentum in the center of mass, $|\mathbf{p}'_{01}| = |\mathbf{p}'_{02}| = |\mathbf{p}_{01}| = |\mathbf{p}_{02}|$. The solid blue vector represents the initial momentum of the first particle in the laboratory frame, $\mathbf{p}_1 = \frac{m_1}{m_2} \mathbf{p}_{01} + \mathbf{p}_{01}$ (remember that $|\mathbf{p}_{01}| = |\mathbf{p}_{02}|$). The dashed blue vector represents the final momentum of the second particle in the laboratory frame, $\mathbf{p}'_1 = \frac{m_1}{m_2} \mathbf{p}_{01} + \mathbf{p}'_{01}$. In red the final momentum of the second particle in the laboratory frame.

In the centre of mass (CM) they are:

$$\mathbf{v}_{01} = \mathbf{v}_1 - \mathbf{V}_{CM} = \frac{m_2}{m_1 + m_2} \mathbf{v}_1 \quad (3.42)$$

Appendix A.3

$$\mathbf{v}_{02} = 0 - \mathbf{V}_{CM} = -\frac{m_2}{m_1 + m_2} \mathbf{v}_1 \quad (3.43)$$

with $V_{CM} = \frac{m_1 v_1 + m_2 v_2}{m_1 + m_2} = \frac{m_1}{m_1 + m_2} v_1$ the center of mass velocity in the laboratory frame. Note that:

$$\mathbf{p}_{01} = \frac{m_2}{m_1 + m_2} \mathbf{p}_1 \longrightarrow \mathbf{p}_1 = \frac{m_1}{m_2} \mathbf{p}_{01} + \mathbf{p}_{01} \quad (3.44)$$

as shown in fig. (A.3.1).

In the CM the non relativistic scattering corresponds to a direction change, i.e to a conserving modulus rotation of the momentum, at a generic angle θ :

$$\begin{cases} |\mathbf{p}_{01}| = |\mathbf{p}'_{01}| \\ |\mathbf{p}_{02}| = |\mathbf{p}'_{02}| \end{cases} \quad (3.45)$$

with $|\mathbf{p}_{01}| = |\mathbf{p}_{02}|$. Therefore after the diffusion, the first particle momentum in the CM, p'_{01} , as a function of the initial momentum in the CM p_{01} , is:

$$\begin{cases} p'_{01x} = p_{01} \cos \theta \\ p'_{01y} = p_{01} \sin \theta \end{cases} \quad (3.46)$$

The relation between the LF and the CM after the diffusion is:

$$\mathbf{v}'_{01} = \mathbf{v}'_1 - \mathbf{V}'_{CM} = v'_1 - \frac{m_1 \mathbf{v}'_1 + m_2 \mathbf{v}'_2}{m_1 + m_2} = \frac{m_2}{m_1 + m_2} (\mathbf{v}'_1 - \mathbf{v}'_2) \quad (3.47)$$

Then:

$$\mathbf{p}'_{01} = m_1 \frac{m_2}{m_1 + m_2} (\mathbf{v}'_1 - \mathbf{v}'_2) = \frac{m_2}{m_1 + m_2} \mathbf{p}'_1 - \frac{m_1}{m_1 + m_2} \mathbf{p}'_2 \quad (3.48)$$

Since \mathbf{p}'_{01} is known, the system of equation:

$$\begin{cases} \mathbf{p}'_{01} = \frac{1}{m_1 + m_2} (m_2 \mathbf{p}'_1 - m_1 \mathbf{p}'_2) \\ \mathbf{p}'_2 = \mathbf{p}_1 - \mathbf{p}'_1 \end{cases} \quad (3.49)$$

can be solved for \mathbf{p}'_1 and \mathbf{p}'_2 . The solution for \mathbf{p}'_1 is:

$$\mathbf{p}'_1 = \mathbf{p}'_{01} + \frac{m_1}{m_1 + m_2} \mathbf{p}_1 = \mathbf{p}'_{01} + \frac{m_1}{m_2} \mathbf{p}_{01} \quad (3.50)$$

as shown in fig. (A.3.1) and, as a consequence, the solution for \mathbf{p}'_2 is:

$$\mathbf{p}'_2 = \mathbf{p}_1 - \mathbf{p}'_1 = \mathbf{p}_1 - (\mathbf{p}'_{01} + \frac{m_1}{m_1 + m_2} \mathbf{p}_1) = \frac{m_2}{m_1 + m_2} \mathbf{p}_1 - \mathbf{p}'_{01} \quad (3.51)$$

and in components:

$$\begin{cases} p'_{2x} = \frac{m_2}{m_1 + m_2} |p_1| - \frac{m_2}{m_1 + m_2} |p_1| \cos \theta \\ p'_{2y} = -\frac{m_2}{m_1 + m_2} \sin \theta |p_1| \end{cases} \quad (3.52)$$

with:

$$|\mathbf{p}'_2|^2 = p'^2_{2x} + p'^2_{2y} = 2 \left(\frac{m_2}{m_1 + m_2} \right)^2 p_1^2 (1 - \cos \theta) \quad (3.53)$$

Appendix A.3

For a comparison with the nuclear recoil due to dark matter discussed in the text, \mathbf{p}'_2 corresponds to the transferred momentum, that in the text we indicate with \mathbf{q} , and 1, 2 correspond to D, T, where D stay for dark matter and T for target. Since the cold dark matter is not relativistic, the kinetic energy and the momentum of the incoming particle are:

$$E = \frac{1}{2}m_D v^2 \quad (3.54)$$

$$p = m_D v \quad (3.55)$$

Said E_R the recoil energy, it is:

$$E_R = \frac{|\mathbf{p}'_2|^2}{2m_T} \equiv \frac{|\mathbf{q}|^2}{2m_T} = \frac{1}{m_T m_D} \left(\frac{4m_D m_T}{m_D + m_T} \right)^2 \frac{p_1^2}{2m_D} (1 - \cos\theta) = E \cdot r \frac{1 - \cos\theta}{2} \quad (3.56)$$

where $r = \frac{4m_D m_T}{(m_D + m_T)^2}$ and $E = \frac{p_1^2}{2m_D}$ is the incoming dark matter energy.

Chapter 4

Experimental Search for Dark Matter Particles

Many experimental efforts are dedicated to the dark matter particle search. Beyond the search at colliders, there are two main categories: the direct and the indirect detection experiments. Each detection technique focuses on a different interaction process. The direct search probes the WIMP interaction off nuclei, the indirect search the WIMP annihilation and the colliders the WIMP production, as summarized in fig. (4.1).

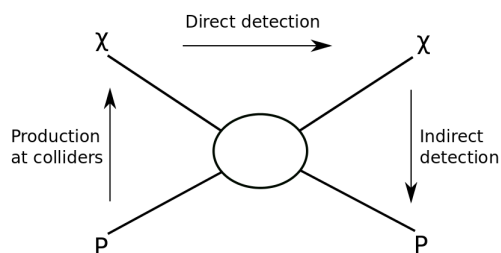


Fig. 4.1: The three interactions typologies exploited for the dark matter search.

This chapter is an analysis of the active projects focusing on the dark matter detection and on the published data. We will discuss the direct experiments in section 4.1, the indirect experiments in section 4.2 and the state of the art of the available results in section 4.3. We remark that the comparison between results is possible according to the conditions discussed in the previous chapter

4.1 Direct detection experiments

The dark matter direct search consists in the detection of a signal produced by the interaction of the halo dark matter particle with the detector material. This task is pursued by very low background detector in underground laboratories. In order to optimize the search, a comparison between the direct detection results obtained through different techniques is crucial. However the different detection principles, the choice of the procedure to reject or subtract the background and the different targets complicate the picture, making this confront one of the most

4.1 Direct detection experiments

discussed issues of the last years.

We will collect the experiments into three classes: high purity crystal detectors, noble liquid detectors and cryogenic detectors.

- **High purity crystal detectors:** constituted by highly radiopure inorganic crystals, such as sodium iodide (NaI) or cesium iodide (CsI), their aim is the observation of single scattering events through the detection of a scintillation signal. Usually the crystals are doped to reduce the gap between the conduction and the valence bands, so that lower recoil energies are detectable. Examples are the popular DAMA (DARk MATter) experiment, constituted by NaI(Tl) (sodium iodide doped with thallium) crystals and the KIMS (Korea Invisible Mass Search) experiments, made of CsI(Tl) (cesium iodide doped with thallium) crystal.

The DAMA result, that is evidence of the annual modulation of the differential rate of events collected in about twenty years of observation, is very discussed because it is in apparent contrast with the null result obtained by other direct detection experiments. In order to shed light on this controversy, experiments that aim to reproduce the DAMA result are in development phase. An example is the SABRE (Sodium-iodide with Active Background REjection) experiment, that will consist in twins NaI(Tl)-detectors that will be located one at the Laboratori Nazionali del Gran Sasso (LNGS), Italy, and the other in Stawell Underground Physics Laboratory (SUPL), Australia [76]. Another challenge is pursued by the DM-Ice experimental program, that is a direct detection experiments that seeks to verify the DAMA results with a target of NaI buried 2450m in the South Pole [77].

- **Noble liquid detectors:** Noble liquids such as xenon (Xe), argon (Ar) and neon (Ne) should allow to detect in coincidence the ionization and the scintillation signal due to WIMP interactions with the noble liquid atoms. This discrimination property, the rapidity of the scintillation decay time (ns) and the possibility to obtain large masses at modest cost make noble liquid a very exploited target. Furthermore these detectors can discriminate between WIMP recoil and electron recoil. Examples are the XENON and the LUX (Large Underground Xenon experiments), that exploit the xenon targets, and DarkSide, that is constituted by argon targets. Xenon and DarkSide are located in the LNGS, while LUX experiment in the Sanford Underground Research Facility (SURF), in the Homestake Mine, in South Dakota. This latter experiment claims to have reached the lowest exclusion limit for WIMP detection. An *exclusion* limit implies the contradiction of the results of previous experiments, for instance the DAMA annual modulation, and this is the reason of the controversy mentioned above.
- **Cryogenic detectors:** the detection principle of very low temperature detectors, constituted by crystals, semiconductor materials or noble liquid, is the measure of temperature variations due to the local energy deposition following the dark matter interaction with nuclei. The cryogenic temperatures lower the energy threshold, allowing the search for smaller dark matter masses. For

4.1 Direct detection experiments

example the CRESST (Cryogenic Rare Event Search with Superconducting Temperature) experiment, located in the LNGS, is constituted by the inorganic scintillator CaWO_4 . The low temperature ($\sim \text{mK}$) allows to probe masses smaller than 10GeV , such that the CRESST-II (last upgrade) collaboration reached the best limit for masses $< 6\text{GeV}$. There are also many detectors constituted by semiconductor materials, for example CoGeNT, CDMS (Cryogenic Dark Matter Search), EDELWEISS are germanium detectors, that work at low temperature. In particular SuperCDMS reached a temperature $\sim \text{mK}$. An example of noble liquid experiment that works at low temperature is DarkSide.

4.1.1 DAMA

The DAMA (DARk MATter) experiment is located at the Laboratori Nazionali del Gran Sasso (LNGS) of the I.N.F.N. (Istituto Nazionale di Fisica Nucleare). It is mainly focused on the dark matter search and precisely its aim is the detection of the signature of the dark matter annual modulation from the Galactic Halo. This section is devoted to the DAMA experiment study, since our aim is to try to understand their result.

Experiment description The DAMA detector is an inorganic scintillator, constituted by a matrix of radiopure Thallium-doped Sodium-Iodide (NaI(Tl)) crystals⁽¹⁾. The general detection principle is based on the collection of radiation emitted by the detector, regardless of the interaction that causes it. The applied procedure to reduce the background (briefly discussed below) are such that the "ambiguous" data, that can be due to the background but that can contain also a dark matter signal, are conserved. In this way constraints on the detectable dark matter candidate are not fixed a priori, because all the possible signals from incoming particles are collected.

It is for this reason that the DAMA results are claimed *model-independent* by the collaboration and this is also why the DAMA results can be consistent with different models [79].

The NaI(Tl) target has an high scintillation yield of ~ 40 photons/ keV_{ee} ⁽²⁾, therefore ideally it could be sensitive to small energy deposition (at the sub-keV level). This high light yield decreases the energy threshold and should allow the search for light dark matter candidates[80], such as the axions of the keV or the sterile neutrinos of the keV. However, although the "physical" energy threshold is at the sub-keV, the software energy threshold is at $\sim 2\text{keV}_{ee}$, because it must take into account the background.

For WIMP candidates, the choice of sodium Na ($m_{\text{Na}} \sim 23\text{GeV}$) and iodide I ($m_{\text{I}} \sim 127\text{GeV}$) as targets would permit a better sensitivity to both possible high and low bullet masses, since the recoil energy is greater if the bullet mass and

¹The advantages of the NaI(Tl) target choice are listed in the DAMA reference [78]

²A keV_{ee} is the amount of energy produced by an electron recoil, with an equivalent nuclear energy recoil. The ratio between the light produced by a nuclear recoil and that produced by an electron recoil is said the nuclear quenching factor ($1\text{keV}/1\text{keV}_{ee} = Q_f$)

4.1 Direct detection experiments

the target nucleus masses are similar, such that the results could be interpreted as a iodide recoil for heavier WIMPs and as a sodium recoil for the lighter ones. Moreover the *spin-independent* cross section is allowed by the high iodide target mass and the *spin dependent* by the most abundant Na and I isotopes, ^{23}Na and ^{127}I , that have unpaired nucleons.

Data taking phenomenology The hypothesized incoming particle provides a nuclear recoil whose energy deposition excites the electrons. The electron de-excitation produces a light-pulse that is detected by the photomultipliers⁽³⁾. Each crystal is connected to two low-background photomultipliers (PMTs) working in coincidence to reduce the photomultiplier noise and to increase the light collected. The experimental setup is such that to have 5.5 to 7.5 photoelectrons/keV, i.e. for 1 keV of energy deposition the resulting photon emission, will induce $5.5 \div 7.5$ photoelectron revealed by the PMTs.

Background reduction attempts Because of the very low-energy signal many precautions are needed to control for the background. The main sources of background are (i) the radioactivity both of the isotopes in the detector material and of the environment such as of the rock surrounding the laboratory, (ii) the primary cosmic rays and (iii) the showers produced by cosmic rays, including for example neutrons, that can simulate a dark matter recoil. To reduce some of these background sources the DAMA apparatus is located in the underground LNGS laboratory at a depth of 3,100 meters-water-equivalent (m.w.e). Internal radiation due to the isotope radioactivity is reduced by the crystal purification, but some elements such as Potassium(K) and Rubidium(Rb) are difficult to separate from Na. This is dangerous because for example the ^{40}K isotope decay indirectly produces γ -rays that provide a signature of 3.2 keVee, a parameter that depends on the energy.

Rejection procedure For the dark matter search, the interesting signals are the *single-hit* events, i.e. the events that occur in a single crystal (since the detection probability of dark matter *multiple-hit* events is negligible). Near the energy threshold the photomultiplier noise can contribute to the single-hit events. This background (reduced also because the photomultiplier work in coincidence) is rejected because the time distribution of scintillation and noise signals are different and therefore they are clearly distinguishable [78].

The detector characteristics and the rejection procedure are chosen in order to reach the main goal of the DAMA project, that is a *model-independent result*. Indeed the dependency on the models is unavoidable, since for example the lightest candidates such as the gravitino or the axions in the $\mu\text{eV} - \text{meV}$ are not detectable. However the annual modulation signature includes many different models and it does not need of priori assumption on the density profile or the couplings. For this reason it is a very relevant result. The absence of other background reduction attempts

³The emitted light-pulse is not absorbed by the material because its energy is lower than the characteristic gap: the excited electrons fill energy states created by the activators (the thallium), that are located between the valence and the conduction bands. Therefore the material is transparent to the light-pulse, that is detected.

4.1 Direct detection experiments

makes the constant signal ambiguous; however the annual modulation, acting as a rejection procedure itself, would contain the meaningful signal.

Results

- The DAMA/NaI was the first set-up for the dark matter annual modulation search. It was an 3×3 array of 9,70 kg of NaI(Tl) crystals with a total weight of ~ 100 kg. With this set-up the DAMA collaboration claimed the detection of an annual modulation after a 14 year observation, with a total exposure of $1.33 \text{ ton} \times \text{yr}$ (the longest and most massive continuous exposure among the direct detection experiments)[81, 82]. They attributed this modulation of the rate, with 6.3σ C.L.(Confidence Level), to the annual modulation of the relative dark matter velocities, as described in the previous chapter.
- The new generation set-up is the DAMA/LIBRA (Large sodium Iodide Bulk for Rare Processes) experiment, that has increases the number of crystals from nine to 25. The total weight is now of ~ 250 kg. Still after this upgrade they confirm the annual modulation observation over 7 years of observation, now with 9.3σ C.L [82].

The energy distribution of the counting rate per day \times kg \times keV $_{ee}$ resulting from a $0.53\text{ton}\times\text{day}$ exposure of the DAMA/LIBRA apparatus is [78]:

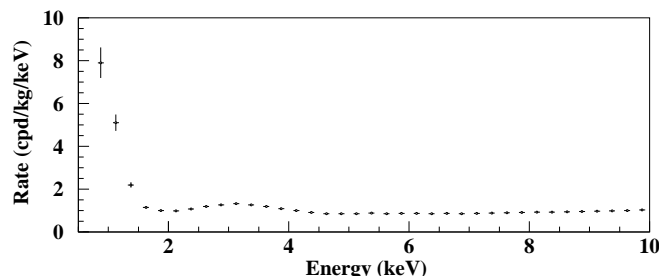


Fig. 4.1.1: Single-hit variation of the counting rate per day \times kg as a function of the deposited energy after a $0.53\text{ton}\times\text{day}$ exposure of the DAMA/LIBRA apparatus. The counting rate has a peak around 3keV_{ee} [78]

The keV axis is somehow misleading, because, as reported in all the DAMA publications, keV stay for keV $_{ee}$, that is the energy that would be detected if the incoming particle was an electron. The proportionality factor between keV and keV $_{ee}$ is the quenching factor Q_f , that is typical of the detector and depends on energy. In the 2-20keV region, DAMA provides quenching factors of (0.30 ± 0.01) and (0.09 ± 0.01) respectively for Na and I. From the graph, the DAMA counting rate as a function of the energy released by the possible interactions, is increasing under $\sim 1.5 \text{ keV}_{ee}$ (that divided for the quenching factor is equivalent to 5keV for Na and 16.6keV for I), has a small peak, i.e. an excess of counts, between 2-4 keV $_{ee}$ ($\simeq 6.6 - 13.3\text{keV}$ for Na and $\simeq 22 - 44\text{keV}$ for I) and above 4 keV $_{ee}$ ($\simeq 13.3\text{keV}$ for Na and $\simeq 44\text{keV}$ for I) is quite constant. Since the constant counting rate is $\simeq 1$ and the peak (red on

4.1 Direct detection experiments

the graph) is roughly between $(1 - 1.5)\text{cpd/kg/keV}_{ee}$, the peak emerges from the background of $(0 - 0.5)\text{cpd/kg/keV}_{ee}$.

The DAMA collaboration publishes only the residuals of the annual modulation as a function of the days, i.e. the term $S_m(E)\cos\omega(t-t_0)$ of eq. (3.26). The residual annual modulation integrated in three different energy intervals is:

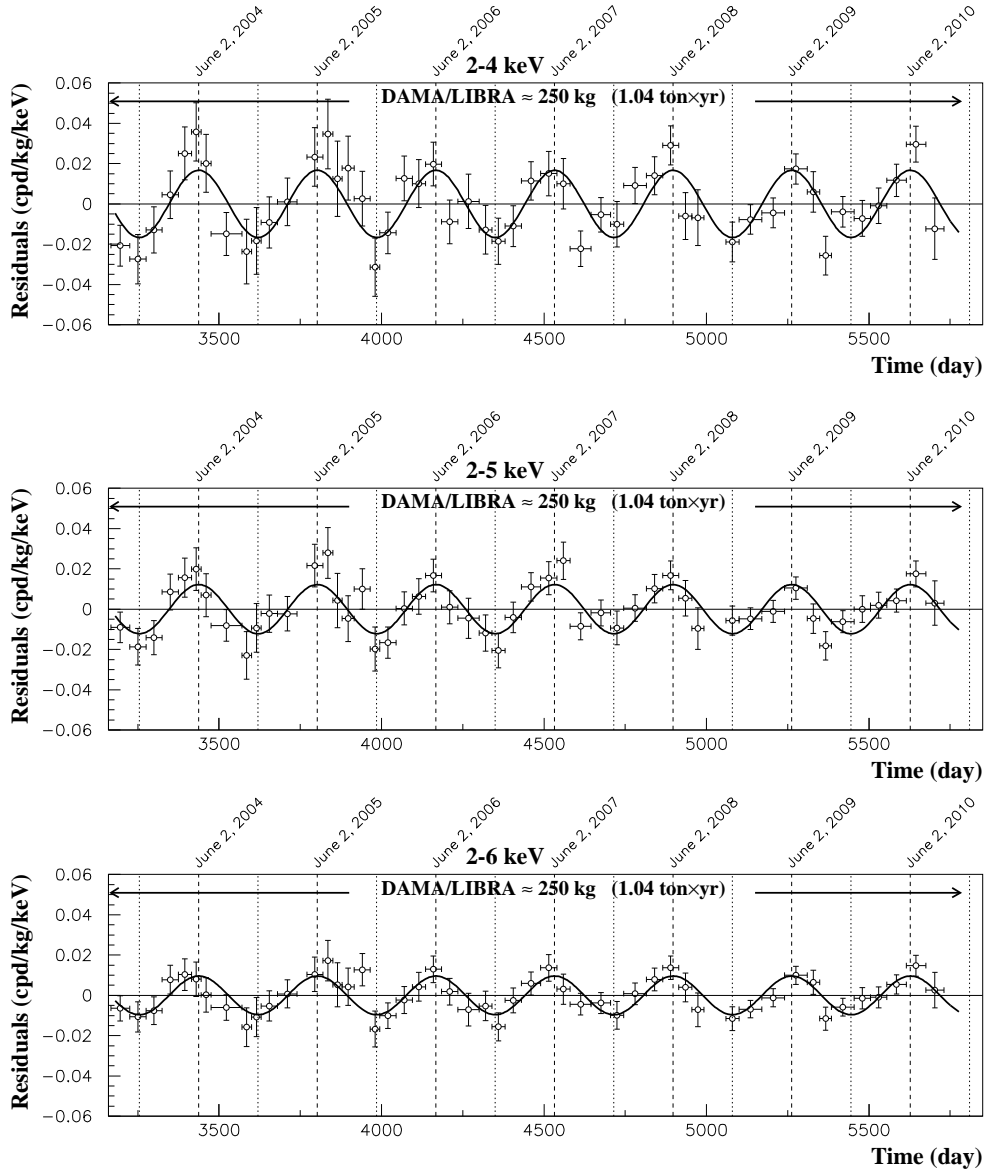


Fig. 4.1.2: The residual annual modulation integrated in three different energy intervals: from the top (i) $2 - 4\text{keV}_{ee}$, (ii) $2 - 5\text{keV}_{ee}$ and (iii) $2 - 6\text{keV}_{ee}$, for a total exposure of $1.33\text{ton}\times\text{yr}$ [83].

After the data analysis the DAMA collaboration conclusion is that the annual modulation is present only in the $2 - 6\text{keV}_{ee}$ energy range, with an amplitude $A = (0.0112 \pm 0.0012)\text{count/day/kg/keV}_{ee}$ with $(9.3\sigma\text{CL})$.

4.2 Indirect detection experiments

The indirect search focuses on the detection of the WIMP annihilation products in standard model particles, that can be detected by telescopes on Earth or by satellites. Telescopes exploitable for the Dark Matter search are of two categories: neutrino telescopes and Imaging Air Cherenkov Telescope (IACT). In what follows we will discuss some experiments belonging to the three indirect detection typologies.

- **Neutrino observatories:** The dark matter search led by neutrino telescopes focuses on the detection of secondary neutrinos produced by dark matter annihilation or decay. More technically they search for the muons produced by the interaction of neutrinos within the detector or with the matter surrounding the detector. The muons are detected exploiting the Cherenkov effect, that is the radiation emission process, activated by the passage of a relativistic charged particle through a transparent medium at a velocity greater than that of light in the same matter.

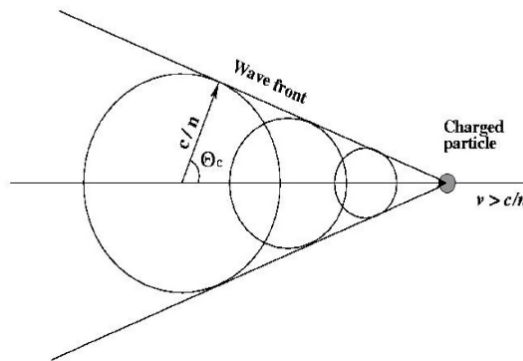


Fig. 4.2.1: The Cherenkov light emission cone.

The neutrino telescopes Ice-Cube and ANTARES (Astronomy with a Neutrino Telescope and Abyss environmental RESearch) use as radiator ice and water respectively, therefore the Cherenkov light is emitted only if the particle velocity v_p is greater than $\frac{c}{n}$ (about $0.76c$ in ice and $0.75c$ in water), where n is the ice or water refraction index. The Cherenkov light is detected in both the experiments by strings of Digital Optical Modules (DOMs), which are evacuated glass spheres, containing the photomultiplier tube to detect the Cherenkov radiation; the DOMs contain also the electronics that can begin to process the signals in place, before sending the data to the surface; this accelerates the data elaboration. The detectors are thought to reconstruct the direction of the incoming μ by fitting the space-time distribution of the detected Cherenkov photons.

- **Imaging Air Cherenkov Telescope (IACT):** MAGIC (Major Atmospheric Gamma Imaging Cherenkov), VERITAS (Very Energetic Radiation Imaging Telescope Array System), HESS (High Energy Stereoscopic System), CTA

4.2 Indirect detection experiments

(Cherenkov Telescope Array) are all ground based telescopes, devoted to the search of Very High Energy (VHE) γ -rays⁽⁴⁾. The interaction of the latter with the atmosphere produces showers of charged particles, whose propagation within the air particles produces the Cherenkov radiation cone detected by the IACTs. The air refraction index is $n = 1.00029$, therefore charged particles with velocity $v > c/n$ can produce Cherenkov radiation. IACT are consolidated as useful tool for the γ -ray astronomy and hence for the dark matter search. As shown in eq. (3.40), γ -ray telescopes cannot connect the signal to a specific point, for instance the Galactic center, because many other sources can be present on the line of sight. However the IACTs can probe the possible signature from the galactic halo, from galaxies nearby or from dwarf spheroidal galaxies, that are the most dominated dark matter objects. So far any γ -signal attributable to dark matter has been detected.

- **Space telescopes:** The favoured position allows the detection of primary cosmic rays. The Fermi satellite (GLAST Gamma-ray Large Area Space Telescope) focuses on the primary γ -ray detection, while for example PAMELA (Payload for Antimatter Matter Exploration and Light-nuclei Astrophysics) or AMS (Alpha Magnetic Spectrometer) detects high energy charged cosmic rays. The expected dark matter signature is the enhancement of the fluxes of positrons, antiprotons or antideuterons, since their origin could be attributed to the dark matter annihilation or decay.

PAMELA published results on a positron excess at 10GeV [84][85], after confirmed also by AMS-02. This result was predicted some years before [86] and the proposed hypotheses for a dark matter interpretation were: (i) a dark matter particle with mass $> 10\text{TeV}$ ⁽⁵⁾ or (ii) a dark matter particle of $\sim 1\text{TeV}$ that annihilates or decays only in leptons. Both the hypotheses have not been excluded. The observation of a positron excess has been confirmed indirectly also by Fermi and HESS experiments⁽⁶⁾ [87].

Another signal that in the past years was hypothesized to be a dark matter signature, was the 511keV γ -ray line from the galactic center, detected by the ESA's INTEGRAL (The European Space Agency's INTERNATIONAL Gamma-Ray Astrophysics Laboratory) satellite. It was thought to be an e^+e^- -annihilation product, that would be connected to the dark matter annihilation in the galaxy center. This hypothesis was ruled out in 2009 [88] and its origin was attributed to other astrophysical sources.

A recent result (2014), provided by the ESA's XMM-Newton (X-ray Multi-Mirror Mission) spacecraft in a spectrum of 73 galaxies [89] and later confirmed by the NASA's CHANDRA X-ray observatory, was the X-ray line at 3.5keV. It is compatible with the hypothesis that a sterile neutrino could account as dark matter and this is one of the main arguments in its favour, as discussed in the dedicated section⁽⁷⁾.

⁴CTA is still in development phase.

⁵A larger WIMP mass could be in agreement with the null results at colliders.

⁶"Indirect" because these results are inferred from the analysis of the detected γ -ray fluxes.

⁷For a schematic but clear discussion refer to

<https://indico.cern.ch/event/325123/contributions/755829/attachments/630486/867688/PPTalks-JC.pdf>

4.3 Experimental results and comparison

The accidental equality between the admissible WIMP mass range and the collider accessible energy scale motivated the WIMP experimental search. Numerous projects have been spending efforts for years in order to obtain some information on the WIMP parameters and further efforts are spent to compare the available results to improve the experimental search. In the light of the analysis realized in the previous chapter, in this section we will discuss the cross section limits as a function of the dark matter mass, for the WIMP paradigm. Firstly consider the $\sigma_{SI} - m_\chi$ plot in fig. (4.3.1).

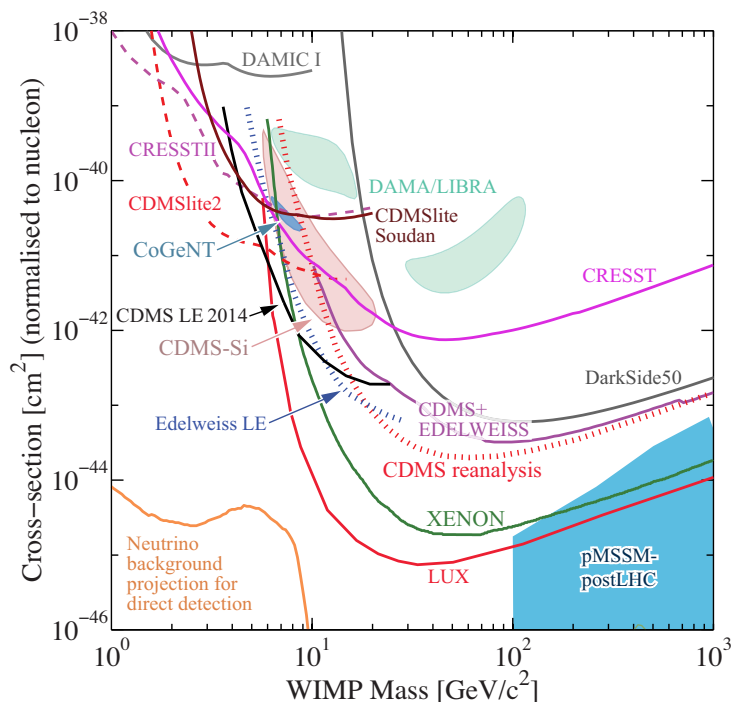


Fig.4.3.1: The σ_{SI} vs m_χ graph for the comparison between the available results. At lower incident dark matter masses the direct detection technique is less efficient due to the lower nuclear recoil energy. The best limit is provided by the LUX experiment[94]. The enclosed area refer to region of possible signal. The green region refers to DAMA annual modulation; the pink region refers to the three events claimed by CDMS-Si as possible dark matter signature; the blue region overlapping the CDMS-Si one refers to the CoGeNT excess. The results of the three experiments are compatible. The blue bottom region on the right refers to an ATLAS non-excluded region, relative to the pMSSM. Taken from [75].

The best limit is provided by LUX between ~ 6 GeV and 1 TeV, with a minimum at about $\sigma_{SI} \sim 10^{-45}$ cm² and $m_\chi \sim 30$ GeV. Towards lighter masses all the direct detection experiments provide less stringent constraints due to their lower sensitivity for lower recoil energy. The coloured enclosed DAMA[90], CDMS-Si[91] and CoGeNT[92] areas are the parameter regions allowed by the three experiments. The blue region, indicated with ATLAS, is a non-excluded region studied by the ATLAS collaboration and referred only to a minimal SUSY model, the phenomenological MSSM, that reduces the MSSM parameters from more than 100 to 19. The ATLAS collaboration affirms that $\sigma_{SI} \sim 10^{-46}$ cm² and $m_\chi \sim 500$ GeV is the favored region

4.3 Experimental results and comparison

[93].

Consider now the $\sigma_{SD} - m_\chi$ plot in fig. (4.3.2).

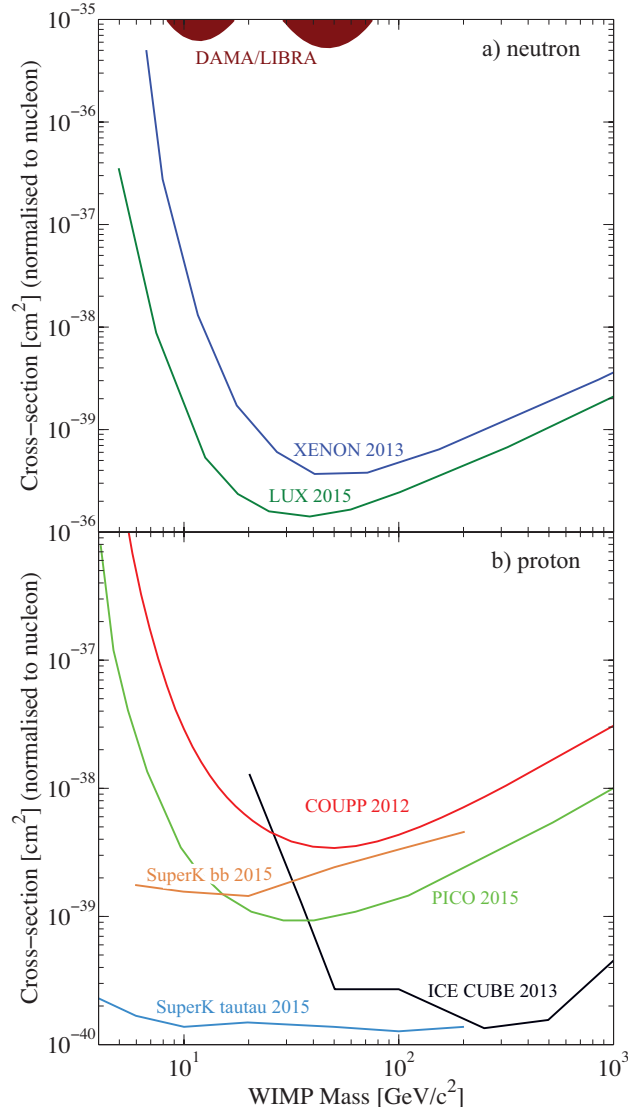


Fig. 4.3.2: The σ_{SD} vs m_χ graph for the comparison between the available results. The Ice-Cube experiment provides the best exclusion limit for $m_\chi \gtrsim 200$ GeV, while Super-Kamiokande provides the best exclusion limit for $m_\chi \lesssim 200$ GeV. Taken from [75].

The two graphs refer to the WIMP spin interaction with neutron or proton. The strongest exclusion limits are provided again by LUX for the WIMP interaction with neutrons and by the Ice-Cube experiment for $m_\chi \gtrsim 200$ GeV and by Super-Kamiokande for $m_\chi \lesssim 200$ GeV for the WIMP interaction with protons⁽⁸⁾.

⁸The observables of the indirect detection technique are the fluxes of primary or secondary particles produced by the dark matter annihilation or decay; starting from the results on fluxes, the upper limit on the cross section off nuclei can be inferred exploiting the physics of the capture process.

4.3 Experimental results and comparison

The collider results, fig. (4.3.3), provided the lowest limit for dark matter masses $m_\chi < 6\text{GeV}$ for the spin independent cross section and the lowest limit in the the whole mass range for the spin-dependent cross section. A comparison between the dark matter search at collider at 13 TeV and the direct detection results is shown in fig. (4.3.3) for the spin-dependent and spin-independent cross sections[95].

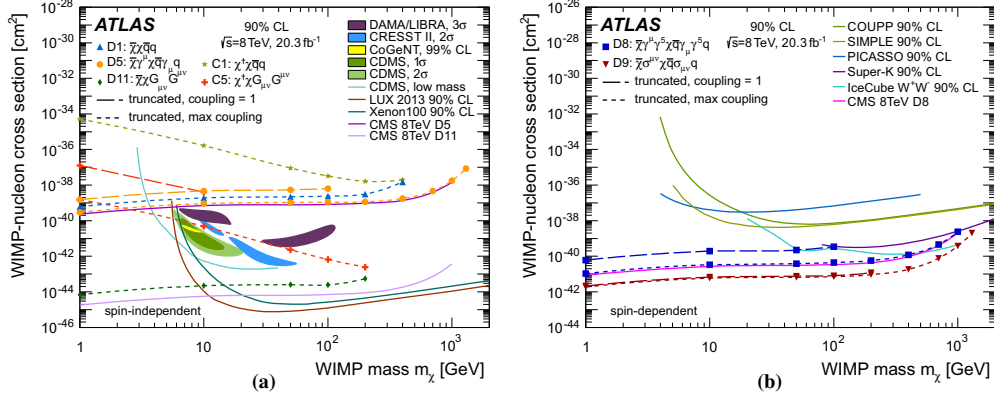


Fig. 4.3.3: In the left panel the σ_{SI} vs m_χ graph for the comparison between the direct detection results and the search at collider. Note that for $m_\chi < 4\text{ GeV}$ the search at collider fixes the lowest upper limit. In the right panel the σ_{SD} vs m_χ plot. The colliders impose the lowest upper limit for the whole mass range.

Taken from [95].

The indirect detection experiments can impose limits on the thermally averaged annihilation cross section times the relative velocity $\langle \sigma \cdot v \rangle$ as a function of the WIMP mass. Since space telescope and IACT experiments observe the products of annihilation or decay of diffuse dark matter and not of dark matter captured in the centre of celestial objects, there is not a connection with WIMP nuclear cross section. This is the reason of the absence of nuclear cross section plots for IACTs experiments or for space telescopes. The plot in fig. (4.3.4) is provided by the Ice-Cube Collaboration⁽⁹⁾.

⁹Fig. (4.3.4) taken from <https://sciencesprings.wordpress.com/2016/06/03/from-icecube-searching-for-dark-matter-using-icecube-cascades/>

4.3 Experimental results and comparison

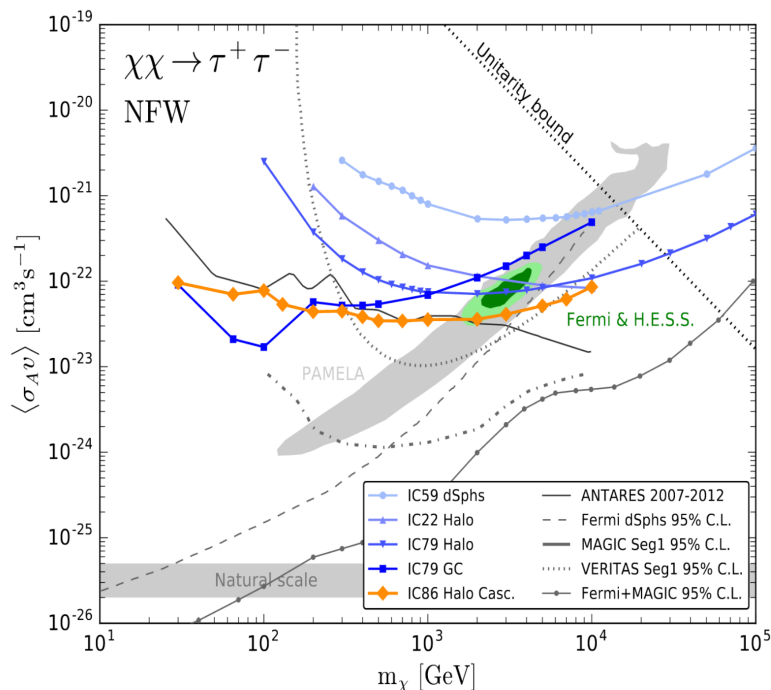


Fig. 4.3.4: The $\langle\sigma v\rangle$ vs m_χ graph for the comparison between the available upper limits. The cross section refers to the channel $\tau^+\tau^-$ and to the Navarro, Frank and White (NFW) density profile.

The figure shows the results/sensitivities in the plane $\langle\sigma v\rangle$ vs m_χ , allowing the comparison between neutrino telescope, IACT and satellite results. The grey region is the parameter space compatible with the PAMELA positron excess while the green region indicates the parameter space that is compatible with the Fermi and HESS indirect results on the positron excess. Clearly the combination of the Fermi and MAGIC results imposes the best upper limit.

From the variety of results illustrated so far, the experimental quest for dark matter, relative to the electroweak mass range, can be splitted in two parts: the search for a low WIMP mass, of the order of 10GeV and the search for a large WIMP mass, of order $\gtrsim 100\text{GeV}$. At this time the latter is the range of interest for the indirect search. The direct detection experiments, together with collider, can probe also the low WIMP mass region and the hints for a positive signal stimulates the arising of more and more projects that aim to verify or exclude these results. The collaboration between direct and indirect search is stricter when the results from the indirect search are provided by neutrino telescopes, due to the theory of the WIMP capture. This latter allows to extrapolate limits on the nuclear cross section from the results on WIMP annihilation, as discussed in section §3.3.2. The competitive results obtained by telescope experiments, both in space and on Earth, for large WIMP masses are impressive, therefore the observation of neutrinos, γ -rays and cosmic rays appears to be a fundamental tool for the dark matter search, despite the difficulty encountered in the comparison of the results. Note that in fig.(4.3.2) the neutrino telescope results refer only to spin-dependent cross section.

4.3 Experimental results and comparison

This is a further complication, since the theory of axial-vector interactions is affected by more unknown parameters than that of scalar couplings. The latter are the most convenient in theoretical simulation, since the dependency on unknown parameters can be handled more easily; that is why the cross section plots for direct detection experiments refer to spin-independent cross section. However this trick is not enough to achieve a reliable comparison among their results. Several assumptions are involved in the extrapolation of the data presented, relative for example to the halo velocity distribution, the mean halo velocity and the local density, beyond the difficulty introduced by the different targets characteristics and the different statistics procedures that affect the outcome and invalidate the comparison. For this reason the so called *exclusion limits* are not definitive constraints and the potential excluded regions of parameter space are still subject to be studied, especially that suggesting a positive signal.

Chapter 5

Numerical Results

As remarked in the previous chapter, the comparison between direct detection experiments and also between direct and/OR indirect detection experiments, is complicated due to the many parameters involved. This last section is dedicated to the numerical analysis of some of these parameters that are crucial for the comparison between direct detection experiments, in order to clarify the ingredients (energy threshold, cross section, nuclear form factor calculation, sensitivities . . .) that are relevant for the evaluation of the results. Since the parameters involved depends on the different targets, in particular on the target mass, the study of their contribution is necessary in order to allow the comparison between the results. We will clarify the experimental limits on the detectable recoil energies and on the probable dark matter masses (section 5.1); the expected counting rate in the most exploited targets, firstly independently on cross section and form factors and secondly discussing the two contributions (section 5.2). We will introduce also a discussion on the WIMP inelastic scattering off nuclei, to fix bounds on the probable dark matter masses (section 5.3). Finally we briefly discuss the section on the neutrino telescope sensitivity for the dark matter indirect search (section 5.4). In the two last sections there are hints about possible future extension of this work, in particular towards the scope to extend this numerical study to the other candidates discussed in deep in previous chapters and to the direct-indirect detection comparison.

5.1 Numerical limits on elastic scattering off nuclei

The direct detection signal produced by the dark matter elastic scattering off nuclei is proportional to the nuclear recoil energy. The recoil transmitted to the nuclei depends on: the bullet mass, the bullet velocity, the target mass and the diffusion angle. This latter is a kinematics factor, while the other terms depends on the dark matter nature and on the target choice. Let us see what are the detection limits as a function of the several parameters.

In the center of mass of the reaction the recoil energy E_R due to the elastic scattering between a dark matter particle of mass m_D and a target nucleus of mass

5.1 Numerical limits on elastic scattering off nuclei

m_T is⁽¹⁾:

$$E_R = E \cdot r \frac{(1 - \cos\theta)}{2} \quad (5.1)$$

where $E = \frac{p_D^2}{2m_D}$ is the incoming dark matter energy, $r = \frac{4m_D m_T}{(m_D + m_T)^2}$, with $0 < r \leq 1$, and θ is the center of mass diffusion angle. The maximum recoil energy as a function of θ and for fixed m_T and m_D is:

$$E_{Rmax} = E \cdot r = \frac{2m_D^2 m_T}{(m_D + m_T)^2} v^2 \quad (5.2)$$

where v is the dark matter velocity. Starting from eq. (5.2), the behaviour of the recoil energy as a function of dark matter masses in the electroweak mass range, for five different targets and for a dark matter velocity $v \equiv v_0 = 220\text{km/s}$, is shown in fig. (5.1.1).

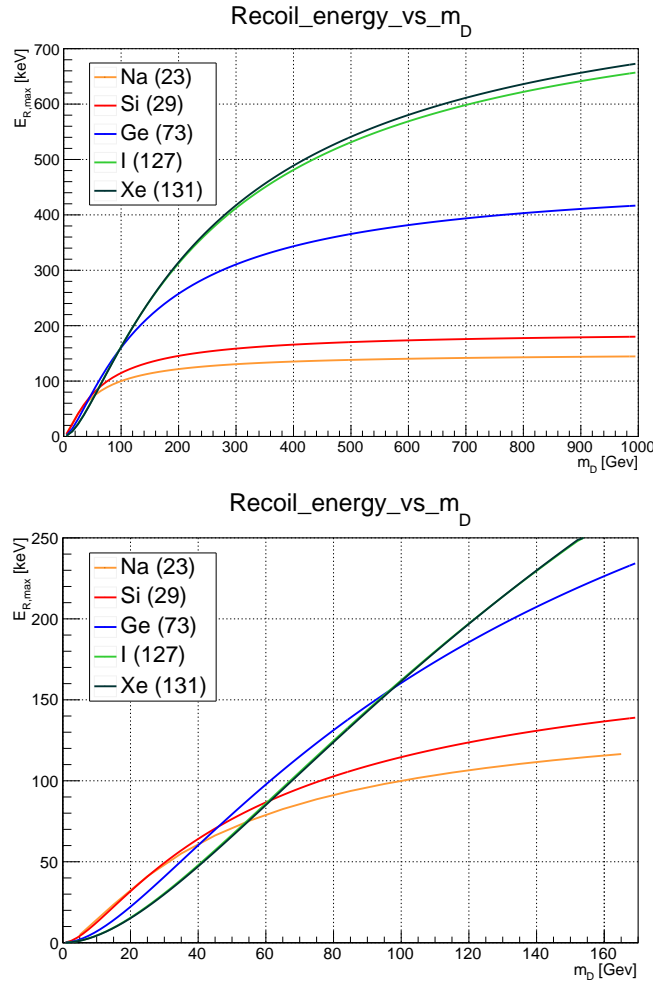


Fig.5.1.1: The maximum recoil energy as a function of a the dark matter mass for different targets. The recoil energy trend is increasing with m_D . For large m_D the maximum recoil energy is greater for heavier targets, while for small m_D the recoil energy is greater for lighter targets. This implies that the recoil energy is maximized for a target mass closer to the dark matter one. In the bottom graph is shown the mass range 0 – 160GeV

¹For the calculus details see the Appendix A.3.1

5.1 Numerical limits on elastic scattering off nuclei

For $m_D < m_T$ the increasing trend with the possible dark matter mass is faster than that for $m_D > m_T$. Furthermore the plot in the bottom of fig. (5.1.1), that is zoomed in the mass range 0 – 160GeV, shows that for smaller dark matter masses the recoil energy is greater for lighter targets, while for larger dark matter masses is greater for heavier targets. This implies that for a fixed m_D , the closer m_T is to m_D , the greater is the recoil energy, as shown in fig. (5.1.2), where the maximum recoil energy is plotted as a function of the possible target masses and for three dark matter masses.

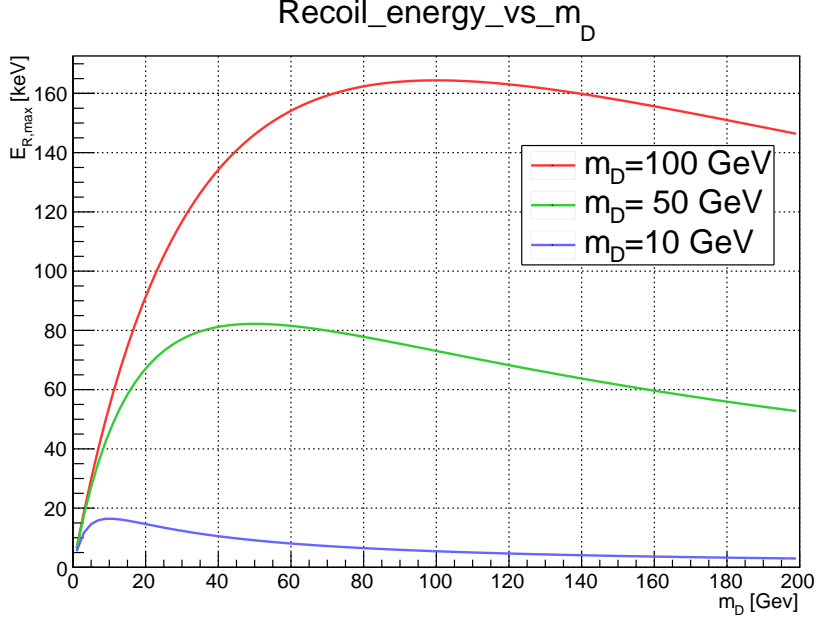


Fig.5.1.2: The maximum recoil energy as a function of the different targets for three dark matter masses. The point of maximum recoil energy is reached for $m_D \equiv m_T$.

If $m_T = m_D \rightarrow E_{Rmax} = E = \frac{1}{2}m_D v^2$. For $10\text{GeV} < m_D \equiv m_T < 1\text{TeV}$ and $v = v_{max} = v_{esc} \simeq \frac{5.44}{3}10^{-3}c$, the most promising recoil is in the range $16.4\text{keV} \lesssim E_{Rmax} \lesssim 1644\text{keV}$, while the minimum recoil energy is fixed by the energy threshold of the detector. These energy recoil ranges can be useful for the target choice if the interest is in a specific dark matter mass.

For a fixed target, that is the situation usually encountered for already active experiments, can be interesting to understand what is the lowest detectable dark matter mass, always exploiting the recoil signal as dark matter signature. Consider the expression of the maximum recoil E_{Rmax} in eq. (5.2). In the most optimistic kinematics, the lowest dark matter mass can be computed through the expression:

$$m_D(\text{GeV}) = \frac{\frac{E_{th}}{[\text{keV}]} \frac{m_T}{[\text{GeV}]} + \frac{m_T}{[\text{GeV}]} \sqrt{2 \frac{m_T}{[\text{GeV}]} \frac{E_{th}}{[\text{keV}]}}}{\left(2 \frac{m_T}{[\text{GeV}]} - \frac{E_{th}}{[\text{keV}]}\right)} \quad (5.3)$$

where m_T is in GeV and E_{th} is in keV. For example for a detector similar to DAMA, with Na as target and with an energy threshold of $E_{th} = 6.7\text{keV}$ ⁽²⁾, the

²Here the energy is in keV. Usually in literature the direct detection energy threshold is given in

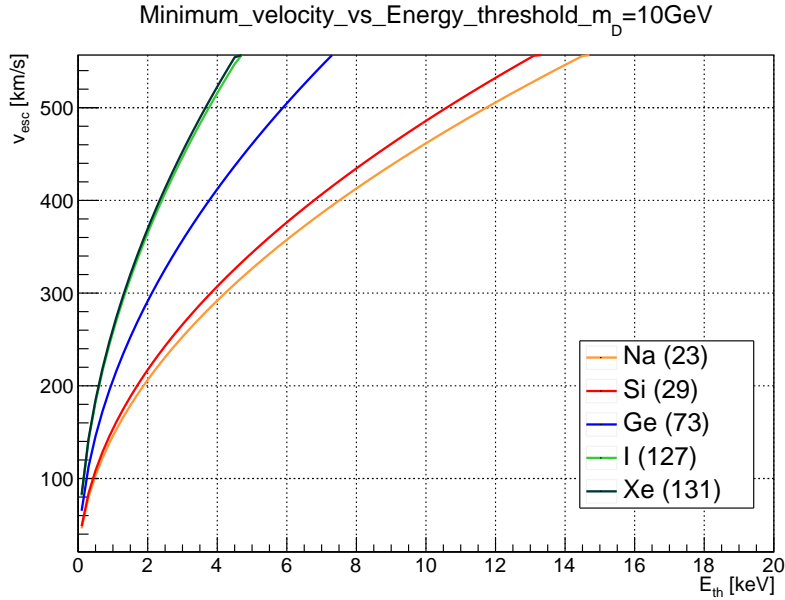
5.1 Numerical limits on elastic scattering off nuclei

lowest probable dark matter mass is $m_D \simeq 14.2\text{GeV}$. So far we have considered $v = 10^{-3}c$. Indeed v can be also $v > v_0$, since $v_{max} = v_{esc} = 544\text{kms}^{-1} \approx \frac{5.44}{3} \cdot 10^{-3}c$. To take into account a different velocity it will be sufficient to divide E_{th} for the adimensional factor $a = \left(\frac{v \cdot 10^3}{c}\right)^2$ in eq. (5.3). For the maximum velocity the a factor will be $a = \left(\frac{5.44}{3}\right)^2$ and the previous estimates will be $m_D > 6.1\text{GeV}$.

Finally, for fixed energy threshold (i.e. for a fixed target) and for a fixed dark matter mass, there is a minimum detectable velocity associated to the incoming dark matter particle:

$$v_{min} = \sqrt{\frac{2E_{th}(\text{keV})}{m_D(\text{GeV})r}} 10^{-3}c \quad (5.4)$$

For example for the sodium target, with $m_T = 23\text{GeV}$, an energy threshold of 6.7keV and $m_D = 10\text{GeV}$ the minimum detectable incoming velocity would be $v_{min} = 1.26 \cdot 10^{-3}c = 378\text{km/s}$. The minimum detectable incoming velocity as a function of the possible dark matter masses can be computed for a fixed energy threshold and different targets or for a fixed target and different energy threshold. The two cases are plotted in fig. (5.1.3). An upper limit on the possible energy threshold can be fixed for the case of $m_D = 10\text{GeV}$ considering that there is a maximum possible velocity, that is the escape velocity $v_{esc} \simeq 544\text{km/s}$. This upper limit implies that for too much high energy threshold the detector are not sensitive to the dark matter particle. For the dark matter mass of 100GeV the minimum velocities are lower than that relative to lighter dark matter masses, as expected according to the kinematics.



keV_{ee} , though it is written in keV, where as said before a keV_{ee} is the amount of energy produced by an electron recoil, with an equivalent nuclear energy recoil. This means for example that the DAMA energy threshold of 2keV is indeed $2keV_{ee}$. Therefore $\sim 2keV_{ee}/Q_{f,Na} \sim 6.7\text{keV}$ for Na and $\sim 2keV_{ee}/Q_{f,I} \sim 22\text{keV}$ for I, where $Q_{f,Na} = 0.3$ for $6.5 < E_R < 97\text{keV}$ and $Q_{f,I} = 0.09$ for $22 < E_R < 330\text{keV}$. For this reason we consider $E_{th,Na} = 6.7\text{keV}$.

5.2 Direct detection event rate in different targets

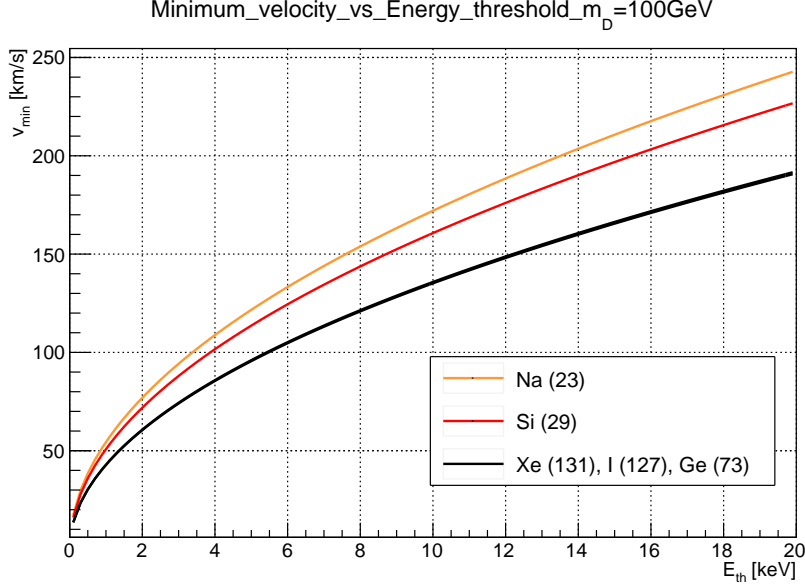


Fig.5.1.3: The minimum detectable incoming velocity as a function of the energy threshold, for a dark matter mass of 10GeV on the top and of 100GeV on the bottom, for five different targets ($^{131}_{54}\text{Xe}$, $^{127}_{53}\text{I}$, $^{73}_{32}\text{Ge}$, $^{29}_{14}\text{Si}$, $^{23}_{11}\text{Na}$).

5.2 Direct detection event rate in different targets

Due to the weakness of the interactions that should couple the dark matter with the ordinary matter, the scattering processes expected in direct detection experiments are rare events and their detection is a challenge for the experimental search. The simulation of the expected signal is in this case a still more fundamental step that allows an careful interpretation of the experimental data, in particular in the optic of a comparison among the results. For this reason in what follows we will study the behaviour of the differential rate as function of the recoil energy detected, in different targets and for several possible dark matter masses in the electroweak range.

The curves in fig. (5.2.1) are the differential rate as a function of the recoil energy for five different targets ($^{131}_{54}\text{Xe}$, $^{127}_{53}\text{I}$, $^{73}_{32}\text{Ge}$, $^{29}_{14}\text{Si}$, $^{23}_{11}\text{Na}$), for a dark matter mass of 100GeV and for a form factor $F(|q|) = 1$ ⁽³⁾. The plotted differential rate is independent from the velocity-independent part of the cross section thanks to the ratio with the factor $R_0/(E_0 r)$, where R_0 , E_0 and r are the terms discussed in the section §3.2.2 and in the previous section §5.1.1. We will name it *rescaled*-differential rate. The multiplication for this term is commonly used to make the results independent from the part of WIMP-target cross section that depends on quark or spin

³The integration of the counting rate involves the form factor due to the transferred momentum dependency on the recoil energy. As discussed later in the text the relation is:

$$q(fm^{-1}) = \sqrt{\frac{2m_T(\text{GeV})E_R(\text{keV})10^{-6}}{0.197\text{GeVfm}}} = \sqrt{(2m_T) \left(\frac{1}{2}m_D v_D^2\right) r} = 2\mu(\text{GeV})v_D(\text{cm/s}) \cdot \frac{0.806}{c} \quad (5.5)$$

Each point of the curve is obtained by integrating on all the possible velocities that can cause the same recoil energy.

5.2 Direct detection event rate in different targets

couplings.

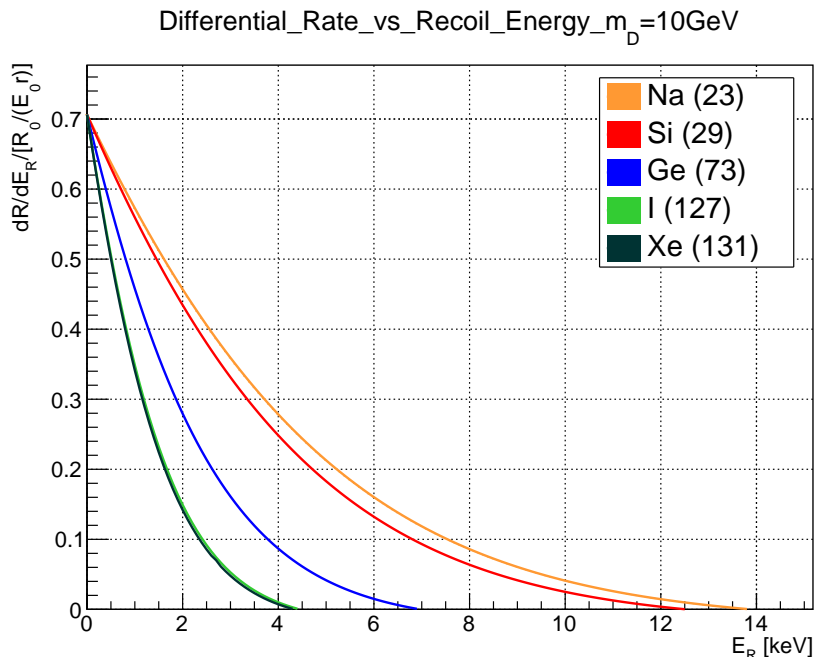


Fig.5.2.1: The scaled differential rate as a function of the recoil energy, for a dark matter masses of 10GeV for five different targets (^{131}Xe , ^{127}I , ^{73}Ge , ^{29}Si , ^{23}Na) and for a form factor $F(|q|) \equiv 1$. The rate is greater for lighter targets for the whole recoil energy range. The division for the factor $R_0/(E_0 r)$ cancels the dependency of the differential rate from the cross section.

The typical form of the differential rate dependency on the recoil energy is[66]:

$$\frac{dR}{dE_R} = \frac{R_0}{E_0 r} e^{-E_R/E_0 r} \quad (5.6)$$

in agreement with the differential rate in fig. (5.2.1). Each point of such differential rate is obtained from the numerical integration of the analytic expression⁽⁴⁾:

$$\begin{aligned} \frac{dR}{dE_R} &= \frac{R_0}{E_0 r} \frac{k_0}{k} \frac{1}{2\pi v_0^2} \int_{v_{min}}^{v_{max}} \frac{1}{v} f(v, v_E) d^3v = \\ &= \frac{R_0}{E_0 r} \frac{k_0}{k} \frac{1}{2v_E} \int_{v_{min}}^{v_{max}} [e^{(v-v_E)^2/v_0^2} - e^{(v+v_E)^2/v_0^2}] dv \quad (5.7) \end{aligned}$$

inferred by the manipulation of eq. (3.9) of [66], together with its appendix A. v_{min} in this case is not the minimum velocity detectable by the detector; it is the minimum velocity that can cause the recoil energy E_R considered.

The differential rate for a fixed dark matter mass of 100GeV is plotted in fig. (5.2.2).

⁴Indeed, as said before, the plot in fig. (5.2.1) and (5.2.2) are the differential rate in eq. (5.7) over the factor $\frac{R_0}{E_0 r}$.

5.2 Direct detection event rate in different targets

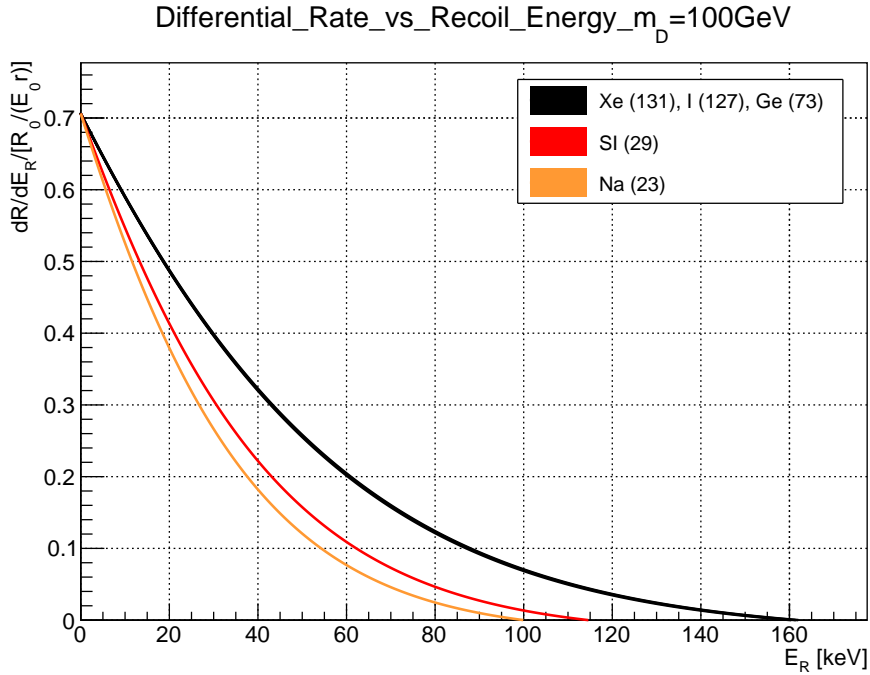


Fig.5.2.2: The differential rate as a function of the recoil energy, for a dark matter mass of 100GeV for five different targets ($^{131}_{54}\text{Xe}$, $^{127}_{53}\text{I}$, $^{73}_{32}\text{Ge}$, $^{29}_{14}\text{Si}$, $^{23}_{11}\text{Na}$) and for a form factor $F(|q|) \equiv 1$. The rate is greater for heavier targets for the whole recoil energy range. The division for the factor $R_0/(E_0 r)$ cancels the dependency on the cross section.

Note that for a dark matter mass of 10GeV the scaled-differential rate for a unit of mass detector is greater for lighter targets, while for a dark matter mass of 100GeV the order is inverted. However, as we will show below, this is due to the multiplicative factor $R_0/E_0 r$, therefore it is not related to a physical effect. Furthermore observe that the recoil energy range for heavier dark matter masses ($[0 - 160]\text{GeV}$ for $m_D = 100\text{GeV}$) is much greater than that of lighter dark matter masses ($[0 - 14]\text{GeV}$ for $m_D = 10\text{GeV}$), as expected from the limits on the maximum recoil energy computed in the previous section, where $E_{R,max} = Er = \left(\frac{1}{2}m_D v^2\right) r$, that is proportional to m_D .

5.2.1 Differential rate for scalar couplings

So far we have not made assumption on the cross section thanks to the scaling with the factor $R_0/(E_0 r)$ discussed above. However this trick does not allow to estimate the order of magnitude of the differential rate. In order to obtain this information let us consider the spin-independent cross section discussed in the section §3.2.3. The cross section is different changing the targets because of the factor $[Zf_p + (A-Z)f_n]^2 \sim A^2 f^2$, where commonly the coefficients f_p and f_n are simplified as $f \equiv f_p \simeq f_n$. The value of σ is obviously unknown, therefore as a consequence its velocity independent part σ_0 is usually fixed arbitrarily. However if we consider $\sigma_0 = \sigma'_0 A^2$ and fix arbitrarily the order of magnitude of the factor σ'_0 (including the factor f), for example to the value $\sigma'_0 = 10^{-40}\text{cm}^2$, we can compute the differential rate considering the dependency on the squared target mass. The dependence of

5.2 Direct detection event rate in different targets

the non-scaled differential rate as a function of the recoil energy for different targets is shown in fig. (5.2.3), for two different dark matter mass, 10GeV and 100GeV and for a form factor $F(|q|) \equiv 1$.

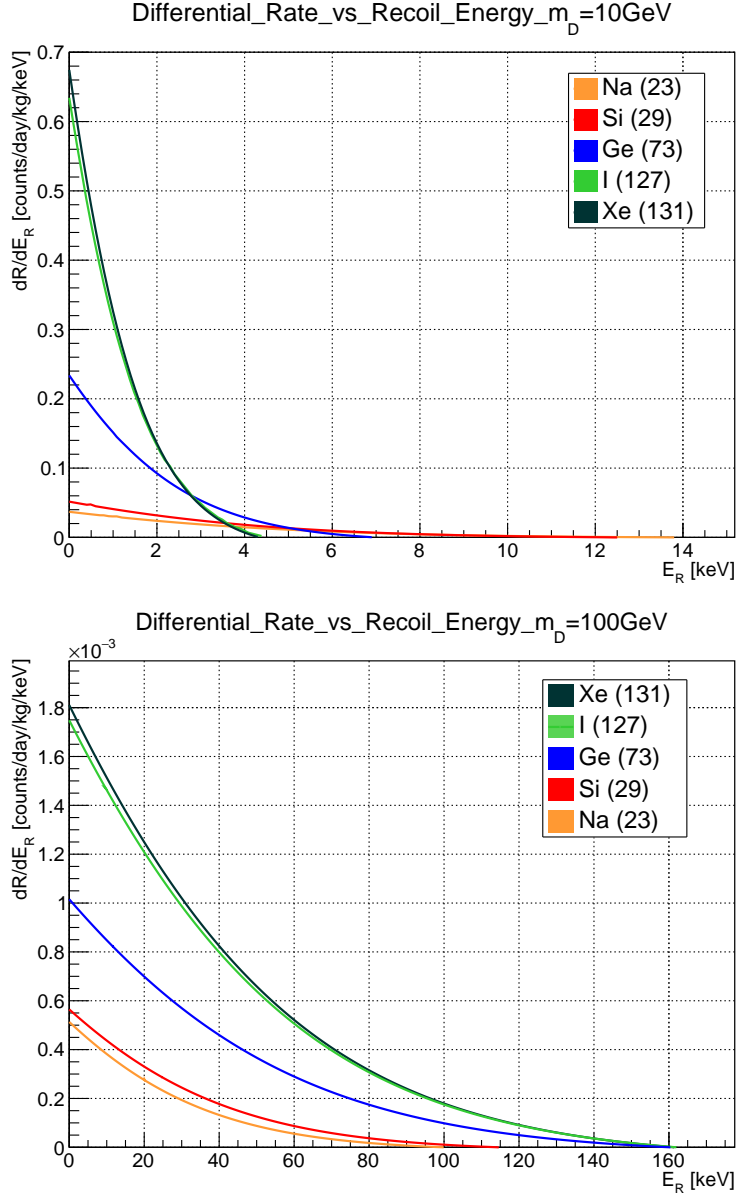


Fig.5.2.3: The non-scaled differential rate as a function of the recoil energy, for a dark matter mass of 10GeV on the top and of 100GeV on the bottom, for five different targets (^{131}Xe , ^{127}I , ^{73}Ge , ^{29}Si , ^{23}Na), for a scalar couplings with $\sigma_0 = \sigma'_0 A^2$ ($\sigma'_0 = 10^{-40} \text{cm}^2$) and for a form factor $F(|q|) \equiv 1$.

Note that, as anticipated, the differential rate is greater for heavier targets for both the dark matter masses considered for the mostly part of the possible recoil energy. However an interesting behaviour present for the 10GeV dark matter mass is discussed in the next paragraph. To conclude this section instead let us evaluate the counting rate integrated over all the possible recoil energies. For each target we compute this total rate through the integration of the curves in fig. (5.2.3).

5.2 Direct detection event rate in different targets

The maximum and minimum recoil energy between which the integration is made are $E_{min} = 0\text{keV}$ and $E_{max} = E \cdot r$. The maximum recoil energy was derived in the previous section and depends on the different targets, while even if the energy threshold characteristic of each detector would shift the minimum recoil energy, here we consider the ideal case, that is $E_{th} \equiv E_{min} = 0$. The total counting rate per day \times kg [cpd/kg] is summarized in table (5.1), for $m_D = 10\text{GeV}$ and $m_D = 100\text{GeV}$. The total rate obtained is exactly inversely proportional to the dark matter mass.

	Rate for $m_D = 10\text{GeV}$	Rate for $m_D = 100\text{GeV}$
$^{129}_{54}\text{Xe}$	0.815 [cpd/kg]	0.0815 [cpd/kg]
$^{127}_{53}\text{I}$	0.790 [cpd/kg]	0.0790 [cpd/kg]
$^{73}_{32}\text{Ge}$	0.454 [cpd/kg]	0.0454 [cpd/kg]
$^{29}_{14}\text{Si}$	0.180 [cpd/kg]	0.0180 [cpd/kg]
$^{23}_{11}\text{Na}$	0.143 [cpd/kg]	0.0143 [cpd/kg]

Table 5.1. Counting rate per day \times kg for five different targets, for $m_D = 10\text{GeV}$ and $m_D = 100\text{GeV}$. The computation is provided through the numerical integration explained in the text.

Considering for example the xenon isotope $^{129}_{54}\text{Xe}$, in 100kg the total rate per day is $\simeq 81$ for a fixed $m_D = 10\text{GeV}$ and $\simeq 8.1$ for $m_D = 100\text{GeV}$. This estimate is derived in the assumption of:

- maxwellian velocity distribution v , with mean value $v_0 = 244\text{km/s}$;
- scalar coupling, with $\sigma = \sigma'_0 A^2/v^2$ and σ'_0 arbitrarily fixed to 10^{-40}cm^2 ;
- local dark matter density $\rho = 0.4\text{GeV}/c^2/\text{cm}^3$;
- unitary form factor $F(|q|) \equiv 1$;
- ideal detectors, with unitary efficiency f .

The order of magnitude of this results is in agreement with eq. (3.10), when the opportune normalization is substituted. What we expect is that in reality the counting rate per day \times kg is lower due to the two suppression factors $F(|q|)$ and f .

A peculiar behaviour of the scalar coupling rate for 10GeV dark matter

The non rescaled differential rate computed for a fixed dark matter mass of 10GeV, shown in fig. (5.2.3), presents an interesting behaviour. Let us focus on the differential rate in the range [0-0.1] cpd/kg/keV. For a recoil energy $E_R \gtrsim 2.75\text{keV}$ for germanium and for a recoil energy $E_R \gtrsim 3.75\text{keV}$ for sodium and silicium, the counting rate per day \times kg \times keV becomes greater than that of the two heavier targets, that is for iodide and xenon.

5.2 Direct detection event rate in different targets

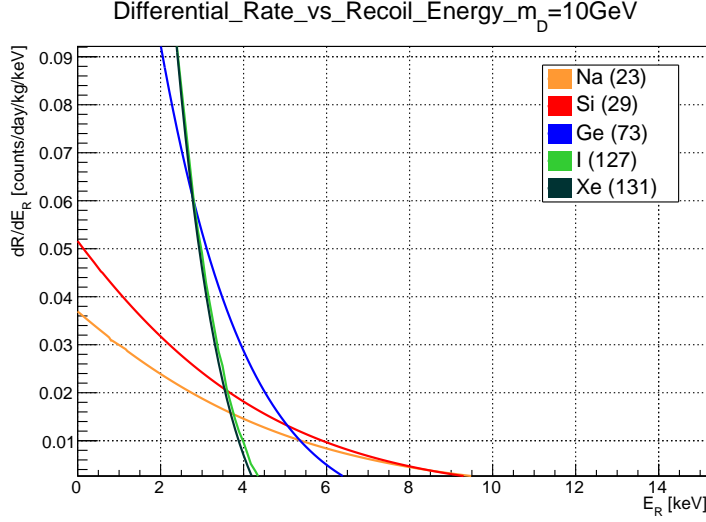


Fig. 5.2.4: The zoomed non-scaled differential rate as a function of the recoil energy in the range $[0-0.1]$ cpd/kg/keV, for a dark matter mass of 10GeV , for five different targets ($^{131}_{54}\text{Xe}$, $^{127}_{53}\text{I}$, $^{73}_{32}\text{Ge}$, $^{29}_{14}\text{Si}$, $^{23}_{11}\text{Na}$), for a scalar couplings with $\sigma_0 = \sigma'_0 A^2$ ($\sigma'_0 = 10^{-40}\text{cm}^2$) and for a form factor $F(|q|) = 1$.

This result could be in agreement with the panorama of the available experimental results. As discussed before, the DAMA collaboration detected, and is detecting, the expected annual modulation of the counting rate due to the Earth rotation velocity around the Sun. This behaviour is compatible with two WIMP mass regions. Here we are interested in the case of a light WIMP, therefore we focus on the hypothesis that the signal is due to a $\sim 10\text{GeV}$ WIMP. However at the same time other experiments discussed before, such as XENON and LUX, affirm that exclusion limits due to their null results, rule out this hypothesis. Nevertheless, with caution, CDMS-Si and CoGeNT published an excess of events, that if interpreted as the detection of a dark matter signal, is compatible with the DAMA results. In this framework our simulation would hint a reconciliation of the two different points of view. For instance the DAMA signature, detected at about 3keV_{ee} , that is at $\sim 10\text{keV}$ for $Q_{f,Na} = 0.3$, would be due to the scalar coupling of a 10GeV dark matter particle with the sodium nucleus; since at 10keV the xenon target counting rate is already null, the observation of a signal in DAMA and a null result in XENON could be not in a contradiction.

However we remark that these estimates are computed only for scalar couplings, for a form factor $F(|q|) = 1$ and for an ideal detector of efficiency $f = 1$. A deeper study of the counting rate requires the estimation of these contributions. A first effort in this sense is discussed below, relative to the analysis of the form factor contribution.

5.2.2 The form factor contribution to the differential rate

So far we have considered a form factor $F(|\mathbf{q}|) = 1$. The numerical integration at the basis of this discussion is elaborated in order to allow the introduction of the counting rate dependency on the transferred momentum. The form factor is a suppression term, more and more important as the transferred momentum (and

5.2 Direct detection event rate in different targets

therefore the recoil energy) is greater. Through this factor the size of the nucleus can be taken into account, since for high energies the nucleus internal structure is *accessible* to the incoming particle and as a consequence the nucleus cannot be approximated as point-like.

We will consider the limit of maximum suppression, i.e. of maximum recoil energy $E_R = E \cdot r$, where $E = \frac{1}{2}m_D v_D^2$ and $r = \frac{4m_D m_T}{(m_D + m_T)^2}$ ⁽⁵⁾.

Consider the form factor in eq. (3.24). The transferred momentum expressed in fm^{-1} is⁽⁶⁾:

$$\begin{aligned} q(fm^{-1}) &= \sqrt{\frac{2m_T(\text{GeV})E_R(\text{keV})10^{-6}}{0.197\text{GeVfm}}} = \\ &= \sqrt{(2m_T) \left(\frac{1}{2}m_D v_D^2\right) r} = 2\mu(\text{GeV})v_D(\text{cm/s}) \cdot \frac{0.806}{c} \end{aligned} \quad (5.10)$$

where μ is the reduced mass $\mu = \frac{m_D m_T}{(m_D + m_T)}$. The Helm form factor discussed in section §3.2.2 is plotted as a function of the transferred momentum in fig. (5.2.5), for a fixed dark matter mass of 100GeV.

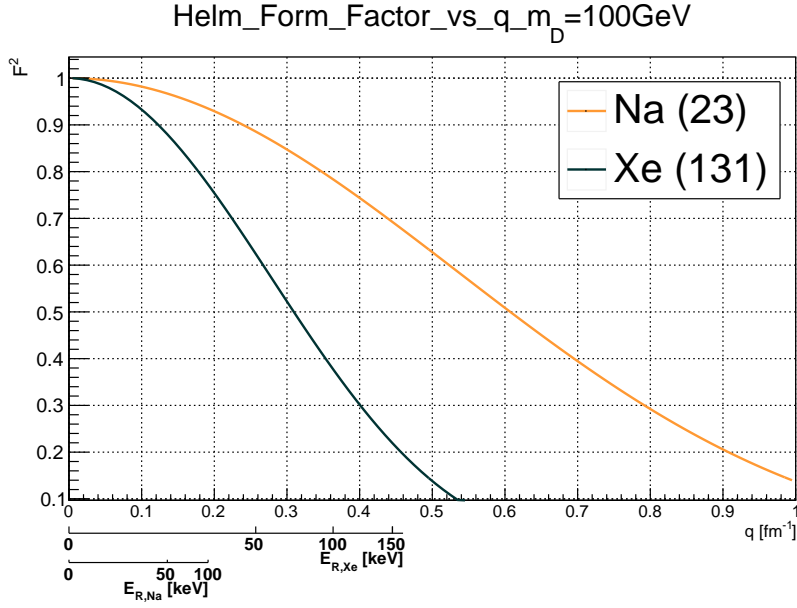


Fig. 5.2.5: The squared Helm form factor $F^2(|q|)$ for a transferred momentum in the range $[0 - 1]fm^{-1}$, for two targets ($^{131}_{54}\text{Xe}$ and $^{23}_{11}\text{Na}$). The two recoil energy scale relative to the two target refer to the case of a fixed dark matter mass of 100GeV.

The form factor relative to the other targets considered in previous sections are between the two curves plotted. The two recoil energy scales are associated to the

⁵This assumption allows also to cancel the dependency on θ , i.e. the diffusion angle in the center of mass.

⁶Since the conversion from Electronvolt (eV) to Hertz (s^{-1}) is:

$$1\text{eV} = 2.41804 \times 10^{14} s^{-1} \quad (5.8)$$

then:

$$1 \frac{\text{GeV}}{c} = 0.806 fm^{-1} \quad (5.9)$$

5.2 Direct detection event rate in different targets

two different targets for a fixed dark matter mass of 100GeV, obtained from eq. (5.10). This graph provides an important information about the value of the form factor at the recoil energies of interest. For xenon the maximum suppression due to the form factor is of the 80% for $E_R = 160\text{keV}$, while for the same maximum recoil energy the suppression is only of the $\sim 10\%$ for Na. The non-scaled differential counting rate in presence of the Helm form factor, for a dark matter mass of 100GeV and for the two targets of xenon and sodium is plotted in fig. (5.2.6).

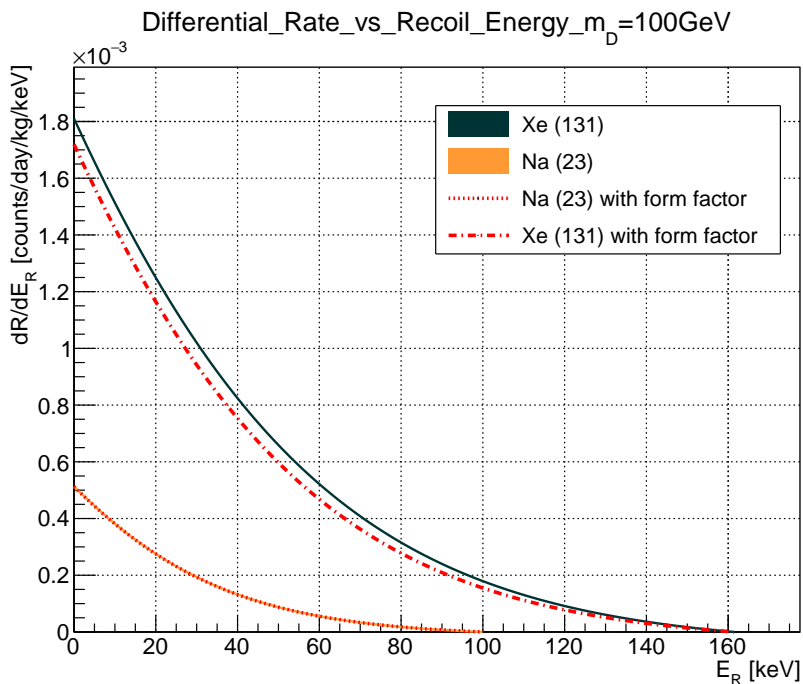


Fig. 5.2.6: The non-rescaled counting rate as a function of the recoil energy for two different targets ($^{131}_{54}\text{Xe}$ and $^{23}_{11}\text{Na}$), for a fixed dark matter mass of 100GeV. The dashed-dot line is referred to the differential counting rate including the Helm form factor.

As expected the form factor suppression is greater for xenon with respect to sodium, for which the counting rate with and without the form factor are indistinguishable on the graph.

Consider now a fixed dark matter mass of 10GeV, relevant for the observations discussed in the previous section.

5.2 Direct detection event rate in different targets

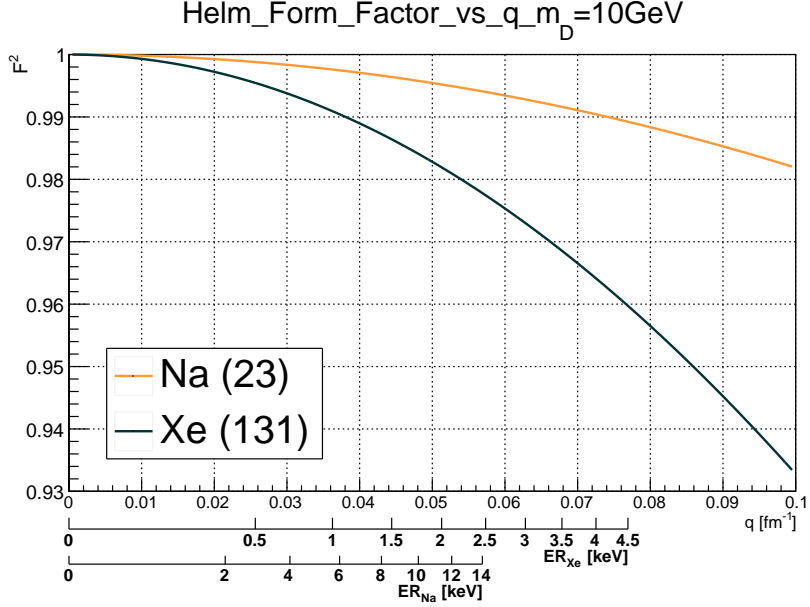


Fig. 5.2.7: The non-scaled counting rate as a function of the recoil energy for two different targets ($^{131}_{54}\text{Xe}$ and $^{23}_{11}\text{Na}$), for a fixed dark matter mass of 10GeV. The dashed-dot line is referred to the differential counting rate including the Helm form factor.

In fig. (5.2.7) the zoomed squared form factor as a function of the transferred momentum is shown. The two energy scales correspond to the recoil energy associated to the two targets, xenon and sodium, for a fixed dark matter mass of 10GeV, computed from the eq. (5.10). As evident, the form factor suppression is irrelevant for this dark matter mass scale. The maximum suppression due to the squared form factor is between $\sim 0.955 - 0.960$ for xenon and between $0 \sim 0.990 - 0.995$ for sodium. A further confirm comes from the comparison between the non-scaled differential counting rate for $m_D = 10\text{GeV}$, computed with and without the Helm form factor, shown in fig. (5.2.8).

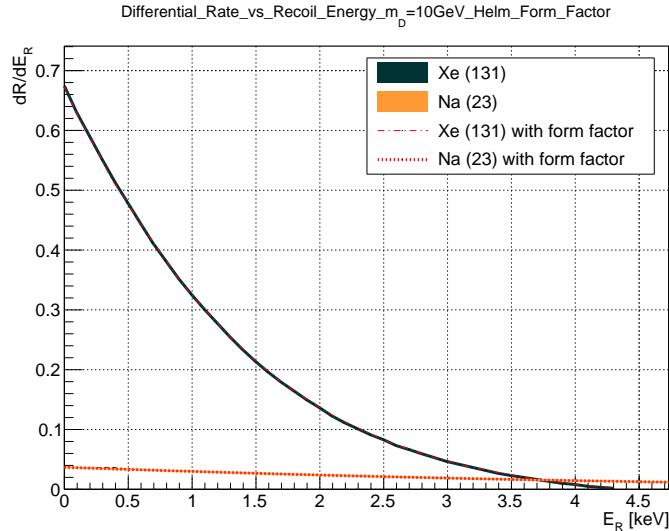


Fig. 5.2.8: The non-scaled counting rate as a function of the recoil energy for two different targets ($^{131}_{54}\text{Xe}$ and $^{23}_{11}\text{Na}$), for a fixed dark matter mass of 10GeV. The dashed-dot line is referred to the differential counting rate including the Helm form factor.

5.3 Numerical limits on inelastic scattering off nuclei

This result is important because allows to affirm that the peculiar behaviour observed in the differential counting rate for different targets and for a fixed dark matter mass of 10GeV, discussed in the previous section, is not influenced by the form factor contribution.

5.3 Numerical limits on inelastic scattering off nuclei

- *This section refers to [71]*

The aim of this section is to put limits on the detectability of lighter dark matter candidates through their inelastic scattering off nuclei. As discussed before, inelastic scattering can occur via atomic or nuclear excitation. Assuming the maximum halo velocity $v_H = v_{esc}$, the minimum probable dark matter mass for the excitation energy of each isotope can be computed through the condition:

$$m_D > \frac{2\Delta E}{|v_{esc} + v_E|^2 - \frac{2\Delta E}{m_T}} \quad (5.11)$$

In [14] only isotopes with nuclear excitation $\Delta E < 100\text{keV}$ are considered since for $\Delta E > 100\text{keV}$ inelastic scattering for WIMP lighter than 100GeV are suppressed by factors > 10 . These isotopes are odd protons-even neutrons or even neutrons-odd protons. In the following table are listed the excitation energies of the most popular isotopes of this kind:

	ΔE (keV)
$^{127}_{53}\text{I}$	37.1
$^{133}_{55}\text{Cs}$	81.0
$^{83}_{36}\text{Kr}$	9.4
$^{129}_{54}\text{Xe}$	39.6
$^{131}_{54}\text{Xe}$	80.2
$^{183}_{74}\text{W}$	46.5

Table 5.2. Excitation energy (ΔE) of the most exploited isotopes with $\Delta E < 100\text{keV}$. Taken from [71]

5.4 Numerical limits on neutrino telescope sensitivity

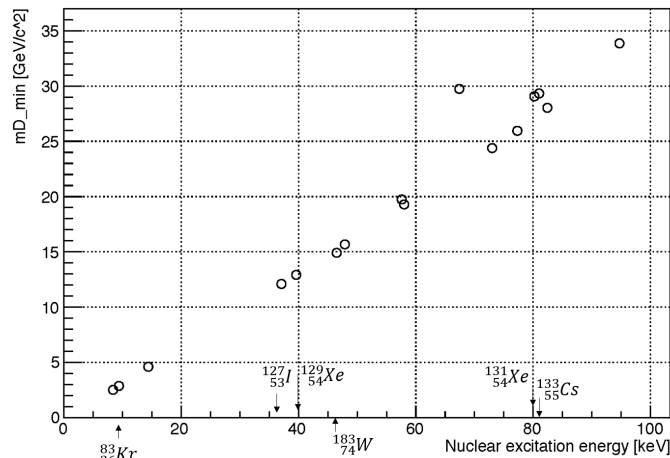


Fig.5.3.1: The minimum detectable dark matter mass as a function of the excitation energies relative to different isotopes. The excitation energies are taken from [14]. Some of them are summarized in table (5.2).

Thanks to the simple eq. (5.11), given the excitation energy of the various isotopes, the minimum dark matter mass detectable through inelastic scattering on nuclei can be inferred. This limit can be useful to clarify if a target is sensitive or not to a precise dark matter mass. For example the graph in fig.(5.3.1) suggests that the lower dark matter mass that can activate a nuclear excitation is between 12 – 13 GeV for $^{127}_{53}\text{I}$ and between 28 – 30 GeV for $^{131}_{54}\text{Xe}$. This simple result allows to establish what experiments have or not have access to inelastic processes that involves nuclear excitation.

It would be interesting to extend this study to atomic excitations due to scattering by WIMPs. Furthermore to shed light on the experimental results, it is necessary to study also inelastic processes characterized by final states not containing the dark matter particle. This latter configuration is possible for candidates different from WIMPs, therefore it is beyond the scope of this work. However it is an interesting hint for a future study.

5.4 Numerical limits on neutrino telescope sensitivity

In the Sun and in the Earth core the temperature is low and the WIMP velocity is non-relativistic, therefore the direct WIMP-annihilation into neutrinos is negligible. The interesting neutrino flux derives from the annihilation or decay of the Standard Model particles produced by the open WIMP-annihilation channel. Each particle of the annihilation channel has an energy $\sim E_\chi \equiv m_\chi$, since the trapped WIMP is on average at rest. Neutrinos produced by the two/three-body decay of these particles have energies equal to $\frac{1}{2}$ or $\frac{1}{3}$ of the WIMP mass. The energy of the muon produced by the deep inelastic scattering $\nu(\bar{\nu}) + N \rightarrow \mu^{-(+)} + X$, that occurs in the detector (in ice or water) or near the detector, in the laboratory reference frame, is [96]:

- $E_{\mu^-} \sim \frac{1}{2}E_{\nu_\mu}$ for $\nu_\mu d \rightarrow \mu^- u$;

5.4 Numerical limits on neutrino telescope sensitivity

- $E_{\mu^+} \sim E_{\bar{\nu}_\mu}$ for $\bar{\nu}_\mu u \rightarrow \mu^+ d$.

These estimations imply that if a detector has an energy threshold E_{th}^μ , the lowest accessible WIMP mass is:

$$m_{\chi,min} \simeq 2E_{th} \quad (5.12)$$

For example, for a generic energy threshold $E_{th} = 20$ GeV, $m_{\chi,min}$ is about 40 GeV.

The estimation (5.12) can be extended to the sterile neutrino candidate. If we consider the sterile neutrino decay $N_1 \rightarrow \gamma + \nu_a$, the active neutrinos energy is $E_{\nu_a} \sim m_{N_1} \sim \text{keV}$, since the interesting sterile neutrino mass range from the dark matter search point of view is $\sim \text{O}(\text{keV})$, as discussed in the previous chapter. The ratio between the sterile neutrino mass and the energy threshold for the muon detection is of the same order of magnitude of (5.12); therefore the neutrino telescopes energy threshold would be of order keV to contribute to the sterile neutrino search via muon-neutrino induced detection.

Conclusions

The cosmological and astrophysical observations impose to the researchers the strenuous and fascinating task of solving the missing mass problem. The cooperation of cosmology and particle physics, together with the experimental efforts, allows to constrain the possible dark matter parameters, that to a first glance appears arbitrarily large. The mass scale relative to the several candidates is discussed. For the axion, proposed as solution of the strong CP problem and whose theoretical background predicts a mass range between 10^{-12} eV to 10^6 eV, the experiments indicate a mass range 10^{-5} eV to 10^{-3} eV. For the sterile neutrino, in order to accommodate with it the dark matter problem, astrophysical observations constrain its mass to be of order of the keV. For the Weakly Interactive Massive Particle (WIMP), the oldest candidate proposed and on which the attention is particularly focused, the mass range is more extended with respect to the interval of 10GeV-1TeV usually encountered in literature, that is only indicative. This restricted interval was considered for the agreement with the experimental limits. Furthermore its fortune is due to the initial common conviction that the electroweak theory could have accommodated the new particle. About that, we discussed the popular 'WIMP Miracle', that is the intriguing coincidence between the WIMP annihilation cross section order of magnitude, that results by cosmological constraints, and the electroweak scale. However, against the expectations, the so far null results at colliders suggest that the possible mediator could be more massive than the gauge bosons of the electroweak theory. The two candidates accommodated in the WIMP proposal and discussed in this work are the supersymmetric neutralino and the Kaluza-Klein photon, this latter belonging to the Universal Extra Dimension (UED) models. As remarked, the resulting allowed mass intervals are quite arbitrary, since new quantum numbers are introduced in both the theories to make stable this potential new particle. The arguments that support the various candidates and the relative theories have been discussed.

The WIMP paradigm is the main topic of the second part of this work. The experimental search dedicates numerous efforts to probe the space of parameters associated to this hypothesis, therefore a deep understanding of its phenomenology and of the available results is necessary. A particular attention is devoted to clarify the conditions under which the comparison between direct and indirect search results is possible. The direct search can provide limits on the possible WIMP nuclear elastic scattering. The indirect search aim to detects the potential WIMP annihilation products. The experimental data are also presented as a combination of direct search and neutrino telescope results, since the comparison is allowed by the common process of nuclear scattering that occurs in the detector for the direct search

Conclusions

and in the WIMP capture process in the center of celestial bodies. These latter processes are relevant for the indirect dark matter search with neutrino telescopes. In these processes the extrapolation of the WIMP nuclear cross section is possible only under the condition of equilibrium between capture and annihilation processes. The estimate of the numerical limit on the minimum WIMP mass detectable by neutrino telescopes, establishes that this latter are more competitive for higher dark matter masses. The comparison between direct detection and space telescope results is not possible because γ and charged cosmic rays cannot be associated to a bordered source. An integral on the halo dark matter density along the line of sight is necessary and the process of WIMP nuclear elastic scattering cannot be exploited. Finally the numerical analysis on the counting rate that occurs in direct detection experiments provides interesting results that could be useful to solve the tension among the available data. For a fixed dark matter mass of 10GeV , for a Maxwellian velocity distribution and for a spin-independent cross section, the counting rate per day $\times \text{kg}$ as a function of the recoil energy results greater for germanium, sodium and silicium with respect to that of iodide and xenon, for recoil energies greater than $\sim 3\text{keV}$. This result is in agreement with the panorama of published data, since the DAMA, CDMS-Si and CoGeNT regions of parameter space are centered in a WIMP mass of $\sim 10\text{GeV}$. Furthermore it would be consistent with the null result in experiments as XENON. The results are checked also in presence of a possible form factor, whose contribution appears to be negligible at the recoil energies involved, while it is an important factor of suppression for larger dark matter masses. The results obtained are potentially relevant but this work need a more deep analysis, in particular through the comparison with experimental data. At this state of the study, we consider the results an interesting hint for future studies.

Bibliography

Chapter 1: Cosmological and Astrophysical Evidences of Dark Matter

- [1] Zwicky F. (1933). *Spectral displacement of extra galactic nebulae*. *Helv. Phys. Acta*, 6(110-127), 15.
- [2] E. W. Kolb, M. S. Turner, *The Early Universe*, Addison-Wesley Publishing Company, (Frontiers in Physics; v.69), 1990.
- [3] S. Weinberg, *Cosmology*, Oxford University Press, 2008.
- [4] Ade P. A. R. et al. (2015). *Planck 2015 results. XIII. Cosmological parameters*. arXiv:1502.01589.
- [5] Montani, G. (2011). *Primordial cosmology*. World Scientific.
- [6] Sachs R. K., Wolfe A. M. (1967). *Perturbations of a cosmological model and angular variations of the microwave background*. *The Astrophysical Journal*, 147(1), 73-90.
- [7] Chen L., Huang Q. G., Wang, K. (2016). *Constraint on the abundance of primordial black holes in dark matter from Planck data*. arXiv preprint arXiv:1608.02174.
- [8] Hawking, S. W. (1975). *Particle creation by black holes*. *Communications in mathematical physics*, 43(3), 199-220.
- [9] Carr B., Kuhnel F., Sandstad M. (2016). *Primordial Black Holes as Dark Matter*. arXiv preprint arXiv:1607.06077.
- [10] LIGO Scientific and Virgo Collaboration (2016). *Observation of gravitational waves from a binary black hole merger*. *Physical review letters*, 116(6), 061102.
- [11] LIGO Scientific and Virgo Collaboration (2016). *GW151226: Observation of gravitational waves from a 22-solar-mass binary black hole coalescence*. *Physical Review Letters*, 116(24), 241103.

Chapter 2: Motivations and Candidates for Dark Matter from Particle Physics

- [12] Weinberg, S. (1978). *A new light boson?*. *Physical Review Letters*, 40(4), 223.
-

BIBLIOGRAPHY

- [13] Wilczek, F. (1978). *Problem of Strong p and t Invariance in the Presence of Instantons*. Physical Review Letters, 40(5), 279.7
- [14] Peccei, R. D., Quinn, H. R. (1977). *CP conservation in the presence of pseudoparticles*. Physical Review Letters, 38(25), 1440.
- [15] Peccei, R. D. (2006). *The strong CP problem and axions*. In Axions (pp. 3-17). Springer Berlin Heidelberg.
- [16] Peccei, R. D. (1996). *QCD, strong CP and axions*. arXiv preprint hep-ph/9606475.
- [17] Baker, C. A. (2006). *Improved experimental limit on the electric dipole moment of the neutron*. Physical Review Letters, 97(13), 131801.
- [18] Coleman S. (1988). *Aspects of symmetry: selected Erice lectures*. Cambridge University Press.
- [19] Forkel, H. (2000). *A Primer on Instantons in QCD*. arXiv preprint hep-ph/0009136.
- [20] Turner, M. S. (1990). *Windows on the Axion*. Physics Reports, 197(2), 67-97.
- [21] Carugno, G. (2015). *Axions: A Brief Introduction*. <https://agenda.infn.it>
- [22] K.A. Olive et al. (2014) and 2015 update. (Particle Data Group). *Axions and Other Similar Particles*, Chin. Phys. C, 38, 090001.
- [23] Golub R., Pendlebury J. M. (1972). *The electric dipole moment of the neutron*. Contemporary Physics, 13(6), 519-558.
- [24] Cabibbo, N. (2008). *Simmetrie Discrete*.
- [25] Dirac P. A. (1949). *Forms of relativistic dynamics*. Reviews of Modern Physics, 21(3), 392.
- [26] Pospelov M., Ritz A. (2005). *Electric dipole moments as probes of new physics*. Annals of Physics, 318(1), 119-169.
- [27] Mohapatra R. N., Pal, P. B. (2004). *Massive neutrinos in physics and astrophysics* (Vol. 72). World scientific.
- [28] Adhikari R. et al. (2016). *A white paper on keV sterile neutrino dark matter*. arXiv preprint arXiv:1602.04816.
- [29] K.A. Olive et al. (Particle Data Group), *Number of Neutrino Types*, Chin. Phys. C, 38, 090001 (2014) and 2015 update.
- [30] Asaka T., Blanchet S., Shaposhnikov M. (2005). *The ν MSM, dark matter and neutrino masses*. Physics Letters B, 631(4), 151-156.
- [31] Merle, A. (2013). *keV neutrino model building*. International Journal of Modern Physics D, 22(10), 1330020.

BIBLIOGRAPHY

- [32] Shaposhnikov M., (2013). *Sterile Neutrinos*. Particle Dark Matter, Bertone G., 228-248.
- [33] Abazajian K. N. et al (2012). *Light sterile neutrinos: a white paper*. arXiv preprint arXiv:1204.5379.
- [34] Boyarsky A., Malyshev D., Neronov A., Ruchayskiy O. (2008). *Constraining dark matter properties with SPI*. Monthly Notices of the Royal Astronomical Society, 387(4), 1345-1360.
- [35] Boyarsky A., Ruchayskiy O., Iakubovskiy D. (2009). *A lower bound on the mass of dark matter particles*. Journal of Cosmology and Astroparticle Physics, 2009(03), 005.
- [36] Abazajian K., Fuller G. M., Patel M. (2001). *Sterile neutrino hot, warm, and cold dark matter*. Physical Review D, 64(2), 023501.
- [37] Boyarsky A., Ruchayskiy O., Iakubovskiy D., Franse J. (2014). *Unidentified line in X-ray spectra of the Andromeda galaxy and Perseus galaxy cluster*. Physical review letters, 113(25), 251301.
- [38] Bulbul E., Markevitch M., Foster A., Smith R. K., Loewenstein M., Randall S. W. (2014). *Detection of an unidentified emission line in the stacked X-ray spectrum of galaxy clusters*. The Astrophysical Journal, 789(1), 13.
- [39] Pal P. B. (2011). *Dirac, majorana, and weyl fermions*. American Journal of Physics, 79(5), 485-498.
- [40] Cirelli, M., Marandella, G., Strumia, A., Vissani, F. (2005). *Probing oscillations into sterile neutrinos with cosmology, astrophysics and experiments*. Nuclear Physics B, 708(1), 215-267.
- [41] Lee T. D., Yang C. N. (1956). *Question of parity conservation in weak interactions*. Physical Review, 104(1), 254.
- [42] Kobzarev I. Y. Okun, L. B., Pomeranchuk, I. Y. (1966). *POSSIBILITY OF OBSERVING MIRROR PARTICLES*. Yadern. Fiz., 3.
- [43] Okun' L. B. (2007). *Mirror particles and mirror matter: 50 years of speculation and searching*. Physics-Uspekhi, 50(4), 380-389.
- [44] Foot R. (2014). *Mirror dark matter: Cosmology, galaxy structure and direct detection*. International Journal of Modern Physics A, 29(11n12), 1430013.
- [45] Foot R. (2012). *Mirror dark matter interpretations of the DAMA, CoGeNT, and CRESST-II data*. Physical Review D, 86(2), 023524.
- [46] K.A. Olive et al. (Particle Data Group), *DARK MATTER*, Chin. Phys. C, 38, 090001 (2014) and 2015 update.
- [47] Lee B. W., Weinberg S. (1977). *Cosmological lower bound on heavy-neutrino masses*. Physical Review Letters, 39(4), 165.

BIBLIOGRAPHY

- [48] Edsjö J., Gondolo P. (1997). *Neutralino relic density including coannihilations*. Physical Review D, 56(4), 1879.
- [49] Griest K., Seckel D. (1991). *Three exceptions in the calculation of relic abundances*. Physical Review D, 43(10), 3191.
- [50] Girardello L., Grisaru M. T. (1982). *Soft breaking of supersymmetry*. Nuclear Physics B, 194(1), 65-76.
- [51] Martin S. P. *A Supersymmetry Primer* (2016). arXiv preprint hep-ph/9709356, 161, 162.
- [52] Hall L. J. Moroi, T., Murayama H. (1998). *Sneutrino cold dark matter with lepton-number violation*. Physics Letters B, 424(3), 305-312.
- [53] Appelquist T., Cheng H. C., Dobrescu B. A. (2001). *Bounds on universal extra dimensions*. Physical Review D, 64(3), 035002.
- [54] Servant G., Tait, T. M. (2003). *Is the lightest Kaluza–Klein particle a viable dark matter candidate?*. Nuclear Physics B, 650(1), 391-419. ISO 690
- [55] Hooper D., Profumo S. (2007). *Dark matter and collider phenomenology of universal extra dimensions*. Physics Reports, 453(2), 29-115. ISO 690
- [56] Coleman S., Mandula J. (1967). *All possible symmetries of the S matrix*. Physical Review, 159(5), 1251.
- [57] Vissani, F. (1998). *Do experiments suggest a hierarchy problem?*. Physical Review D, 57(11), 7027.
- [58] Weinberg, S. (1989). *The cosmological constant problem*. Reviews of Modern Physics, 61(1), 1.ISO 690
- [59] Kolb E. W., Chung D. J., Riotto A. (1998). *WIMPzillas!*. arXiv preprint hep-ph/9810361.
- [60] Griest K., Kamionkowski M. (1990). *Unitarity limits on the mass and radius of dark-matter particles*. Physical Review Letters, 64(6), 615.

Chapter 3: The Phenomenology of WIMP Candidates

- [61] Bergstrom L., Ullio P., Buckley J. H. (1998). *Observability of γ rays from dark matter neutralino annihilations in the Milky Way halo*. Astroparticle Physics, 9(2), 137-162.
- [62] Jungman G., Kamionkowski M., Griest K. (1996). *Supersymmetric dark matter*. Physics Reports, 267(5), 195-373.
- [63] Lisanti, M. Strigari, L. E., Wacker, J. G., Wechsler R. H. (2011). *Dark matter at the end of the Galaxy*. Physical Review D, 83(2), 023519.

BIBLIOGRAPHY

- [64] Fox P. J., Kribs G. D., Tait T. M. (2011). *Interpreting dark matter direct detection independently of the local velocity and density distribution*. Physical Review D, 83(3), 034007.
- [65] Catena R., Ullio P. (2010). *A novel determination of the local dark matter density*. Journal of Cosmology and Astroparticle Physics, 2010(08), 004.
- [66] Lewin J. D., Smith P. F. (1996). *Review of mathematics, numerical factors, and corrections for dark matter experiments based on elastic nuclear recoil*. Astroparticle Physics, 6(1), 87-112.
- [67] Goodman M. W., Witten E. (1985). *Detectability of certain dark-matter candidates*. Physical Review D, 31(12), 3059.
- [68] Helm, R. H. (1956). *Inelastic and elastic scattering of 187-MeV electrons from selected even-even nuclei*. Physical Review, 104(5), 1466.
- [69] Engel J. (1991). *Nuclear form factors for the scattering of weakly interacting massive particles*. Physics Letters B, 264(1-2), 114-119.
- [70] Starkman G. D., Spergel D. N. (1995). *Proposed new technique for detecting supersymmetric dark matter*. Physical review letters, 74(14), 2623.
- [71] Ellis J., Flores R. A. Lewin, J. D. (1988). *Rates for inelastic nuclear excitation by dark matter particles*. Physics Letters B, 212(3), 375-380.
- [72] Wikström G., Edsjö J. (2009). *Limits on the WIMP-nucleon scattering cross-section from neutrino telescopes*. Journal of Cosmology and Astroparticle Physics, 2009(04), 009.
- [73] Gould A. (1987). *Resonant enhancements in weakly interacting massive particle capture by the earth*. The Astrophysical Journal, 321, 571-585.
- [74] Blennow M., Edsjö J., Ohlsson, T. (2008). *Neutrinos from WIMP annihilations obtained using a full three-flavor Monte Carlo approach*. Journal of Cosmology and Astroparticle Physics, 2008(01), 021.

Chapter 4: Experimental Search for Dark Matter Particles

- [75] K.A. Olive et al. (Particle Data Group), *DARK MATTER*, Chin. Phys. C, 38, 090001 (2014) and 2015 update.
- [76] Shields, E. K. (2015). *SABRE: A search for dark matter and a test of the DAMA/LIBRA annual-modulation result using thallium-doped sodium-iodide scintillation detectors*.
- [77] Pettus W. C. (2015). *Cosmogenic Activation in NaI Detectors for Dark Matter Searches*. (Doctoral dissertation, THE UNIVERSITY OF WISCONSIN-MADISON).

BIBLIOGRAPHY

- [78] Bernabei R. et al (2008). *The Dama/Libra apparatus*. Nuclear Instruments and Methods in Physics Research Section A: Accelerators, Spectrometers, Detectors and Associated Equipment, 592(3), 297-315. ISO 690
- [79] Belli P. (2016). *Results and strategies in dark matter detection*. International Journal of Modern Physics D, 25(05), 1630013.
- [80] Bernabei R. et al. (2008). *Investigation on light dark matter*. Modern Physics Letters A, 23(26), 2125-2140.
- [81] Bernabei et al (1999). *WIMPs search by scintillators: possible strategy for annual modulation search with large-mass highly-radiopure NaI (TI)*. Nuclear Physics B-Proceedings Supplements, 70(1), 79-84.
- [82] Bernabei (2002). *Results with the DAMA/NaI (Tl) experiment at LNGS*. Nuclear Physics B-Proceedings Supplements, 110, 61-63.
- [83] Bernabei et al (2013) *Final model independent result of DAMA/LIBRA-phase1*. The European Physical Journal C, 73(12), 1-11.
- [84] Adriani O. et al. (2009). *An anomalous positron abundance in cosmic rays with energies 1.5–100 GeV*. Nature, 458(7238), 607-609.
- [85] Adriani, O. (2013) *The cosmic-ray positron energy spectrum measured by PAMELA*. arXiv preprint astro-ph/1308.0133.
- [86] Cirelli M., Kadastik M., Raidal M., Strumia A. (2009). *Model-independent implications of the e^\pm , cosmic ray spectra on properties of Dark Matter*. Nuclear Physics B, 813(1), 1-21.
- [87] Aharonian F. et al. (HESS Collaboration)(2008). *Energy spectrum of cosmic-ray electrons at TeV energies*. Physical Review Letters, 101(26), 261104.
- [88] <http://sci.esa.int/integral/45320-galactic-positron-annihilation-not-a-signal-of-dark-matter>
- [89] Bulbul E., Markevitch M., Foster, A., Smith R. K., Loewenstein M., Randall S. W. (2014). *Detection of an unidentified emission line in the stacked X-ray spectrum of galaxy clusters*. The Astrophysical Journal, 789(1), 13.
- [90] Bernabei R. et al. (2012). *DAMA/LIBRA RESULTS AND PERSPECTIVES OF THE SECOND STAGE*. Current Problems in Nuclear Physics and Atomic Energy, 21.
- [91] Agnese R. et al. (2013). *Silicon detector dark matter results from the final exposure of CDMS II*. Physical review letters, 111(25), 251301.
- [92] Aalseth C. E. et al. (2011). *Results from a search for light-mass dark matter with a p-type point contact germanium detector*. Physical Review Letters, 106(13), 131301.

BIBLIOGRAPHY

- [93] Aad G. et al (ATLAS Collaboration)(2015). *Summary of the ATLAS experiment's sensitivity to supersymmetry after LHC Run 1—interpreted in the phenomenological MSSM*. Journal of High Energy Physics, 2015(10), 1-76.
- [94] Akerib D. S. et al (2016). *Improved limits on scattering of weakly interacting massive particles from reanalysis of 2013 LUX data*. Physical review letters, 116(16), 161301.
- [95] Aad G .et al. (ATLAS Collaboration) (2015). *Search for new phenomena in final states with an energetic jet and large missing transverse momentum in pp collisions at sqrt s= 8 TeV with the ATLAS detector*. The European Physical Journal C, 75(7), 1-43.

Chapter 5: Numerical Results

- [96] Hughes I. S., (1991). *Elementary Particles*. Cambridge University Press, 3th edition.

